UPMC HILLMAN CANCER CENTER ACADEMY

FRIDAY, JULY 31, 2026

ABSTRACT BOOK

UPMC | HILLMAN CANCER CENTER

University of Pittsburgh

Welcome

Thank you for joining us today to honor our hard-working scholars and laboratories from the Hillman Academy! We strive to provide cutting-edge research and career preparatory experiences to a diverse group of highly motivated high school students who are interested in pursuing higher education and careers in STEM fields. In this hands-on summer program, scholars are placed in laboratories directed by dedicated faculty and trainee mentors across the University of Pittsburgh Campus.

Over the course of its history, the Hillman Academy has become an award-winning science, technology, engineering, and mathematics (STEM) program that prepares students for successful college careers and beyond. The Academy was initiated in 2009 under the directorship of Michael Lotze, MD, and has grown to the program it is today with generous support from the NIH, Doris Duke Charitable Foundation, Jack Kent Cooke Foundation, UPMC, Hillman Foundation, Ear and Eye Foundation, Beckwith Funds, Stan Marks Foundation, Shadyside Hospital Foundation, University of Pittsburgh, grateful parents and patients, and the many University faculty, trainees, and staff who give selflessly of their time.

Please join us in honoring these students and mentors, as well as the hard work they did this summer to complete an authentic research project. We are so glad that you chose to join us today and are pleased that you have given your scholar a chance to work with our talented faculty, students, and fellows!

Hillman Academy Staff

Program Director: David Boone

Associate Director: Joseph Ayoob

Project Manager: Steven Jones

Hillman Academy Site Directors

Cancer Biology (CB): Dr. Deborah Galson and Dr. Ines Lohse

Computer Science, Biology and Biomedical Informatics (CoSBBI): Dr. David Boone

Computational Biology (CompBio): Dr. Joseph C. Ayoob and Dr. Keisuke Ishihara

Immunology and Cancer Immunotherapy (ICI): Dr. Tullia Bruno and Dr. Greg Delgoffe

Ophthalmology (VISION): Dr. Yuanyuan Chen

Pathobiology: Dr. Andrew Duncan and Dr. David Gau

Surgery: Dr. Emilia Diego

Tech Drive X (TDX): Dr. David Maestas and Serafina Lanna

Women's Cancer Research Center (WCRC): Dr. Partha Roy and Dr. Michelle M. Williams

Thank You

This program was made possible with the help of the following people and organizations.

Funding

National Cancer Institute (NCI) Youth Enjoy Science (YES) R25

Doris Duke Charitable Foundation (DDCF)

Hillman Foundation

Stan Marks Foundation

Ear and Eye Foundation

Pittsburgh Cure Sarcoma

Buncher Foundation

University of Pittsburgh

Magee Women's Research Institute

National Institutes of Health NCI CURE - past

The Beckwith Institute - past

Shadyside Hospital Foundation - past

UPMC Center for Engagement and Inclusion – past

Jack Kent Cooke Foundation - past

UPMC Parking and Security – past

Partners

Fund for the Advancement of Minority Education (FAME)

Homeless Children's Education Fund (HCEF)

Pittsburgh Public Schools (PPS)

Remake Learning

YWCA

MPowerhouse

Investing Now

Propel Schools

STEM PUSH Network

Precollege STEM Programs at Pitt

The Citizen Science Lab

Gene Team

BioZone

Community Engagement Centers

Pittsburgh Promise

Neighborhood Learning Alliance

Propel Schools

Grateful parents and patients


NIH
NATIONAL
CANCER
INSTITUTE


DORIS DUKE
CHARITABLE FOUNDATION


HILLMAN
FAMILY FOUNDATIONS


the
pittsburgh
promise


remake
learning


HOMELESS
CHILDREN'S
EDUCATION
FUND


MAGEE-
WOMENS
RESEARCH INSTITUTE
& FOUNDATION


PITTSBURGH CURE
SARCOMA


FAME
FUND FOR ADVANCEMENT OF MINORITIES THROUGH EDUCATION


Pittsburgh
Public Schools

Hillman Academy Leadership Team

Dr. John Byrd

Dr. Kathryn Schmitz

Dr. Christopher Bakkenist

Dr. Devin Dressman

Dr. David Boone

Dr. Joe Ayoob

Steven Jones

Administration

Beth Baic

Genine Bartolotta

Michael Becich

Amanda Bytzura, MBA

Rob Ceccehetti

Heather Culp

Dawn Cziczin

Bridget Deasy, PhD

Josh Derby

Keith Durst

Carrie Fogel

Megan Hamilton

Harry Hochheiser

Steven Jones

Barbara Karnbauer

Jon Klosinski

Vladislav Leskovtec

Alison Lithgow

Renee Mandell

Christy McCrory

Kelsey Meyer

George Michalopoulos, MD, PhD

John Moretti, MHA, MBA

Carolyn Nolte

Liron Pantanowitz, MD, PhD

Cyndy Patton

Glenn Peterson

Bryce Petrunich

Toni Porterfield

Rayleigh Reynolds

Fritz Roth

Jose-Alain Sahel

Kirsten Schwoegl

Amanda Shaheen

Sanjeev G. Shroff

Lawton Snyder

Alejandro Soto-Gutierrez, MD, PhD

Lola Thompson

Fangling Tian

Dr. Toren Finkel

Gina Toy-Cuttler

Shyam Visweswaran

Nicole Webb

Justin Wideman

Bethany Wintermantel

Emily Woodard

Xiaojie Yu

Technology

Dianna Fennell

Scot Dunsmore

Bryan Krinberg

Mark Schramm

Roland Frasher

Ethan Hay

Interpreters and Future Deaf Scientist Partners

Naveh Berner-Kadish
Heather Gray
Julie Ann Mountain
Dr. Megan Majocha
Gregory Mendenha

Hendrix Undergrads

Sanskruti Ghanti
Pranit Koppolu

Pittsburgh Cure Sarcoma High School Interns

Sophie O'Toole
Cruz Sanders

TECBio REU @ Pitt Mentoring Committee

Lydia Aluko
David Anthony Jr
Prisha Banushali
Cooper Ferrance
Emma Killmeyer
Diana Manzanes
Patricia Rodriguez-Moreno
Ebise Tarekegn

Instructors, TAs, and Education Team

Jacqueline Avila
Isabelle Chickanosky
Maria Constanza Potilinski
Katherine Davoli
Adam Forrest
Daniel Gao
Anthony Gebrane
Lexi Hill
Tom Hintelmann
Huda Issa Atiya
Naveen Kumar Tangudu
Chris Merkel
Stephanie Podguski
Saira Rizwan
Shriya Siddhartha
Kristin Wannemo
Sierra White
Hamza Yazdani
Liyun Zhang

Speakers, Lecturers, and Guests

Issam Al Diri
Joshua Anderson
John Ash
Roshni Batt
Silke Becker
Marlene Behrmann

Speakers, Lecturers, and Guests (cont.)

David Boone, PhD

Bryan Brown, PhD

Alex Chang

Yuanyuan Chen

Isabelle Chickanosky

Carlos Cosme

Andrew Craig

Chi-An Daugavietis

Amal Elhaw

Julia Foldi

Len Frisbie

Steven K. Galson, MD, MPH, MSSM

Jessie Galson, PhD, MSSM

Brittany Gomez

Kayla Hodges

Caden Horton

Eileen Huang

Priyasha Itani

Anna Kane, PhD

Semmie Kim

Paul Kingchinton (Kip)

Rajay Lindsay

Roger Loughney

John Maier

Ugonna Mbaekwe

Caelan McCormack

Douglas McCormack, JD

Noelle Michel

Christopher Morii-Sciolla

Yana Najjar

Carola Neumann

Craig Nicholson

Steffi Oesterreich

Nate Paine

Sudipta Pathak

Rebecca Pfeiffer

Dhivyaa Rajasundaram

Billy Reynolds, PhD

Santiago Rivero

Brent Schlegel

Maria Silvaggio

Claudette St. Croix, PhD

Wyatt Stoll

Swathi Suresh

Shikhar Uttam

Andreas Vogt

Yaya Wang

Gillian Williams

Ethan Wolfe

Professional Development Seminar Series Speakers

Mohammed Ali Al-Nagash

Armin Aryannejad

Joe Ayoob

Amelia Balet

Katherine Beavis

David Boehm

Tullia Bruno

Sam Butler

Jonathan Cho

Carolyn De La Cruz

Gianna DeBole

David Donahue

Adriana Duncan

Mia Fritz

Victoria Garcia

Viraj Govani

Donise Griffin

Najih Haider

Gloria Hao

Honghao (Harvey) Xu

Alexis Henderson

Rachel Hyzny

Ruth Joel

Kylie King

Professional Development Seminar Series Speakers (cont.)

Guldane Kocyigit

Nana Kwame Dwomoh

Joshua Le

Sean Lee

Taylor Monitz

Lucia Nanda

Alzbeta Novotna

Asher Peng

Sunny Pham

Lauriane Pinto

Shamael Rahamani

Ethan Richlak

Neha Shetty

Eduplast Team

Caroline Tyndall

Nithila Vijayan

Hunter Waltermire

Jerome Watts

Alastair Watts

Andy Weng

Sarah-Beth Winikoff

William Zhang

Offices and Departments

University of Pittsburgh

UPMC Hospital System

UPMC Hillman Cancer Center

UPMC Children's Hospital of Pittsburgh

Pitt School of Medicine

Ear and Eye Institute

UPMC St. Margaret

UPMC Security Office

UPMC Volunteer office

Disability Resources and Services

Pitt IT/ Technology Help Desk

Pitt Health Sciences IT

Panther Central

Department of Biomedical Informatics

Department of Ophthalmology

Computational and Systems Biology

Department of Immunology

Department of Pathology

Department of Cell Biology

Department of Surgery

Aging Institute

Cellular & Molecular Pathology Graduate Training Program

Center for Biologic Imaging

Center for Transcriptional Medicine

Department of Bioengineering

Magee-Womens Research Institute

McGowan Institute of Regenerative Medicine

University Counsel

And the many other departments that support this program

Mentors

Thanks to the hundreds of mentors across campus each of which is recognized on the individual student abstracts and site schedule

UPMC HCC Summer Academy
Cancer Biology Site 2026 Research Symposium

July 31, 2026, 8:30 am-12:45 pm

Auditorium in Assembly Building on 5051 Center Ave

Join Zoom Meeting: https://pitt.zoom.us/j/98430307436 Passcode: 683008

8:30 AM **Welcoming Remarks -** CB Site Education Team:
Deborah L. Galson, PhD (Site Director) & Ines Lohse, PhD (Site Co-Director)

8:45 AM **#1** **Melanie Lam**
PI: Diwaker Davar, MD, MSc; Lab Mentor: Drew Hurd, BS

9:00 AM **#2** **Victoria Chernetska**
PI: Bridget Deasy, PhD; Lab Mentor: Olena Abakumova, PhD; Jacob Harris, BS

9:15 AM **#3** **Cruz Sanders**
PI: Bridget Deasy, PhD; Lab Mentor: Olena Abakumova, PhD; Jacob Harris, BS

9:30AM **#4** **Kaisra Setiawan**
PI: Ahmad P. Tafti, PhD; Ines Lohse, PhD

9:45 AM **#5** **Sophie O'Toole**
PI: Joel Greenberger, MD; Amitava Mukherjee, PhD; Lab Mentor: Renee Fisher, BS

10:00 AM **#6** **Andy Weng**
PI: Wei Du, MD, PhD; Lab Mentor: Jian Xu, PhD; Jianyang Bao, PhD; Oliver Freund

10:15 AM **#7** **Najih Haider**
PI: Wei Du, MD, PhD; Lab Mentor: Jian Xu, PhD; Jianyang Bao, PhD; Logan Sund, BS

10:30-10:45 AM **---------- BREAK ----------**

10:45 PM **#8** **Maeve Beresford**
PI: Ken Urish, MD, PhD; Lab Mentor: Beth Knapick, BS; Jewelia Rempuszewski, BS

11:00 AM **#9** **Ismael Bey**
PI: Jessie Nedrow, PhD; Lab Mentor: Angel Cortez, BS

11:15 AM **#10** **Zhanyu (Eric) Jiang**
PI: Ines Lohse, PhD; Kurt Weiss, MD; Lab Mentor: Ecem Ayvaz Golcuk, PhD

11:30 AM **#11** **Anish Goyal**
PI: Ines Lohse, PhD; Kurt Weiss, MD; Lab Mentor: Ecem Ayvaz Golcuk, PhD

11:45 AM **#12** **Stephanie Chen**
PI: Kathy Shair, PhD; Lab Mentor: Joshua Walston, PhD

12:00 PM **#13** **Vesta Homayoun**
PI: Allison Bean, MD, PhD; Lab Mentor: Hiroki Kaneta, PhD

12:15 PM **#14** **Ayanna Hall**
PI: Tatiana Moiseeva, PhD; Lab Mentor: Rohan Harolikar, BS

12:30 PM **#15** **Enrique Ochoa**
PI: Jianying Zhang, PhD; Lab Mentor: Vasyl Pastukh, MD, PhD

12:45 PM **#16/17** **Sanskruti Ghanti & Pranit Koppolu (Undergrads @ Hendrix College)**
PI: Allison Bean, MD, PhD *PI: Karen Schoedel, MD; Lab Mentor: Ecem Ayvaz Golcuk, PhD*

1:00 PM **------ LUNCHEON (Atrium, Crane Shed) ------**

2:30 PM **ACADEMY-WIDE CLOSING CEREMONY (Assembly Auditorium)**

Computational Biology Site Agenda

2026 Research Symposium • Hillman Academy

July 31, 2026
3396 Fifth Ave, Pittsburgh, PA 15213
Room 10105
Virtual link: https://pitt.zoom.us/j/93921815682

9:30 – 10:00 AM	**Students check their slides on shared computer**
10:00 – 10:05 AM	**Dr. Keisuke Ishihara and Dr. Joe Ayoob, CompBio Site Head**
10:05 – 10:20 AM	**Allison Shi** Mentors: Dr. Jianhua Xing, Dr. Yong Lu
10:20 – 10:35 AM	**Ethan Varghese** Mentors: Dr. Jim Faeder, Achyudhan Ramesh Kutuva
10:35 – 10:50 AM	**Break**
10:50 – 11:05 AM	**Ahana Vyas** Mentor: Dr. Dennis Kostka, Elizabeth Gilfeather
11:05 – 11:20 AM	**Saranya Saripalli** Mentors: Dr. David Koes, Fareeda Abu-Juam
11:20 – 11:35 AM	**Hongyi Wang** Mentors: Dr. Fritz Roth, Dr. Warren van Loggerenberg
11:35 – 11:45 AM	**Group Photo**
11:45 – 12:30 PM	**Lunch for Students, Mentors, Family, and Friends**

Hillman Academy - CoSBBI

July 31, 2026, 8:00 AM

Murdoch Building, 8th floor classroom

https://us02web.zoom.us/j/85754282549?pwd=elordlNjOE43cFNXOEM4M3RhNGRjZz09

8:00 AM **Welcoming Remarks**

David Boone, PhD

8:05 AM **CoSBBI Scholars Research Presentations – Session 1**

Saanvi Jain
Mentor: Dr. Andriry Bandos
Francesco Keuwo
Mentors: Drs. Rafael Ceschin and William Reynolds
Deilyla Rue
Mentors: Drs. Margaret Rosenzweig and Ruth Modzelewski
Sarah Beth Winikoff
Mentor: Dr. Marissa Gogniat and Lindsey Jorda
Mia Zhao
Mentor: Dr. Uma Chandran
Nana Kwame Dwomoh
Mentors: Dr. Natasa Miskov-Zivanov, Haomiao Luo, and Niloofar Arazkhani

9:40 AM **CoSBBI Scholars Research Presentations – Session 2**

Erick Zhao
Mentors: Dr. Murat Akcakaya, Yifan Zuo, and Ege Ozkoc
Daniel Bandos
Mentors: Dr. Jacob Biehl and Calvin Brinkman
Nixie Grey
Mentors: Dr. Nev Jones, Lauren Fowler, Shannon Pagdon, and Eidolon Kelly
Shreyan Bansal
Mentors: Dr. Liang Zhan, Kun Zhao, and Siyuan Dai
Ayush Srivastava
Mentor: Dr. Xinghua Lu and Alexander VanHelene
Ruth Joel
Mentor: Dr. Olga Kravchenko

11:15 AM **CoSBBI Scholars Research Presentations – Session 3**

Parker Budney
Mentors: Joshua Anderson and Dr. Shyam Visweswaran
Ariella Mensah-Agyekum
Mentors: Dr. Matt Wohlever and Angela Kayll
Tisha Joshi
Mentor: Dr. Inhee Lee
Divya Thirumala
Mentor: Ethan Wolfe
Nevaeh Thompson
Mentors: Dr. Ana Radovic, Kayla Odenthal, and Yueru Tu
Lucia Nanda
Mentor: Dr. Lujia Chen

12:45 PM **Lunch – Baum 4th floor foyer and 407A/B RSVP REQUIRED**

2:30 PM **Hillman Academy Closing Ceremony**

Assembly Building – First Floor Auditorium
5051 Centre Ave or **Zoom for students**:
https://us02web.zoom.us/j/86021100717?pwd=dmVQQ0NvYzFnMUVIOUxKWFdwd2U5UT09

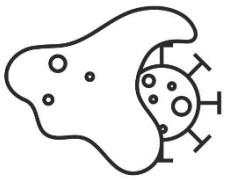

Immunology and Cancer Immunotherapy

Hillman Summer Academy Final Day

Friday, July 31, 2026

9:30 AM-2:30 PM EST (West Wing Auditorium)

Time	Presenter and Mentor
9:30-9:45 AM	Breakfast (optional)
9:45-10:00 AM	**Opening remarks** *Drs. Tullia Bruno and Greg Delgoffe*
10:00-10:15 AM	**Ashton Creech** *Mentor: Dr. Greg Delgoffe*
10:15-10:30 AM	**Sofia Melani** *Mentors: Dr. Tullia Bruno, Dr. Allie Casey, and Charu Arora*
10:30-10:45 AM	**Veda Krishna** *Mentor: Dr. Adam Soloff*
10:45-11:00 AM	**Lacqueeta Oduogo** *Mentor: Dr. Adam Soloff*
11:00-11:15 AM	*Short networking break*
11:15-11:30 AM	**Melody Ann Marsh** *Mentor: Dr. Jishnu Das*
11:30-11:45 AM	**David Boehm** *Mentor: Dr. Jishnu Das*
11:45-12:00 PM	**Aleya Hamilton** *Mentor: Dr. Tina Sumpter*
12:00-12:15 PM	**Kylie King** *Mentor: Dr. Dayana Rivadeneira*
12:15-12:30 PM	*Short networking break*
12:30-12:45 PM	**Nathaniel Javorski** *Mentors: Dr. Dario Vignali, Dr. Creg Workman, and Sam Butler*
12:45-1:00 PM	**Catherine Yang** *Mentor: Dr. Amanda Poholek*
1:00-1:15 PM	**Eric Peng** *Mentor: Dr. Xiaoming Hu, and JiajingShan*
1:15 PM	**Final remarks, group picture, and grab and go lunch** *Migrate to Assembly Building*
2:30 PM	**Start of final ceremony in Assembly Auditorium**

We would love for you to join us in person, but if you must join virtually, here is the zoom link:

https://pitt.zoom.us/j/96376428009

Pathobiology

2026 Research Symposium • Hillman Academy

July 31, 2026

S120 BST, 200 Lothrop St., Pittsburgh, PA 15261
Virtual: https://pitt.zoom.us/j/97160327501

9:00 AM **Morning Mixer**
Join us for coffee, juice, and pastries.

9:15 AM **Welcome**
Drs. Andrew Duncan & Dave Gau, Pathobiology Site Heads

9:30 AM **Oral Presentations** (10 min. presentations + 5 min. questions); introductions by lab mentors

9:30 AM **Myles Denton**
Lab, Dr. Christiano Alves; *Mentor,* Dr. Igor Gomes dos Santos

9:45 AM **Rhea Patel**
Lab, Dr. Bharat Bhushan; *Mentor,* Dr. Siddhi Jain

10:00 AM **Lotus Soletti**
Lab & Mentor, Dr. Amanda Clark

10:15 AM **Adham Hendawy**
Lab & Mentor, Dr. Rodrigo Florentino

10:30 AM **Sebastian Lamana**
Lab & Mentor, Dr. Lanuza Faccioli

10:45 AM **BREAK**

11:00 AM **Vishruth Vignesh**
Lab, Dr. Dave Gau; *Mentors,* Alyssa Arminan & Alison Buck

11:15 AM **Josiah Chalmers**
Lab, Dr. Julia Kofler; *Mentors,* Riley Sawka, Mark Stauffer, & Hossein Tahmasebi Dehkordi

11:30 AM **Gianna Mazer**
Lab, Dr. Christi Kolarcik; *Mentor,* Stefanie Taiclet

11:45 AM **Ella Belcher**
Lab, Dr. Ivona Pandrea; *Mentors,* Dr. Samuel Johnson & Dr. Cuiling (Amy) Xu

12:00 PM **Gabrielle Wilkins**
Lab & Mentor, Dr. Tim Perkins

12:15 PM **Lunch – S120 BST**

2:30 PM **Closing Ceremony**
Assembly Building, First Floor Auditorium
5051 Centre Ave, Pittsburgh, PA 15213

Department of Surgery

2026 Research Symposium • Hillman Academy

July 31, 2026
Hillman Cancer Center 5115 Centre Ave
Cooper Conference Room AB (Ground Floor)
https://pitt.zoom.us/j/93921202458
Meeting ID: 939 2120 2458

10:00 AM – 10:15 AM	**Opening Remarks** *Dr. Emilia Diego*
10:15 AM – 10:25 AM	**Mia Fritz** *Mentor: Dr. Elizabeth Bailey*
10:25 AM – 10:35 AM	**Isabel Ulis** *Mentor: Dr. Samer Tohme*
10:35 AM – 10:45 AM	**Asher Peng** *Mentor: Dr. Robert Tessler*
10:45 AM – 10:55 AM	**Honoria Saxton** *Mentor: Dr. Melanie Scott*
10:55 AM – 11:05 AM	**Blake Whiteman** *Mentors: Dr. Joshua Brown & Dr. Christine Leeper*
11:05 AM – 11:15 AM	**Bradyn Whiteman** *Mentor: Dr. Genia Dubrovsky*
11:15 AM – 11:25 AM	**Amaia Dodds** *Mentor: Dr. Erin Bayley*
11:25 AM – 12:00 PM	**Group Discussion and Q&A**
12:00 PM – 1:00 PM	**Lunch**
2:30 PM At Assembly Building	**Graduation Ceremony**

TECH DRIVE X

2026 Research Symposium • Hillman Academy

July 31, 2026
CNBIO Building, 300 Technology Drive, Pittsburgh PA 15213; **Room 203**
Zoom link: https://pitt.zoom.us/j/96344265712; Meeting ID: 963 4426 5712; Passcode: 060277

9:00 **Welcome & Refreshments**

9:15 **Welcome by Site Directors Dr. David Maestas and Serafina Lanna**

9:30 **Research Presentations**

9:30 **Khamya Cobb-Hewlett**
Lab, Dr. Jonathan Vande Geest; *Mentor*, Jacqueline Avila

9:45 **Shirish Krishna Bollineni**
Lab, Dr. Jonathan Vande Geest

10:00 **Aayushi Vardhan**
Lab, Dr. Jonathan Vande Geest; *Mentor*, Dr. David Maestas

10:15 **Anna Bittner**
Lab, Dr. David Vorp; *Mentor*, Dr. Kiran McLoughlin

10:30 **Nithila Vijayan**
Lab, Dr. Amrita Sahu; *Mentor*, Jagruti Kosaraju

10:45 **Break**

11:00 **Despina Gambotto**
Lab, Dr. TK Kozai; *Mentor*, Camila Garcia

11:15 **Aaditya Kasture**
Lab, Dr. TK Kozai; *Mentor*, Vanshika Singh

11:30 **Preston Oakes**
Lab, Dr. TK Kozai; *Mentor*, Dr. Anna Korol

11:45 **Isha Vyawahare**
Lab, Dr. Jay Tan

12:00 **Grace Yang**
Lab, Dr. Bistra Iordanova

12:15 **Group Picture**

12:30 **Lunch**

2:30 **Closing Ceremony at The Assembly Building**

Hillman Summer Students Research Meeting 2026 - VISION

July 31st, 2026, 9:30 to 1:00 pm EST
IN-PERSON meeting at MHP-PAV 4.221A

Zoom link: https://pitt.zoom.us/j/96614385629

Each session will be started by a brief intro of each student by his/her mentor followed by a 10 min presentation leaving 2-3 min Q&A and picture time.

9:30-9:40 am Start the OPT site meeting

9:40-9:55 am William Zhang (Mentor: Dr. Issam Al Diri)

9:55-10:10 am Zainab Al-Nagash (Mentor: Drs. Constanza Potilinski and John Ash)

10:10-10:25 am Noa Litwin (Mentor: Dr. Yuanyuan Chen)

10:25-10:40 am Benjamin Shuai (Mentor: Dr. Liyun Zhang)

10:40-10:55 am Break and Awards Announcement

10:55-11:10 am Patrick Johnson (Mentor: Dr. Rebecca Pfeiffer)

11:10-11:25 am Christie Koyo (Mentor: Mx. Katherine Davoli)

11:25-11:40 am Sophie Filipink-Smith (Mentor: Dr. Patrick Mayo)

11:40-11:55 am Shivum Telang (Mentor: Dr. Daniel Gao)

11:55-12:30 pm Pictures, Award announcement and Lunch

Womens Cancer Research Center Site Agenda

2026 Research Symposium • Hillman Academy

July 31, 2026
Assembly Building, Room 2001
5051 Centre Ave
https://pitt.zoom.us/j/96875684045
Passcode: 266100

10:30 am **Welcome**
Michelle Williams, Womens Cancer Research Center Site Head

10:45 am **Research Presentations** (10-12 min. presentations + 3-5 min. questions); introductions by lab mentors

10:45 am **Shamael Rahamani**
Mentors: Dr. Partha Roy & Masoumeh Baghaei

11:00 am **Amelia Balet**
Mentors: Dr. Steffi Oesterreich & Dr. Adrian Lee & Alex Opsahl

11:15 am **Angelina Li**
Mentors: Dr. Lan Coffman & Dr. Huda Issa Atiya & Dr. Len Frisbie

11:30 am **Helena Khalil**
Mentors: Dr. Nadine Hempel & Shriya Kamlapurkar

11:45 am **---Break----**

12:00 pm **Manal AL Hussein**
Mentors: Dr. Abir Mukherjee & Paulina Keskinidis

12:15 pm **Sunny Pham**
Mentors: Dr. Michelle Williams & Angelica Phan

12:30 pm **Sai Saharsh Gumudavelly**
Mentors: Dr. Wayne Stallaert & Janet McLaughlin

12:45 pm **Lunch – Assembly Building, Room 2001**

2:30 pm **Closing Ceremony – Assembly Building, Richards Auditorium**

Characterizing a neutralizing antibody against CD36

Introduction: Ovarian cancer is the deadliest gynecological cancer affecting 21,000 women yearly. It involves abnormal cell growth in the ovaries and fallopian tubes. It is often diagnosed late due to subtle symptoms, resulting in high mortality rates. CD36, a lipid transporter is highly expressed in cancer cells adjacent to adipocytes and facilitates tumor growth. Previously studies have shown that cancer cell specific inhibition of CD36 reduces ovarian tumor growth. We generated an antibody against CD36 and here we evaluated its effect on CD36 function.
Hypothesis: We hypothesize that inhibiting CD36 using a neutralizing antibody would reduce tumor growth by targeting both cancer and stromal cells
Research Methods: THP1 cells were treated with phorbol 12-myristate 13-acetate (PMA) to induce macrophage-like differentiation. Western blotting and flow cytometry was used to check for CD36 protein expression. Subsequently, we performed lipid uptake assay using fluorescent dye tagged oxidized LDL to determine if an antibody against CD36 can block intracellular lipid transport.
Results: We used THP-1 treated (macrophage-like) cells as a model system to probe the functionality of CD36 antibody. We show that PMA treatment increases CD36 expression using western blot and flow cytometry. These cells were also used to perform lipid uptake assay. The CD36 antibody, however, could not block lipid uptake.
Conclusion: While the CD36 antibody generated can recognize the protein and can be used for analysis of CD36 expression, it cannot block CD36 function (lipid uptake). Therefore, the antibody does not function as a neutralizing antibody. CD36 plays a significant role in ovarian cancer progression and could be a valuable biomarker for early detection, as well as a promising therapeutic target. Future research will aim to translate these findings into clinical applications to enhance patient outcomes.

Improvement of DNA Delivery with Lipid Nanoparticles (LNPs) to Cells using the Histone H1 Protein

Scholar: Zainab Al-Nagash

High School/State: Pittsburgh Science and Technology Academy, PA

PI of Lab: John Ash, PhD

Mentors: Frank Dyka, PhD; Maria Constanza Potilinski, PhD

Site: Biology and Translational Medicine in Vision (VISION)

Background/Purpose: Lipid nanoparticles (LNPs) are used as non-viral delivery vesicles for nucleic acids because of their ability to protect genetic cargo and promote cellular uptake. Although LNPs are effective for mRNA delivery, plasmid DNA delivery is less efficient because DNA must reach the nucleus for gene expression; however, conventional LNPs do not specifically target the nucleus.

We hypothesize that a DNA-binding protein containing a nuclear localization sequence (NLS) will improve nuclear plasmid DNA delivery. This study investigates a "piggyback" strategy using Histone H1, which naturally contains both an NLS and DNA binding capability. Histone H1 is first bound to plasmid DNA before LNP formulation, creating nanoparticles carrying a DNA-protein complex instead of DNA alone. Then, it will facilitate nuclear transport of plasmid DNA, increasing transfection efficiency. Efficiency will be evaluated by comparing LNPs containing naked plasmid DNA with LNPs containing Histone H1-bound DNA.

Methods: Histone H1 protein production began with cloning the Histone H1 gene into an expression vector, followed by protein expression in *E. coli*. Histone H1 was then isolated through His-tag purification, concentrated and quantified with a spectrophotometer measuring absorption at 280nm. LNP transfection was subsequently performed in HEK293 cells (human embryonic kidney) using a plasmid encoding the red fluorescent protein (RFP) mCherry and varying concentrations of Histone H1. MCherry expression was detected with a fluorescence microscope.

Results: We analyzed mCherry expression in HEK293 cells qualitatively through fluorescence microscopy and observed an increase in cell numbers with red fluorescence in samples with high concentrations of Histone protein indicating improved nuclear delivery of plasmid DNA.

Conclusion: The results demonstrate that a “piggyback” strategy using a DNA binding protein with a NLS potentially enhances current LNPs.

Future Investigations: These promising initial results need to be quantified, and the underlying mechanisms and cellular pathways need to be investigated in detail.

Identification and Mechanistic Exploration of Vacuole- Like Mystery Structures in CDH1 Suppressed Breast Cancer Cell Lines

Scholar: Amelia Balet
High School/City/State: The Ellis School, Pittsburgh, PA
PIs: Steffi Oesterreich and Adrian Lee
Mentor(s): Alex Opshal
Site: WCRC

Invasive Lobular Carcinoma (ILC) is the second most common histological type of breast cancer. ILC cells grow in single file lines because of a reduction of functional E-cadherin by the CDH1 gene. E-cadherin drives cell-to-cell adhesion and its loss leads to impaired cell adhesion, tumor suppression, and cell structure. Previously, my mentor discovered vacuole-like “mystery structures” in the cytoplasm of multiple E-cadherin negative cell lines but not in many of their E-cadherin positive counterparts. Their size and presence in other breast cancer cell lines lead us to question if these mystery structures were the result of macropinocytosis.

To test this, we hypothesized that the inhibition of macropinocytosis using EIPA will lead to fewer cells presenting mystery structures. The cell lines used were T47D Parental (Ecad +) and T47D with CRISPR CDH1 KO (Ecad -). In the first experiment, the cells were incubated with different concentrations of EIPA and a constant concentration of TMR dextran, a stain for macropinosomes, then imaged. In a second experiment, the same cell lines were incubated with EIPA for 72 hours in a cell growth-monitoring incubator. These two experiments identified the optimal concentrations of 10 uM and 25 uM for maximum macropinocytosis inhibition without significantly decreasing cell viability. Finally we incubated the cell lines EIPA for 24 hours, then stained them with EPCAM, and imaged them via confocal microscopy

As shown in Figure 1, macropinocytosis inhibition was most effective with an EIPA concentration between 25-55 uM; however, the viability of T47D cells significantly decreased when the concentration of EIPA was 25 uM or higher (Figure 2). These results indicated that the concentrations of EIPA used in the IF staining assay should be 10 and 25 uM for 24 hours. As of July 24, the results for the third assay are incoming.

Figure 1. Initial Count of Macropinosomes From the EIPA Inhibition Assay

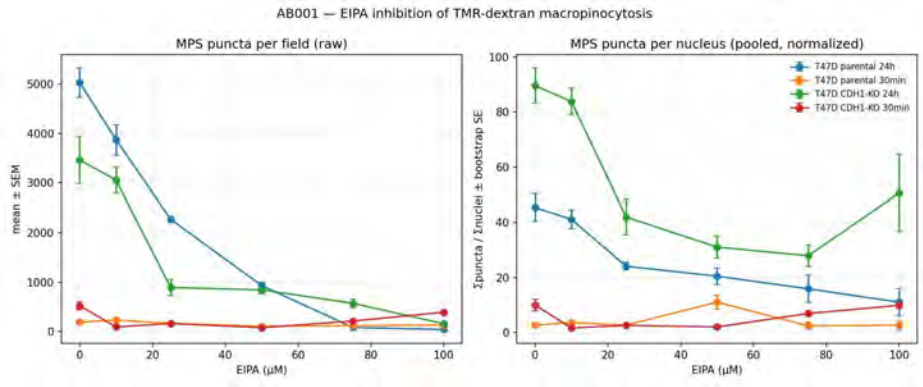

Figure 2. Normalized Cell Count vs. Time In Media Containing EIPA

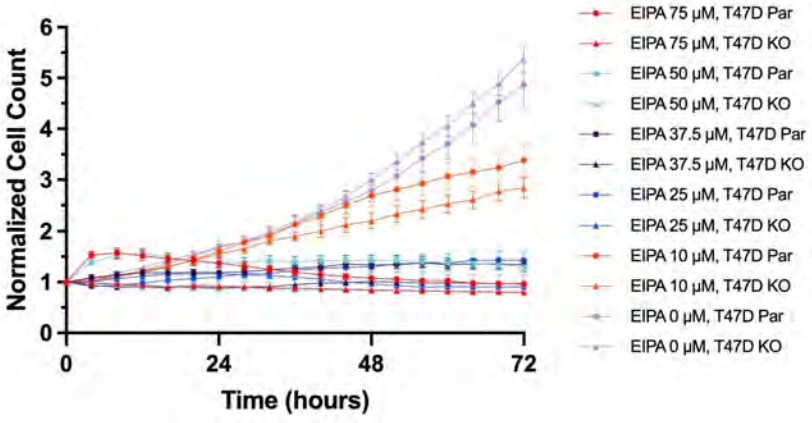

Works Cited

Christgen, M., Kandt, et al. (2022), Inter-observer agreement for the histological diagnosis of invasive lobular breast carcinoma. J Pathol Clin Res, 8: 191-205. https://doi.org/10.1002/cjp2.253

Commisso, C., Davidson, S., Soydaner-Azeloglu, R. *et al.* Macropinocytosis of protein is an amino acid supply route in Ras-transformed cells. *Nature* 497, 633–637 (2013). https://doi.org/10.1038/nature12138

Commisso, Cosimo et al. “Determining the macropinocytic index of cells through a quantitative image-based assay.” *Nature protocols* vol. 9,1 (2014): 182-92. doi:10.1038/nprot.2014.004

El Khalki, Lamyae, et al. “Triple-Negative Breast Cancer and Its Correlation with Viral Agents.” *Immunological Implications and Molecular Diagnostics of Genitourinary Cancer*, 2023, pp. 229–248, www.sciencedirect.com/topics/pharmacology-toxicology-and-pharmaceutical-science/lobular-carcinoma-in-situ, https://doi.org/10.1016/b978-0-323-85496-2.00019-1. Accessed 23 June 2026.

Fangquan Chen, Hu Tang, Junhao Lin, Limin Xiang, Yanjiao Lu, Rui Kang, Daolin Tang, Jiao Liu, Macropinocytosis inhibits alkaliptosis in pancreatic cancer cells through fatty acid uptake, Carcinogenesis, Volume 45, Issue 12, December 2024, Pages 953–964, https://doi.org/10.1093/carcin/bgae045

National Center for Biotechnology Information. "PubChem Compound Summary for CID 1795, "Eipa" *PubChem*, https://pubchem.ncbi.nlm.nih.gov/compound/Eipa. Accessed 22 July, 2026.

Lau MT, Klausen C, Leung PC. E-cadherin inhibits tumor cell growth by suppressing PI3K/Akt signaling via β-catenin-Egr1-mediated PTEN expression. Oncogene. 2011 Jun 16;30(24):2753-66. doi: 10.1038/onc.2011.6. Epub 2011 Feb 7. PMID: 21297666.

Mendonsa, Alisha M et al. “E-cadherin in contact inhibition and cancer.” *Oncogene* vol. 37,35 (2018): 4769-4780. doi:10.1038/s41388-018-0304-2

Wang, Bing-Yen et al. “Inhibition of Na+/H+ exchanger (NHE) 7 by 5-(N-ethyl-N-isopropyl)-Amiloride displays anti-cancer activity in non-small cell lung cancer by disrupting cancer stem cell activity and downregulating PD-L1 expression.” *American journal of cancer research* vol. 13,10 4721-4733. 15 Oct. 2023

Development and Preliminary Validation of a Low-Cost Cyclic Fatigue Tester for Surgically Bent Spinal Fusion Rods

Daniel Bandos[1], Rishi Basdeo[2], Calvin Brinkman[3], Ted Andrews, MD[4], Jacob Biehl, PhD[3]
[1]Gateway High School, Monroeville, PA; [2]Carnegie Mellon University, College of Engineering, Pittsburgh, PA; [3]University of Pittsburgh, School of Computing and Information, Pittsburgh, PA; [4]University of Pittsburgh Medical Center, Department of Neurological Surgery, Pittsburgh, PA

Abstract

Spinal fusion rods are contoured intraoperatively with French Benders, which can induce kinking and frequent re-bending that may reduce fatigue strength. To evaluate such a reduction, a low-cost cyclic fatigue tester was designed, built, and programmed by repurposing a 3D printer frame. Under higher cyclic loads, the tester successfully fatigued rods to failure. Lower loads produced no observed failures. These preliminary results support the fatigue tester's feasibility for future fatigue testing studies.

Introduction

Spinal fusion is the standard surgical treatment for deformities such as scoliosis. During these procedures, surgeons contour cobalt-chromium (CoCr) alloy rods to a patient's spinal curvature using French Benders, a manual tool that demands considerable technical skill and can introduce localized kinking that compromises fatigue strength[1]. A recent literature and case review by Fakunle et al.[2] documented this difficulty and observed experienced surgeons re-bending rods repeatedly to achieve adequate fit—a practice that may further degrade fatigue life. Building on this work, the present study aims to directly compare the effects of bend geometry and re-bending under controlled conditions, using an accessible, low-cost testing platform. Its immediate objective was to develop an apparatus for cyclically fatiguing surgical rods and to establish, through preliminary testing, its feasibility for such comparisons.

Methods and Materials

A custom fatigue tester, modeled on the professional-grade Instron® testing system, was designed, programmed, and built in-house. The build repurposed the frame of an Ender 3® 3D printer; the main structure comprised a dual lead-screw actuated cart driven by two NEMA 17 stepper motors (42-40 1.5 A 0.4 N·m), a 100kg S-type load cell for force measurement, and two (1-13 mm) drill chucks to secure the rod. Electrical components included an Arduino Uno, two A4988 stepper drivers, an HX711 load-cell amplifier, and appropriate wiring and soldering.

The tester's maximum effective force, verified both mathematically and experimentally, was 200 N, which is insufficient to fatigue clinical CoCr rods. Accordingly, 3 mm diameter copper rods were chosen as an inexpensive surrogate to validate the apparatus and cycling protocol. In a force-based protocol, each rod was cyclically bent and compressed to a target force. Rods were pre-bent at three points—30° bends one inch from each end (for uniaxial seating in the drill chucks) and a 60° bend at the center—forming an approximate 120-30-30° triangle. All bends were formed around a 19.25 mm radius V-groove wheel to simulate French Bending, and a paper template was used to keep pre-bending history consistent across specimens. Failure was defined as a 7 mm difference between maximum and minimum displacement within a cycle. For the higher-force failure trials, a cap of 2,000 cycles was subsequently added to prevent excessively long runs while still allowing failure to be observed. Several force-control settings were evaluated to identify the most effective cycling protocol.

Results

The tester applied cyclic loading to failure at 100 N, 80 N, and 75 N. The number of cycles to failure varied notably between trials but indicated fewer cycles for larger force, as expected. Compression to failure produced a maximum effective force of approximately 125 N. Lower-force cycling led to no observable damage: rods survived 10,000 cycles at 30 N and 4,000 cycles at 60 N without any change in cycling range.

Discussion and Conclusion

The tester's ability to fatigue rods to failure confirms that the apparatus functions as intended. The substantial variation in cycles to failure is attributed primarily to inconsistencies in manual pre-bending. Although only a limited range of forces and durations was examined, these preliminary data demonstrate the apparatus's potential for systematically fatiguing rods of differing pre-strain histories to determine how French Bender–induced kinking and re-bending affect fatigue life.

Immediate future experimentation would compare four specimen conditions—French-bent and large-radius-bent rods, each with and without a subsequent re-bend—to isolate the contributions of bend geometry and re-bending. The longer-term aim of this work is a mechanism capable of intraoperatively shaping patient-specific CoCr rods from augmented-reality scans. This mechanism will base its contouring technique around the preliminary results gathered in this study and aims to shape rods that yield greater fatigue strength than those bent and re-bent with French Benders. Future testing of CoCr rods will be performed on a more capable machine to quantify the mechanism's potential to improve spinal fusion rod bending and surgical workflow.

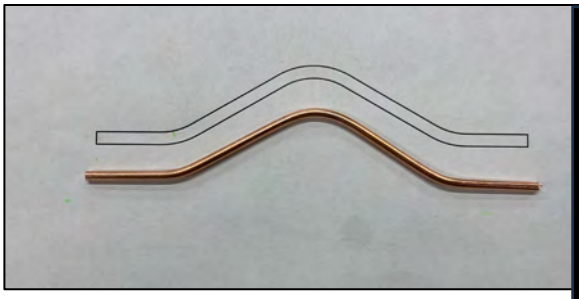

Figure 1 (above): *Copper Rod bent around 19.25mm radius V-groove wheel according to paper template. Three bends were done on each rod: 30-degree angles 1 inch from each end and a 60-degree angle at the center of the rod.*

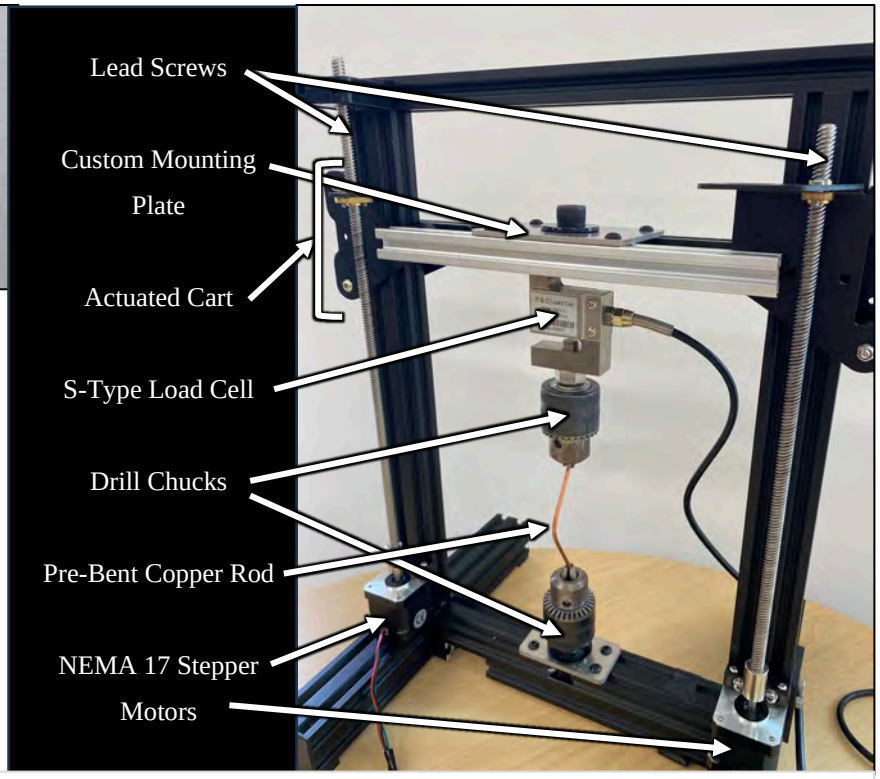

Figure 2 (right): *Custom-built and custom-programmed fatigue tester to cyclically load rods to failure. Lead screws translate the rotational motion from the stepper motors into linear motion to actuate the cart. The custom mounting plate secures the load cell to the actuated the cart, the load cell reads the force exerted on the rod, and the drill chucks secure the rod at both ends to prevent slippage.*

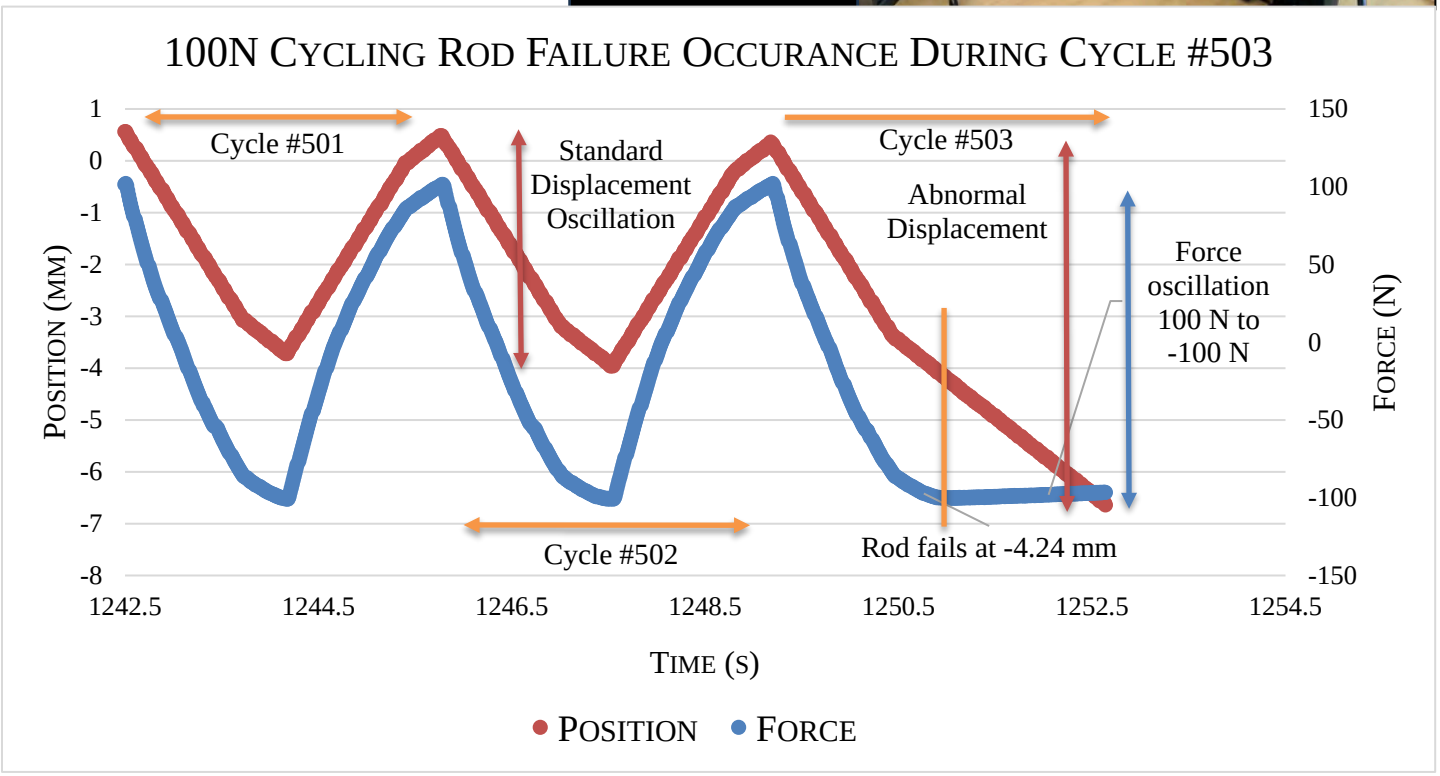

Figure 3: *Final three cycles before failure of a copper rod cycled at 100N. Near -4.24 mm, the rod approached the target oscillation force, but failed before reaching it, continuing to plastically deform until the 7 mm failure criterion (the difference between upper and lower displacement) was met.*

References

1. Lindsey C, Deviren V, Xu Z, Yeh RF, Puttlitz CM. The effects of rod contouring on spinal construct fatigue strength. Spine (Phila Pa 1976). 2006;31(15):1680-1687.
2. Fakunle O, O'Laughlin K, Waldorff E, Zhang C, Magro M, Goodwin R. How good are we at rod bending?—a review of the literature and a case series of experienced pediatric and adult scoliosis surgeons. J Spine Surg. 2025;11(3):591-599.

Fine-Tuning Large Language Models to Simulate the Role of Therapists

Shreyan Bansal[1], Liang Zhan, PhD[2], Siyuan Dai[2], Kun Zhao[2]
[1]North Allegheny Senior High School, Wexford, PA; [2]University of Pittsburgh, Pittsburgh, PA

Abstract

The goal of this study was to determine how effectively a large language model (LLM) could perform as a therapist. To maximize performance, existing models were fine-tuned on a private dataset consisting of therapist responses from anonymized therapy sessions. This study compares the effectiveness of three different models, Qwen2-7B-Instruct, Qwen3.5-9B, and Llama 3.1-8B-Instruct, before and after fine-tuning using various evaluation metrics, namely BLEU, ROUGE, BERTScore, cosine similarity, and LLM-as-a-Judge.

Introduction

Recently, top artificial intelligence (AI) companies have taken a special interest in fields outside of those typically associated with technology, namely philosophy. With LLMs dominating logical tasks such as researching and coding, the focus has shifted to increase emotional and ethical reasoning capabilities. Emotional intelligence is especially unique due to its extremely subjective and sensitive nature. By specifically training LLMs on therapist speech, this study tries to mimic therapist techniques and have the LLM adopt said skills.

Methods

The initial dataset was cleaned using Python and agentic coding tools such as Claude Code. Sessions were isolated and split into speaker roles, with either “Therapist:” or “Client:” as a label. Dialogues were compiled into a list of dictionaries with three keys, “Instruction”, “Input”, and “Output”. The value of Instruction consisted of a generic system prompt informing the LLM of its role and task. The value of Input held the last 30 therapist-client dialogue pairs. Output was filled with the real therapist’s response. The list was converted into a JSON file and split into two datasets, 80% going towards a training dataset and the remaining 20% towards a testing dataset. LLaMA-Factory was utilized to train Qwen2-7B-Instruct, Qwen3.5-9B, and Llama 3.1-8B-Instruct using supervised fine-tuning (SFT) with LoRA. For the GPUs, the models were trained across two NVIDIA A6000s. After training, a variety of evaluation metrics were used, specifically BLEU, ROUGE, BERTScore, cosine similarity, and LLM-as-a-Judge. BLEU and ROUGE check pure, lexical overlap, showing similarities in vocabulary and phrasing. BERTScore and cosine similarity show similarities in meaning at the token and response level respectively. LLM-as-a-Judge accounts for qualitative data, being able to analyze the models’ responses based on factors other than pure numbers.

Results

Holistically speaking, the study was a success. All 3 models had an increase in performance across all metrics. As can be visibly observed in (Table 1), improvements after fine-tuning were drastic. Every metric clearly showed great improvement, except for BERTScore. While an increase was present, it is significantly less than other metrics. This is due to the typical clustering of BERTScore around the values of 0.85-0.95 when rescale_with_baseline is disabled. When shown in perspective, as in (Figure 1), visible improvements are easily seen across all 3 models.

Discussion

For further advancements, one of the most direct ways of increasing model performance is increasing the parameter count of the model. Due to available compute, the highest parameter model that was used was 9 billion, with Qwen3.5. With a higher parameter count, any given model can pick up on more complex patterns, resulting in a more accurate prediction. Furthermore, if a larger percentage of parameters are tuned, then more of the total model will be affected by the training dataset. More on the dataset, a larger dataset would also provide more techniques for the model to use and more examples to train on. Furthermore, while the dataset was cleaned extensively, some errors still slipped through resulting in certain instances of the model replying with an empty string. Refining the data cleaning would result in less mistakes and a lower percentage of empty outputs. This study also did not include think blocks in the dataset, which could boost model reasoning capabilities. With all these changes, the models would, without a doubt, perform much better. To evaluate these changes, real, experienced therapists could judge responses based on taught, conventional practices to essentially replace LLM-as-a-Judge with a more concrete and thorough analysis.

Table 1. Average evaluation metrics for each model, before and after fine-tuning, rounded to 3 significant figures

Model Name	BLEU	ROUGE-1	ROUGE-2	ROUGE-L	BERTScore	Cosine Similarity	LLM-as-a-Judge Rating
Llama 3.1 Base	0.00377	0.0841	0.0117	0.0582	0.822	0.167	4.69
Llama 3.1	0.0154	0.151	0.0220	0.131	0.857	0.268	7.25
Qwen 2 Base	0.00261	0.0700	0.0110	0.0459	0.816	0.166	4.12
Qwen 2	0.0140	0.152	0.0230	0.133	0.851	0.266	6.88
Qwen 3.5 Base	0.00171	0.0548	0.00808	0.0380	0.791	0.176	4.19
Qwen 3.5	0.00876	0.147	0.0198	0.133	0.857	0.268	6.56

Figure 1. BERTScore distribution for each model, before and after fine-tuning

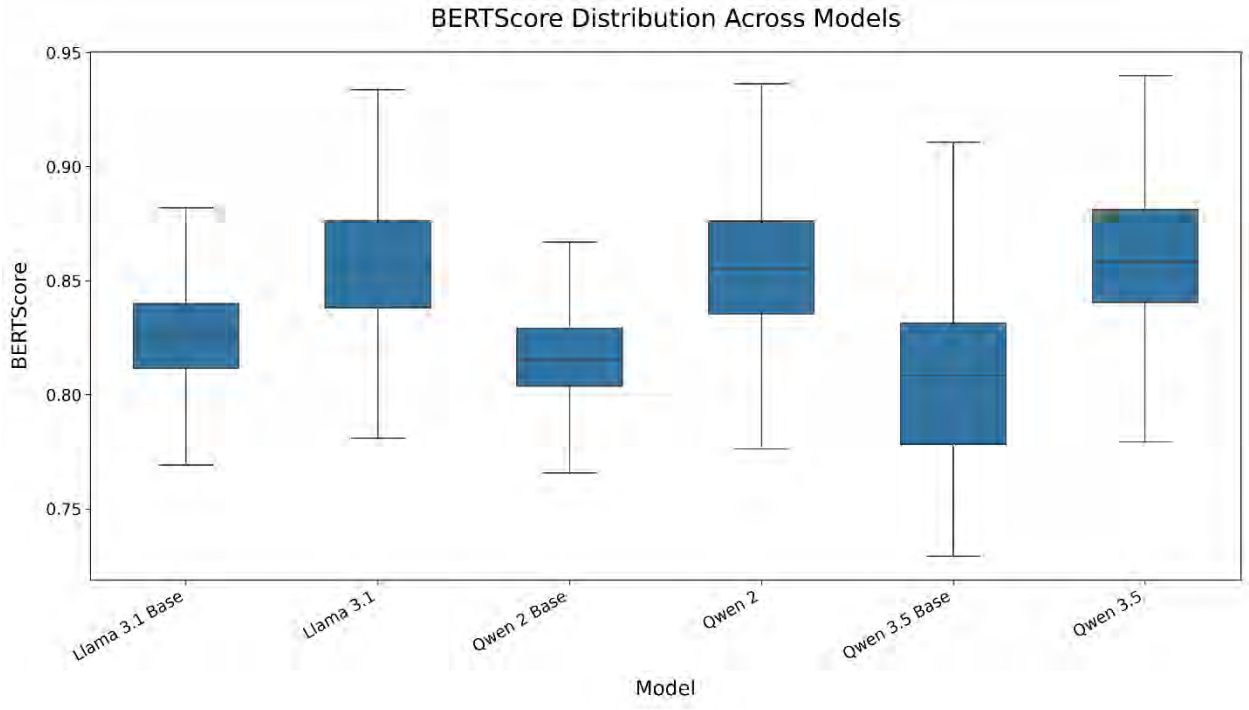

Western diet increases comorbidity development in Macaques

Scholar: Ella Belcher
School: Taylor Allderdice
Lab: Ivona Pandrea, MD, PhD
Mentors: Samuel D. Johnson, PhD; Amy Xu, PhD
Site: Pathobiology

Introduction: People with HIV experience elevated levels of chronic inflammation and have a high risk of co-morbidity development such as cardiovascular, kidney, and liver diseases. An unhealthy diet can cause increased inflammation and incidence of these same diseases. However, how diet influences the trajectory of co-morbidity development in people with HIV remains poorly understood.

Purpose: To determine the impact of diet on the microbiome, inflammation, and tissue pathology to better understand its potential contribution to HIV/SIV-associated disease.

Methods: Four male uninfected pigtailed macaques were fed a conventional diet (control), and five uninfected male pigtailed macaques were fed a Western diet, which was high in sugar and saturated fat. Tissue and fecal samples were taken at serial time points. 16S rRNA sequencing was used to determine the microbiome composition using fecal samples. Hematoxylin and eosin staining were used to evaluate tissue pathology. Immunohistochemistry using antibodies against UCP1, Synaptopodin, CD68, Ki67, and LPS were performed.

Results: Macaques that were fed the Western diet displayed hepatic steatosis, aortic plaque formation, lymph node histiocytosis, and intestinal barrier dysfunction, suggesting increased gut microbial translocation. This was accompanied by microbiome dysbiosis, with observed microbial richness decreasing from approximately 800 to 600 operational taxonomic units (OTUs) after approximately 300 days on the diet ($P=0.046$). Histology demonstrated hepatic steatosis, atherosclerosis, histiocytosis, and inflammation. Immunohistochemistry found increased gut microbial translocation, renal cellular proliferation, and macrophage infiltration in glomeruli and colon.

Conclusion: Administration of a Western diet, rich in sugar and saturated fats to pigtailed macaques induced microbiome dysbiosis, and a pro-inflammatory environment that resulted in

hepatic steatosis, aortic plaque formation, lymph node histiocytosis, and intestinal barrier dysfunction. These findings provide a baseline for evaluating the contribution of diet to HIV/SIV-associated comorbidities.

Future directions: Future studies will compare these findings with SIV-infected macaques to further determine the inter-relationships between diet, co-morbidity development, and disease progression.

Retention of Doxycycline and Minocycline Susceptibility When *Staphylococcus epidermidis* Joint Infection Isolates Are Non-Susceptible to Tetracycline

Scholar: Maeve Beresford
College: Fox Chapel Area High School (‘26); University of Pittsburgh (‘30)
Lab: Dr. Kenneth Urish, MD, PhD
Mentor: Jewelia Rempuszewski, BS; Beth Knapick, BS
Site: Cancer Biology

Staphylococcus epidermidis is an opportunistic pathogen that causes infection, particularly by forming protective biofilms on implanted medical devices such as prosthetic joints. The treatment of a *S. epidermidis* infection typically utilizes the long-term oral antibiotic tetracycline, which stops protein production in bacteria by acting as an allosteric inhibitor at the A-Site on mRNA. When *S. epidermidis* exhibits tetracycline resistance, the pool of suitable oral therapeutics narrows significantly, as alternative agents carry higher risks of drug interactions and adverse patient reactions. Thus, this study investigates whether there is retention of doxycycline and minocycline susceptibility when *Staphylococcus epidermidis* joint infection isolates are non-susceptible to tetracycline. Eleven gram-positive prosthetic joint infection isolates that were evaluated as non-susceptible to tetracycline in hospital screening were tested for retention of both doxycycline and minocycline susceptibility. Sensitivity was determined using doxycycline gradient diffusion test strips and minocycline gradient diffusion test strips. All eleven tested isolates demonstrated complete minocycline susceptibility, with an average minimum inhibitory concentration (MIC) of 0.24±0.14 μg/mL, while all tested isolates demonstrated intermediate doxycycline susceptibility, with an average MIC of 5.19±2.58 μg/mL. Our study shows that although doxycycline MICs were elevated, standard tetracycline resistance is unable to predict minocycline resistance in *S. epidermidis*. These findings give direct clinical support that minocycline could be a strong alternative treatment for patients facing tetracycline-resistant infections.

Observing effects of doxorubicin on K7M2 cell line

Ismael Bey
Science and Technology Academy, Pittsburgh, PA
PI: Jessie Nedrow
Mentor(s): Jessie Nedrow, Angel Cortez
Cancer Biology Site

Background. Osteosarcoma is the most common type of bone cancer and occurs mostly in individuals aged 10-30. Standard treatment for osteosarcoma consists of chemotherapy (i.e. doxorubicin) and surgery. Although this treatment is effective for patients with resectable disease, it has heavy side effects that can have a large impact on physical and mental health. The Nedrow lab is researching the potential of transarterial radioembolization therapy (TARE) with Actinium-225 (^{225}Ac), an extremely potent radioisotope, to treat osteosarcoma. To test how effective a treatment is in osteosarcoma cell lines, a cell viability assay can be utilized. The objective of this work is to develop a standard cell viability protocol with Doxorubicin, an SOC control.

Methods. Murine (mouse-derived) osteosarcoma cells, K7M2, were used to test how different molar amounts of Doxorubicin, ranging from 5000 µM to 0.1 µM, affect cell viability. The Cell Counting Kit-8 (CCK-8) assay was used to measure viability 5 days post-treatment.

Results. The results of the CCK assay showed that the higher concentration of doxorubicin led to lower viability in the cell line. As the dosage of doxorubicin got lower, the viability of the cells got higher, essentially telling us the assay worked just as planned. The concentration of doxorubicin at which the cell viability was 50%, also known as the IC50, was between 22 and 34nM. Some of my results were unreadable on the microplate reader. This is because I accidentally added twice as much CCK-8 solution to that well.

Conclusion. The cell viability assay protocol was established. This protocol will be utilized in future works to contrast the therapeutic effectiveness of ^{225}Ac-TARE as compared to SOC chemotherapy. This protocol will help identify osteosarcoma cell lines to further evaluate with ^{225}Ac-TARE in murine models, including models that are resistant to SOC chemotherapy.

Isolation of Extracellular Vesicles from Endothelial Colony Forming Cells to Determine Therapeutic Potential

Scholar: Anna Bittner

High School/College/City/State: Keystone Oaks High School, Pittsburgh, PA

PI of group/lab: Dr. David A. Vorp, Ph.D.

Mentor: Kiran Mcloughlin, Ph.D.

Site: Technology Drive X

Introduction: Ischemic disease is characterized by endothelial degradation/destruction and eventually causes tissue necrosis. Cell therapy, which involves delivering therapeutic cells, can restore tissue functionality. Cell therapy can be successful; however, the risks, including infection, outweigh the benefits. Cell-free therapy (CFT) involves derivation of therapeutic cell products without direct cell delivery. Extracellular vesicles (EVs) are CFT candidates, with our lab showing mesenchymal stem cell (MSC)-derived EVs as a promising candidate for regeneration. This project will optimize the isolation of EVs from endothelial colony forming cells (ECFCs) as a candidate for ischemic repair.

Methods: ECFC media optimization compared combinations of basal media, growth factors, and serum types. AlamarBlue was performed to establish viability between groups. ECFCs were scaled up in candidate media, and EVs were isolated using tangential flow filtration (TFF) and ultrafiltration (UF) tubes centrifuged for 55 minutes at 3000g. Nanoparticle tracking analysis (NTA) determined EV concentration. Silk films were prepared and soak-loaded with ECFC-EVs to test mature endothelial cell (HUVECs/HAECs) response to EVs in a vascular graft biomaterial environment.

Results: The optimal media for ECFC-EV isolation was found to be RoosterCollect with 5% Exosome-Depleted FBS and complete growth factors. NTA established that the TFF-EV concentration was 1.32e9 particles (P) per mL, while the UF-EV concentration was 89.40e9 P/mL. After 72 hours, AlamarBlue showed EVs positively impacted HUVEC proliferation, but negatively impacted HAEC proliferation.

Conclusion: When cultured in RoosterCollect with 5% Exosome Depleted FBS and complete growth factors, ECFCs supply sufficient EVs that can be isolated via TFF and concentrated via UF. HUVEC cells benefited from EVs, while HAEC cells were hindered. Future experiments could explore other ways to isolate EVs, such as ultracentrifugation, and compare results with TFF and UF isolation methods, to further optimize ECFC-EVs as a CFT candidate.

Identification of Cellular Programs within Diabetic Kidney Disease

Scholar: David Boehm Jr.

High School/College/City/State: PGH Scitech --> Duquesne

PI: Jishnu Das, PhD

Mentor: Mary D. Cundiff, PhD

Site: ICI

Diabetic kidney disease, also called diabetic nephropathy, is a serious complication of type 1 and type 2 diabetes. It occurs when persistently high blood sugar and blood pressure damage small blood vessels and filtering units called glomeruli in your kidneys, impairing their ability to filter waste and excess fluid. In this project, I analyzed publicly available single-cell RNA sequencing (scRNA-seq) data to compare gene expression in kidney cells from individuals with diabetes versus healthy controls. These data were processed using Seurat, an R package for single-cell RNA sequencing analysis, to identify the genes that were significantly differentially expressed. Using these data, volcano plots were created to visualize these differences across multiple kidney cell types. We then utilized an interpretable machine learning method called SLIDE to analyze and identify gene programs specific to diabetic kidney disease. These gene programs highlighted biological processes related to cellular stress, inflammation, metabolic dysfunction, and tissue remodeling. Some of the pathways are already being targeted by drugs, whilst others are experimental, that could be utilized in the future.

TGenerative AI Modeling of Lamina Cribrosa Microstructure for High-Throughput Glaucoma Biomechanics Research

Scholar: Shirish Bollineni

High School/College/City/State: North Allegheny Senior High School, Pittsburgh PA

PI of group/lab: Dr. Vande Geest

Mentor(s): Dr. Vande Geest**Mentor(s):** Dr. Vande Geest

Site: Tech Drive X

Background: The lamina cribrosa (LC), a mesh-like connective tissue structure in the optic nerve head, varies uniquely between individuals like a fingerprint, and specific structural vulnerabilities within this architecture are believed to contribute to glaucoma, a leading cause of irreversible blindness. However, studying LC variability across large populations is limited by the time and cost required to scan and reconstruct sufficient numbers of human samples. This project aims to address that limitation by developing a generative AI model capable of producing realistic synthetic LC tissue volumes, reducing dependence on scarce experimental data.

Methods: We curated 230 high-resolution LC tissue volumes (1039 × 1039 × 167 voxels each) and processed them into randomized 3D chunks suitable for model training. A generative model was then trained on this dataset to learn the structural patterns of LC tissue and produce novel, AI-generated tissue volumes.

Results: Initial outputs successfully captured plausible trabecular architecture resembling real LC morphology. A preliminary test "stitch," combining multiple generated chunks into a larger continuous structure, was successful in producing a coherent, structurally intact tissue sample.

Conclusion: These early results demonstrate the feasibility of using generative AI to synthesize anatomically realistic LC microstructure, offering a promising path toward reducing reliance on limited experimental tissue samples. While the model has not yet been fully validated against real tissue, the successful preliminary stitch suggests the approach can scale to larger, structurally coherent volumes. Future work will focus on refining the model, performing a full-scale stitching test, and 3D printing both AI-generated and real LC samples for direct physical comparison to assess whether synthetic structures are viable substitutes for biomechanical testing in glaucoma research.

Assessing UTICalc Precision Under Demographic Shift

Parker R. Budney[1], Joshua W. Anderson, MS[2]
[1]Seneca Valley High School, Pittsburgh, PA; [2]University of Pittsburgh, Pittsburgh, PA

Abstract
Clinical prediction models often result in unequal performance across heterogeneous populations. Using patient data from over 1562 young febrile children from Children's Hospital of Pittsburgh, we investigate the varying precision of UTICalc, a logistic regression model developed to predict the risk of urinary tract infections. We estimated changes in model precision across each U.S. state's demographic composition to infer the impact on performance if deployed to other populations without additional training data.

Introduction
Clinical prediction models that use race as a predictor may compound healthcare disparities. Because the U.S. demographics vary regionally, the impact of model bias may differ across patient populations[1]. Additionally, minority groups are often underrepresented in training data, which can affect model performance[2,3]. We investigate UTICalc, a clinical decision support tool that uses electronic health record (EHR) data to estimate urinary tract infection (UTI) risk in children aged 12–24 months before invasive testing[4]. Version 1 (V1) included race (Black vs. non-Black) as a predictor, whereas Version 3 (V3) excluded it. Previous work found that removing race improved recall bias but increased precision bias[5,6]. Because precision depends on disease prevalence, which may vary across populations, it is an important performance metric for models deployed under new patient populations[7]. Reported precision bias (difference in precision of Black vs. non-Black) was 16 percentage points for V1 and 23 percentage points for V3, despite similar overall precision (0.422 vs. 0.427)[6].

Methods
Using EHRs from over 1562 patients at Children's Hospital in Pittsburgh with approximately 25% Black patients[4], we estimate how precision may vary when considering the demographics of different state populations. The performance of UTICalc was measured using the precision of the underlying logistic regression model's predictions conditioned on race. We calculate a pooled precision metric to weight performance by demographic composition:

$$precision_{pooled} = P(Y = 1 \mid \hat{Y} = 1, R = 0) \cdot P(R = 0) + P(Y = 1 \mid \hat{Y} = 1, R = 1) \cdot P(R = 1)$$

where $\hat{Y}$ is UTICalc's prediction, Y is the true UTI status, and R is race. $P(R = 0)$ represents the proportion of the population that is Black, and $P(R = 1)$ is the proportion that is non-Black. We obtain current population estimates for all 50 states, D.C., and Puerto Rico from the US Census[8] under "Race alone or in combination with one or more other races," We measure the difference in $\text{precision}_{\text{pooled}}$ for V1 and V3 to assess the impact of race as a predictor.

Results
V1 conditional precision values were 0.293 for Black and 0.451 for non-Black. V3 conditional precision values were 0.254 for Black and 0.484 for non-Black. The lowest proportion of Black population according to the U.S. Census was Montana at 1%, and the highest was D.C. at 44.4%. Figure 1a maps the difference in $\text{precision}_{\text{pooled}}$ between V1 and V3 of the contiguous U.S. and includes each state's racial composition (percentage Black). Figure 1b maps these results for Hawaii, Alaska, and Puerto Rico. Precision decreased the least from V1 to V3 in D.C., Mississippi, and Georgia (0.69, 0.85, and 0.95 percentage points, respectively), where the Black race composition was the highest (>30%). Precision decreased the most in Montana, Wyoming, and Idaho (1.77, 1.76, and 1.75 percentage points, respectively), where the Black race composition was the lowest (<2%).

Discussion
Our results indicate race introduces a tradeoff: V1 has higher recall bias[6], but reduced precision bias compared to V3. Although V3 had a lower $\text{precision}_{\text{pooled}}$ than V1 across most populations, the magnitude of difference was related to racial composition. In populations with a greater black population, pooled precision generally decreased less from V1 to V3, whereas in populations with smaller black populations, precision experienced a greater decrease. This is due to V1 achieving a higher precision for Black patients than non-Black patients compared to V3. As the weight assigned to Black patients increased, the pooled precision estimate therefore increased. In populations with similar demographics, we expect UTICalc would not have a substantial difference in racial bias with respect to precision. However, we recommend additional training data in populations with substantially different demographics.

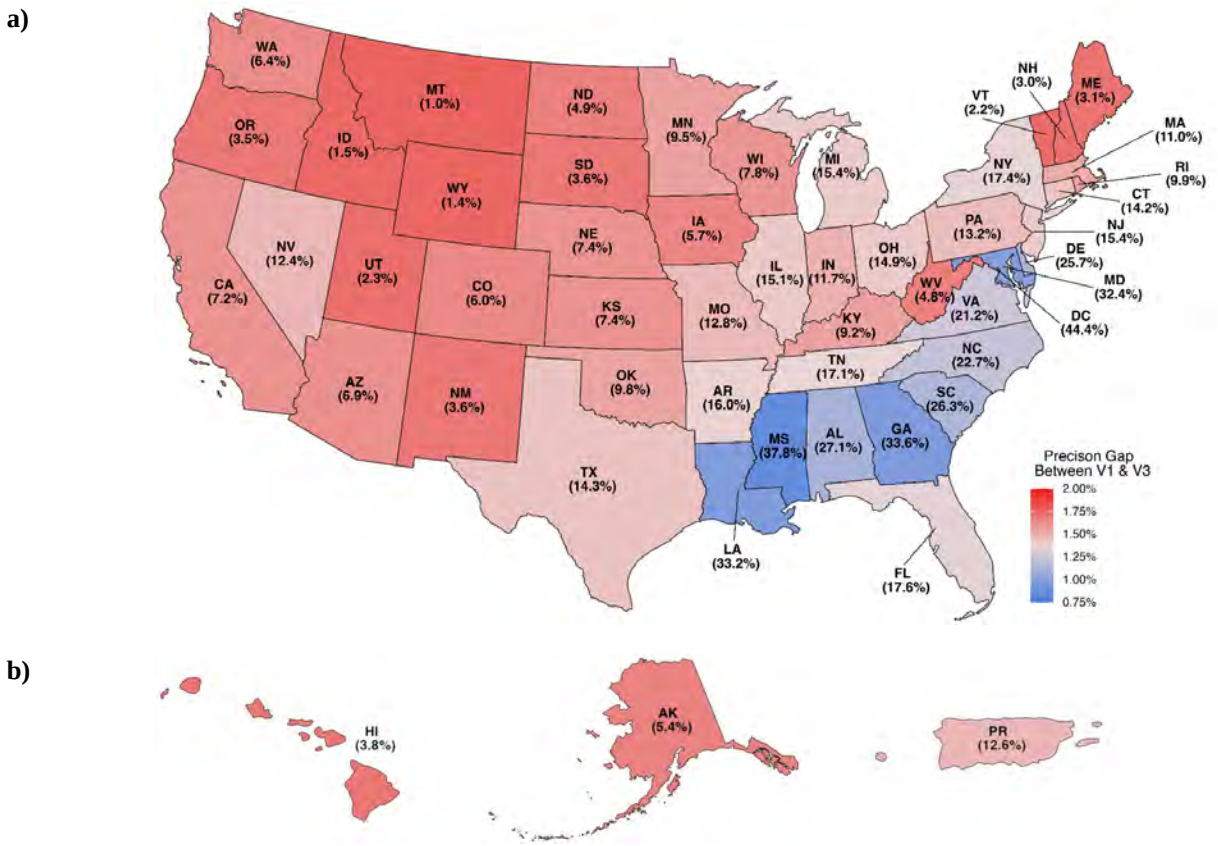

Figure 1. Difference in pooled precision between V1 and V3 across (a) the contiguous U.S. and (b) Hawaii, Alaska, and Puerto Rico.

References

1. Subbaswamy A, Adams R, Saria S. Evaluating model robustness and stability to dataset shift. In: International conference on artificial intelligence and statistics 2021 Mar 18 (pp. 2611-2619). PMLR.
2. Celi LA, Cellini J, Charpignon ML, Dee EC, Dernoncourt F, Eber R, Mitchell WG, Moukheiber L, Schirmer J, Situ J, Paguio J. Sources of bias in artificial intelligence that perpetuate healthcare disparities—a global review. PLOS digital health. 2022 Mar 31;1(3):e0000022.
3. All of Us Research Program Investigators. The "All of Us" research program. New England Journal of Medicine. 2019 Aug 15;381(7):668-76.
4. Shaikh N, Hoberman A, Hum SW, Alberty A, Muniz G, Kurs-Lasky M, Landsittel D, Shope T. Development and validation of a calculator for estimating the probability of urinary tract infection in young febrile children. JAMA pediatrics. 2018 Jun;172(6):550-6.
5. Shaikh N, Lee MC, Stokes LR, Miller E, Kurs-Lasky M, Conway I, Shope TR, Hoberman A. Reassessment of the role of race in calculating the risk for urinary tract infection: a systematic review and meta-analysis. JAMA pediatrics. 2022 Jun;176(6):569-75.
6. Anderson JW, Shaikh N, Visweswaran S. Measuring and reducing racial bias in a pediatric urinary tract infection model. AMIA Summits on Translational Science Proceedings. 2024 May 31;2024:488.
7. Monaghan TF, Rahman SN, Agudelo CW, Wein AJ, Lazar JM, Everaert K, Dmochowski RR. Foundational statistical principles in medical research: sensitivity, specificity, positive predictive value, and negative predictive value. Medicina. 2021 May 16;57(5):503.
8. U.S. Census Bureau. ACS demographic and housing estimates: American Community Survey 1-year estimates data profiles, Table DP05 [Internet]. Washington (DC): U.S. Census Bureau; 2024 [cited 2026 Jul 22]. Available from: https://data.census.gov/table/ACSDP1Y2024.DP05?q=demographics+by+state&moe=true

Candidate Transcription Factors in Human White Matter: Expression Validation by qPCR

Scholar: Josiah Chalmers
High School: Pittsburgh Science and Technology Academy, Pittsburgh Pennsylvani**a**
Lab: Julia Kofler, MD
Mentor: Riley Sawka
Site: Pathobiology

Background: Neuropathological analysis of postmortem human brain tissue provides many opportunities for neuropathologists to diagnose and investigate various disease mechanisms. In Alzheimer's disease (AD), diagnosis is primarily based on the pathology of the gray matter in the brain. While AD is commonly linked to gray matter pathology, white matter (WM) abnormalities are frequently seen in AD patients. Oligodendrocytes are key to maintaining WM, but their contribution to AD pathology remains poorly understood. Preliminary transcriptomic analysis identified eight transcription factors specific to oligodendrocytes (MEF2C, ARX, JDP2, FOSL2, NEUROD1, MXD1, KLF11, and DLX4) that exhibited altered activity levels in patients with late-stage AD compared with non-AD controls. Seven of these eight transcription factors were specific to oligodendrocytes or oligodendrocyte precursor cells. Transcription factors are responsible for regulating a variety of downstream targets, so changes in activity levels can have widespread effects. Although transcriptomic analysis has identified altered transcription factor activity, confirming the expression levels of these transcription factors is a critical first step to validate the computational findings before investigating their regulatory roles in oligodendrocyte dysfunction.

Methods: RNA from two human white matter samples from the Alzheimer's Disease Research Center brain bank (CW23-18 and CW23-19) was isolated and converted to cDNA and analyzed using quantitative PCR. Expression levels of the oligodendrocyte markers (OLIG2 MBP, MOG) and transcription factors of interest (MEF2C, ARX, JDP2, FOSL2, NEUROD1, MXD1, KLF11, and DLX4) were quantified. The gene expression relative to housekeeping gene GAPDH was calculated using the ΔCT method.

Results: Quantitative PCR showed that all transcription factors of interest except DLX4 were expressed in both human WM samples. Expression levels were consistent across samples, while DLX4 was undetectable, suggesting its expression was below the assay detection limit.

Conclusion: Our findings confirm the presence of our transcription factors of interest in human white matter, confirming them as relevant targets for future studies into oligodendrocyte dysfunction in AD.

Assessing LMP1 Knock-In Efficiency in EBV-Negative and EBV-Positive HEK293 Cells Using the Casilio System

Scholar: Stephanie Chen

Highschool: North Allegheny Senior High School, Wexford, PA

PI: Dr. Kathy Shair, Ph.D.

Mentor(s): Dr. Joshua Walton, Ph.D., Dr. Kathy Shair, Ph.D.

Site: Cancer Biology

Background: Epstein-Barr Virus (EBV) is a ubiquitous human herpesvirus that establishes a life-long infection in 95% of the human adult population worldwide. It is an oncogenic virus that is strongly linked to various human malignancies including nasopharyngeal carcinoma and a subset of Hodgkin's lymphomas. Latent Membrane Protein 1 (LMP1) is the primary oncogene of EBV that plays an essential role in transforming EBV-induced B-cells and driving cancer growth. The LMP1 oncogene exists as seven major geographic stains. These variants evolved through genetic variation and natural selection, and they are named after the regions where they were first discovered or are most predominant. This project aims to investigate the knock-in (KI) efficiency of LMP1 variants into the EBV genome within Human Embryonic Kidney 293 (HEK293) cells using the Casilio System. Casilio is an imaging system that combines nuclease-deficient CRISPR-Cas9 (dCas9) with Pumilio (PUF) RNA-binding proteins to enable live-cell visualization of specific genomic loci.

Methods: HEK293 cells and EBV-positive HEK293 (293-EBV+) cells were seeded into two collagen-coated 24-well plates with FluoroBrite DMEM and 10% FBS. Once 70% confluence was reached, the HEK293/293-EBV+ cells were co-transfected with plasmids encoding the CASILIO components (dCas9; pCR8_sgBamHI-W-20xPBSc / pmax-iRFP670_PUFc for EBV genome labelling; pCR8_sgLMP1-1-25xPBS9R / pmax-PUF9R_mRuby2 together with a 20ng LMP1 KI template for LMP1 KI labelling) using the X-tremeGENE 9 DNA Transfection Reagent at a 3:1 ratio of transfection reagent (uL) to DNA (ug). After 48 hours, half of the media volume in each well was removed and replaced with an equal volume of 7nM Hoechst 33342 working solution to achieve our target concentration of 3.5nM. The cells were incubated for an additional 1-3 hours before being placed in the BioTek Cytation 5 for imaging using a 4x and 20x objective under DAPI, Cy5, and TRITC channels. The KI efficiency will be calculated as (mRuby2+ cells / iRFP670+ cells) × 100.

Results: Imaging confirmed successful nuclear Hoechst staining and detected iRFP670 (EBV genome) and mRuby2 (LMP1 KI) signal. However, our ability to visually assess KI efficiency from raw images alone was limited due to low signal intensity and foci appearing outside nuclear boundaries, which are likely due to background signal, nonspecific binding, or autofluorescence.

Conclusion: We aim to perform image analysis in CellProfiler using a speckle counting method to assess LMP1 KI efficiency. Determining the KI efficiency of LMP1 is essential because B-cell immortalization assays depend on cells successfully carrying the intended LMP1 variant.

The effect of vitamin B6 on the survival of muscle cells after oxidative or inflammatory stress.

Scholar: Victoria Chernetska

High School: Brashear High School, Pittsburgh, PA

PI of group/lab: Bridget M. Deasy

Mentors: Jacob Tyler Harris, Matthew Shi, Olena Sergiyivna Abakumova, Bridget M. Deasy

Site: Cancer Biology

Background: Reactive oxygen species (ROS) are highly reactive oxygen-containing molecules that can cause oxidative and inflammatory stress and damage cellular components. ROS have been linked to age-related chronic diseases, including cardiovascular diseases, diabetes, and Alzheimer's disease. With age, mitochondrial function declines, and ROS-producing systems such as NADPH oxidases and cytochrome P450 enzymes become dysregulated, leading to excessive ROS. As global life expectancy increases, oxidative and inflammatory stresses grow increasingly concerning. Vitamin B6 is a potent antioxidant, neutralizing ROS like superoxide, hydrogen peroxide, and hydroxyl radicals, as well as being a coenzyme for amino acid production. Thus, this study investigates the effect of vitamin B6 on the survival of muscle cells after oxidative or inflammatory stresses from both aging and additional supplementation of ROS.

Methods: Immortalized mouse myoblast cell lines (C2C12) and human muscle cells were treated with vitamin B6. Cell culturing was done to measure the amount of C2C12 cells grown with the addition of vitamin B6 compared to a control. C2C12 cells were given hydrogen peroxide to test the effects of vitamin B6 after additional oxidative stress. Cell division times were measured with human muscle cells to test the effects of vitamin B6 on cell proliferation speed.

Results: Vitamin B6 increased cell proliferation and decreased cell death for C2C12 cells compared to a control, both with and without the addition of hydrogen peroxide. The effect of vitamin B6 on human muscle cells is inconclusive due to a lack of data.

Conclusion: Our study shows that vitamin B6 promotes growth and neutralizes harmful ROS in C2C12 cells following both aging and additional ROS. Hence, vitamin B6 has the potential to promote muscle cell health in humans. Further studies will be done to confirm this result and investigate the concentrations of vitamin B6 needed to maintain positive effects.

Quantifying Regional Differences in Intimal Hyperplasia

Scholar: Khamya M. Cobb-Hewlett[1]
High School/College/City/State: Northgate High School, Pittsburgh, PA

PI of group/lab: Dr. Jonathan Vande Geest[1,2,3]

Mentor(s): Jacqueline L. Avila[1], Katarina M. Martinet[1]

Site: 300 Technology Drive

[1]Department of Bioengineering, University of Pittsburgh, Pittsburgh, PA, United States, [2]McGowan Institute for Regenerative Medicine, University of Pittsburgh, Pittsburgh, PA, United States, [3]Department of Mechanical Engineering and Material Science, University of Pittsburgh, Pittsburgh, PA, United States

Introduction: Intimal Hyperplasia (IH) narrows blood vessels via smooth muscle cell proliferation, disrupting normal flow; initiating endothelial injury in diseased states. While existing techniques analyze overall IH thickness, methods detecting regional variations are scarce. This study develops a MATLAB image processing scheme to quantify regional differences across control, inhibitor, and TGFβ3 groups. We hypothesize that this tool will capture and quantify regions of IH growth variations.

Methods: Using a total of 30 H&E images, a MATLAB image processing scheme was created and used to calculate IH layer thickness in microns via pixel ratios. To minimize human error, we manually outlined every image three times using the roispline function to create masks. The script then automatically outputted the thicknesses for the greatest region, least region, and overall area of the IH layer.

Results: The MATLAB scheme detected regions with greatest thickness from 101.4 ± 13.6 µm in the control, 92.5 ± 7.3 µm in TGFβ3, to 215.8 ± 64.3 µm in the inhibitor (**Fig. 2B**). Regions with least thickness from 23.1 ± 2.5 µm in control, 29.1 ± 1.9 µm in TGFβ3, and 21 ± 4.7 µm in the inhibitor (**Fig. 1B**). The IH area is non-significantly different across all groups **(Fig. 3).**

Conclusions: All groups showed a linear pattern within regions of Northeast, Southeast, Southwest, and Northwest, (**Fig. 1A, Fig. 2A**). While IH growth occurred universally, the inhibitor group exhibited both the least (**Fig. 1B**) and the greatest amount of growth (**Fig. 2B**). Furthermore, this group displayed the highest standard error of the mean (SEM), driven directly by its specific image processing scheme.

Figures

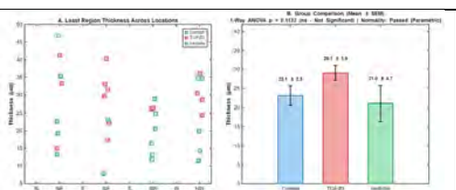

Figure 1. A scatter plot (**A**) and bar graph (**B**) for the least region's thickness.

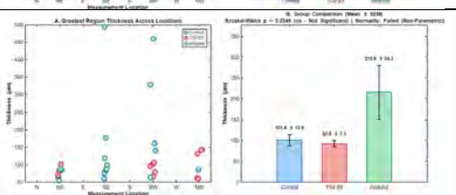

Figure 2. A scatter plot (**A**) and bar graph (**B**) for the greatest region's thickness.

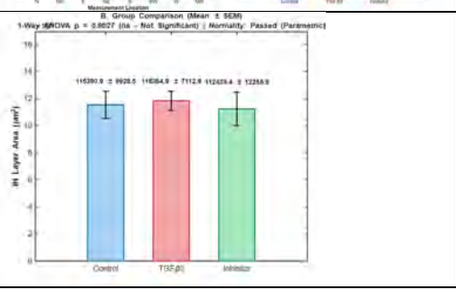

Figure 3. A bar graph for the IH area.

Title: Validating a Tool to Understand How Metabolites in Lymph Influence T Cells

Scholar: Ashton Creech

High School/College/City/State: Athens High School, Troy, MI

PI of group/lab: Greg Delgoffe, PhD

Mentor(s): Arianna Creech

Site: Immunology and Cancer Immunotherapy (ICI)

Introduction: Metabolite availability plays a vital role in the survival and expansion of T cells. This study investigated to see if a physiological media made to represent lymph fluid, lymph-like media (LyMe), could be used to better understand how lymph metabolites influence T cell fate and function in its natural environment in the body. However, from a previous experiment we learned that the original LyMe recipe inhibited T cells to survive. We hypothesize this was due to excessive ROS causing oxidative damage to the T cells. In standard T cell culture mediums, β Mercaptoethanol (BME) sequesters the excessive ROS that is created when T cells are activating and proliferating. Our goal is to find the optimal concentration of BME in LyMe which allows for T cell survival.

Procedure: To find the optimal concentrations of BME in Lyme, eight different conditions were created from 0 to .25x(13.75uM) and doubling until 16x (880uM) of BME along with control R10. T cells were harvested from the spleens of OTI mice, then activated via peptide activation in their specific media condition that they would be cultured in. Flow cytometry and cell trace violet were used to measure survival, proliferation, and activation.

Results: The flow cytometry data showed that higher BME concentrations in LyMe correlated with an increase in cell survival, proliferation, and increase of activation markers (CD44, CD69, CD25). However, T cells in R10 had higher survival and proliferation then all the LyMe conditions. R10 had lower percentages of CD44, CD69+ activation, but higher CD44, CD25+ populations compared to T cells in LyMe with BME.

Discussion: Higher concentrations of BME in LyMe proved to be more optimal for survival, proliferation, and activation. Future plans involve testing higher concentrations of BME in LyMe to see if it is more optimal.

Optimizing Cell Seeding and Growth Parameters to Enable CRISPR-Based ALS Research

Scholar: Myles Denton

High School: Gateway Senior High School, Monroeville, Pennsylvania

Lab: Christiano Alves, PhD

Mentor: Igor Gomes dos Santos, PhD

Site: Pathobiology

Amyotrophic lateral sclerosis (ALS) is a progressive neurodegenerative disease marked by motor neuron degeneration, muscle weakness, paralysis, and death. A hallmark of ALS pathology is mislocalization of the nuclear protein TDP-43, causing nuclear loss of function and toxic cytosolic aggregation. To model this process and support CRISPR-based gene editing studies of ALS-relevant pathways, we use human neuroblastoma (Be(2)-C, SH-SY5Y) and HEK293T cell lines exposed to various gene editing strategies and stressors across a range of concentrations. Reliable modeling depends on reproducible cell density and health, but standard culture protocols often fail to account for well-to-well and passage-to-passage variability. In our hands, cells plated in 96-well plates were frequently lost during bioimaging and staining, leaving insufficient numbers for downstream analysis, while inconsistent growth complicated transfection and stress-response assays. To address this, we optimized culture conditions for all three cell lines in 96-well plates, assessing cell density 24 hours post-seeding on poly-D-lysine (PDL), fibronectin, and uncoated surfaces, and characterizing growth across seeding densities (5, 10, 20, 40, and 80 × 10^3 cells/well) at 24, 48, and 72 hours. We found that HEK293T and Be(2)-C cells lose most cells from uncoated wells regardless of density, with 20 × 10^3 cells/well optimal for reaching 50–75% confluency on coated surfaces. SH-SY5Y cells lose cells regardless of coating, indicating a higher seeding density (80 × 10^3 cells/well) is required. Ongoing work includes evaluating post-trypsinization recovery on coated versus uncoated surfaces and stressor dose- and time-response relationships (four stressors, three time points, three doses). Together, these results establish a standardized workflow that improves reproducibility for in-vitro ALS modeling and CRISPR-based functional studies by defining coating requirements and optimal seeding densities for reliable downstream assays.

The Psychological Impact of Variants of Uncertain Significance (VUS) in Breast Cancer Genetic Testing: The Role of Age and Race/Ethnicity

Scholar: Amaia Dodds
Mentor: Dr. Erin Bayley
High School/City/State: North Allegheny Senior High School, Wexford, PA
Site: Surgery

Abstract:
Variants of Uncertain Significance (VUS) in breast cancer genetic testing can cause psychological distress because the clinical meaning of the result remains unclear. This proposed study will evaluate the psychological impact of VUS results among women and examine differences across age and racial/ethnic groups. Findings may improve genetic counseling, patient education, and care following a VUS result.

Introduction:
Genetic testing for hereditary breast cancer has advanced from screening a few high-risk genes to using multigene panels, improving risk identification but increasing the detection of Variants of Uncertain Significance (VUS), meaning there is insufficient evidence to determine if a variant is pathogenic or benign. Although clinical guidelines advise that medical management should not change, receiving a VUS result may increase anxiety and uncertainty. Minority populations are more likely to receive VUS results due to underrepresentation in genetic research. This proposed study will examine whether psychological outcomes differ by age and race/ethnicity.

Methods:
A survey will be developed for women ages 20–70 without breast cancer who have received a VUS result. Surveys completed privately will assess anxiety, stress, uncertainty, understanding of VUS, communication with healthcare providers, social support, sleep quality, counseling utilization, financial barriers, and the impact on future medical decisions using rating scales.

Expected Results:
We anticipate that younger women and women from minority racial/ethnic groups will report higher distress levels. Greater understanding of VUS results, communication with healthcare providers, and social support are hypothesized to show lower distress.

Future Directions:
Understanding these psychological effects may help identify patients who would benefit from additional counseling, encourage more inclusive genetic research, and help reduce anxiety among patients receiving VUS results.

Automating Knowledge-Assisted Literature Mining for Biological Interaction Analysis

Nana Kwame Dwomoh[1], Niloofar Arazkhani[2], Dr. Natasa Miskov-Zivanov[2]
[1]Brown University, Providence, RI; [2]University of Pittsburgh, Electrical and Computer Engineering, Pittsburgh, PA

Abstract
In this project, we automated the process of both extracting biological interactions from published literature and evaluating those interactions through an evidence pipeline; these tasks were previously only available manually through the KALIMBA web interface. Originally designed as human-in-the-loop tools for domain experts to use manually, we wanted to test the process of omitting the expert in the process and build an automation that can successfully run a large number of papers.

Introduction
Biology-based literature continues to grow at exponential rates, much more than researchers can analyze by hand. Thus, extracting and studying interactions established across so many papers is an inefficient process. Our lab developed KALIMBA to address this issue. It extracts interactions from papers using readers that utilize LLMs, NLP, and LLM + NLP, represents the results in the standardized BioRECIPE format, and can evaluate the interactions using an evidence pipeline called BELL. The problem, however, is that KALIMBA's tasks are entirely manual, meaning extracting or evaluating interactions requires the user to select and carry out their operations paper by paper, which is tedious and slow when analyzing large datasets of papers. Our objective was to automate the process of extraction and the running of the evidence pipeline.

Methods
We programmed two scripts using JavaScript that can call KALIMBA's operations. The first tool, KALIMBA extractor, reads a list of PubMed papers, usually presented in .xlsx format, retrieves each available abstract from PubMed, then extracts the interactions under the user-prompted methodology (LLM, NLP, LLM+NLP), and then produces the interactions in the BioRECIPE tabular format, which contains regulator and regulated entities, sign, mechanism, and source. The second tool, the BELL runner, reads a table in the BioRECIPE format and runs KALIMBA's BELL pipeline over every interaction: the query stage collects supporting evidence for each interaction from various databases (INDRA, OmniPath, STRING, SIGNOR, Reactome, BioGRID, and PCnet) and then matches each entity to a standard identifier; the score stage assigns a confidence score and flags conflicting evidence; the explain stage produces a typed-out justification. Additionally, each completed item is recorded in a progress log, which allows interrupted sessions to begin where they stopped rather than restart.

Results
The finished scripts allow a simple and easy method to extract biological interactions from papers and also evaluate those interactions. To demonstrate, we supplied the script with a dataset of 167 papers, ran extraction through each method: LLM, NLP, and the hybrid, and ultimately ran those outputs through BELL, which was able to successfully provide evidence support, entity grounding, confidence scores, evidence conflict, and justification for each interaction.

Discussion
By converting KALIMBA's manual extraction and BELL’s evidence evaluation into an efficient process, the scripts can provide immediate, practical use, especially when dealing with large data sets. This ultimately accelerates scientific research at a pace that manual processes could never match.

References

[1] N. Arazkhani and N. Miskov-Zivanov, "BELL: Biomodel Evidence and LLM based Logic," in Proc. 18th Int. Workshop on Bio-Design Automation (IWBDA), 2026, pp. 26–30.

[2] N. Arazkhani, M. Kotecki, B. Cochran, and N. Miskov-Zivanov, "KALIMBA: Knowledge-Assisted Literature Mining for Biological Interaction Analysis," in BioNLP 2026, San Diego, CA, USA, 2026, pp. 880–889, doi: 10.18653/v1/2026.bionlp-1.71.

[3] E. Holtzapple, G. Zhou, H. Luo, D. Tang, N. Arazkhani, C. Hansen, C. A. Telmer, and N. Miskov-Zivanov, "The BioRECIPE Knowledge Representation Format," ACS Synth. Biol., vol. 13, no. 8, pp. 2621–2624, 2024, doi: 10.1021/acssynbio.4c00096.

[4] Miskov-Zivanov Lab, "KALIMBA," University of Pittsburgh. [Online]. Available: https://boheme.pitt.edu/kalimba. [Accessed: Jul. 24, 2026].

Title: Mapping the connections between the left and right brain in the frontal eye fields

Scholar: Sophie Filipink-Smith

High School/College/City/State: Winchester Thurston, Pittsburgh, PA

PI of group/lab: Dr. Patrick Mayo

Mentor(s): Dr. Patrick Mayo, Emily Lopez

Site: Vision

The frontal eye field (FEF) plays a vital role in vision, helping to coordinate and execute eye movements. FEF is located in the frontal cortex, and it has a clear contralateral mapping: the left FEF controls eye movements into the right visual field and vice versa. Although this organization can explain much of how eye movements work, coordination between the two sides of the brain is necessary for eye movements to avoid competing movement plans and to make eye movements that are vertical. Our goal is to study the spatial pattern of connection across the hemispheres in FEF to better learn how the hemispheres coordinate. We used retrograde AAV, a virus designed to travel backwards ("retrograde") through neural circuits, and injected it into five places on the left hemisphere of a macaque brain. Each virus injection included a protein that would fluoresce into a separate color, enabling us to view the spatial pattern in the opposite hemisphere. Histological slides of the NHP brain were prepared and mounted, and an OLYMPUS live cell microscope was used to scan each slide through different filters at 4x resolution. This produced an image of each slide with clear separation between each injected AAV virus. We tracked where each virus was injected, what color it produced, and how much labeling appeared in the opposite hemisphere. By analyzing the pattern in the non-injected hemisphere, we found that there was a spatial segregation that was consistent with a structured connection between the hemispheres that maintain spatial information. In future work, we aim to better quantify the specific retinotopic locations of the injected and projecting neurons to generate a clear map of the connections across the hemispheres.

Optimizing First-Case On-Time Starts in Plastic Surgery at UPMC Magee-Womens Hospital

Scholar: Mia Fritz

College: University of Pittsburgh, Oakland, Pennsylvania

Lab: Dr. Elizabeth Bailey, MD

Mentor: Dr. Elizabeth Bailey, MD

Site: Surgery

Background: First-case start time timeliness relies on preoperative preparation. Failure to start on time results in inefficient use of resources, increased costs, and time wasting. At UPMC Magee Women's Hospital, plastic surgery first-case “on time” starts ranged between 24% and 40% of the time over the last 6 months, leading to decreased operating room efficiency. UPMC aims for a 70% “on time” start performance, with an “on time” start defined as the patient entering the operating room (OR) at or before the scheduled time. A quality improvement (QI) project was begun to identify delay causes and implement processes to reduce first start case delays.

Methods: A Gemba walk was performed to measure the preoperative process, and identify bottlenecks, delays and system failures. Current state process mapping and an Ishikawa diagram were utilized for root-cause analysis. Data was collected over a period of about 3 weeks, recording potentially influential components, including the surgeon, the anesthesiologist, if it was a combined case, arrival times, and OR availability. Past months data was analyzed using Pareto and run charts, along with bar graphs, demonstrating relationships between potential delay causes, variance in case start times, and root-cause attributions.

Results: Over the data collection period, 20 first start cases were evaluated along with 203 past cases ranging from 1/2/2026 to 6/30/2026. Past data showed a 78.37% average delay rate with an individual case delay percentage of 74.05% and combined case delay percentage of 83.33%. The most frequent cause of delay was the surgeon, 56.49%, with the second most frequent cause being anesthesia, 27.27%. Patient, Room, Lab/Paperwork and Other made up the other 16.23% of delay time. The mean start delay was 10.84 minutes.

Conclusion: First start case delays are multifactorial with the most prominent being surgeon and anesthesia delays. The higher rate of delay observed in combined cases highlights the additional collaboration needed between multiple surgical teams. Plan-Do-Study-Act process improvement plans will begin and be repeated until the necessary improvements in start time percentage have been made. This will then be standardized and maintained.

Effects of Age and Sex on Serum Extracellular Vesicle miRNA Cargoes

Scholar: Sanskruti Ghanti

College: Hendrix College, Conway, Arkansas

Lab: Musculoskeletal Regenerative Rehabilitation Laboratory

Mentor: Allison Bean, MD, PhD

Site: Cancer Biology

Background: Age-related declines in skeletal muscle regeneration capacity are associated with loss of skeletal muscle mass and strength, increasing mobility impairment and morbidity. Extracellular vesicles (EVs) are abundant circulating nanoparticles containing cargoes including microRNAs (miRNAs) that can induce phenotypic changes in target cells, and have potential to promote regeneration after injury. In mice, serum EVs from young males were more pro-regenerative than those from aged males, suggesting age-related EV phenotype changes may reduce regenerative capacity. Whether this holds for human EVs, or differs by sex, remains unevaluated. The objective of this project is to evaluate interactions of age and biological sex on EV miRNA content.

Methods: Circulating serum EVs were isolated from healthy young (18-30 year old) and aged (>60 year old) male and female adults (n=6/group) using size exclusion chromatography. RNA was isolated with Qiagen miRNeasy Serum/Plasma Kit to select for small RNAs. DNA libraries were prepared using QIAseq miRNA Library Kit and sequenced using Illumina NextSeq. miRNA sRNA-Seq analysis was performed with alignment to the human reference genome (GRCh38), followed by differential miRNA analysis. mRNA targets of differentially packaged miRNAs were identified, and predicted transcriptomic pathway differences were evaluated through Gene Ontology and Kyoto Encyclopedia of Genes and Genomes enrichment analyses using clusterProfiler.

Results: Age was associated with increased miRNA cargo expression in aged vs young, with 9 miRBase and 7 MirGeneDB miRNAs showing consensus differential packaging (edgeR/DESeq2 agreement), suggesting age-related upregulation of specific EV miRNA cargo, with no notable sex differences.

Conclusion: Findings demonstrate that age strongly influences EV miRNA packaging, with effects consistent between males and females. Future studies will validate findings and link differences in EV miRNA cargo to changes in skeletal myoblast phenotype *in vitro* following EV treatment to enhance therapeutic efficacy of EVs for skeletal muscle regeneration following injury in aged skeletal muscle.

Investigating the migration of osteosarcoma cells in response to the conditioned media of Inflammatory Conditions like Asthma and COPD

Scholar: Anish Goyal

School & Location: Radnor High School, Radnor, PA

Lab: Ines Lohse, PhD; Kurt Weiss, MD

Mentor: Ines Lohse, PhD

Site: Cancer Biology

Osteosarcoma is the most common primary bone cancer in adolescents and young adults and is characterized by high metastatic potential to the lungs. Preliminary clinical data from our lab shows a higher survival rate and delayed metastatic onset in patients with inflammatory comorbid lung conditions such as asthma and chronic obstructive pulmonary disease (COPD). This project aims to investigate how the inflammatory preconditioned lung microenvironment impacts the migration of osteosarcoma cells. To elucidate the mechanisms underlying these clinical observations, we obtained *in vitro* models of healthy and inflammatory lung tissues. Primary human lung fibroblasts representing three conditions: healthy control (PCS-201-013), asthma (PCS-201-015), and COPD (PCS-201-017) were cultured in 10 cm dishes for 72 hours to collect conditioned media containing secreted exosomes, growth factors, and other signaling molecules. The harvested conditioned media from each cell line will serve as chemoattractant or chemorepellent in a 4-arm Boyden chamber migration assay. Saos-2 or Saos-LM2 osteosarcoma cells will be seeded in the upper chamber and allowed to migrate toward the bottom chamber under the following conditions: plain culture medium (negative control), healthy fibroblast conditioned media (positive control), asthma conditioned medium, and COPD conditioned medium. Cell migration will be quantified using crystal violet staining to determine whether preconditioned inflammatory lung microenvironments stimulate or repel osteosarcoma cells. The different types of lung fibroblasts showed distinct morphologies: control healthy fibroblasts maintained elongated spindle shapes, while asthma and COPD fibroblasts exhibited noticeable stress-associated morphological changes. Based on our preliminary clinical findings, we hypothesized that conditioned media from inflammatory fibroblasts would significantly decrease osteosarcoma migration compared to the conditioned media from healthy fibroblasts.

Introduction:

Genotoxic therapies (targeted and chemotherapy) are widely used as a treatment option against a variety of cancers, especially breast. The Stallaert lab has shown that breast cancer cells that survive treatment with genotoxic agents can become polyploid through endoreplication, a process in which DNA replication is decoupled from cell division. The paths towards whole genome duplication (WGD) force the cell into a state of G0, halting cell cycle progression. However, cells can exit G0, duplicate their genomes again, and reenter G0, creating polyploid populations which can buffer problematic mutations and provide excess genetic material to accumulate productive mutations, promoting tumor evolution and progression. This has been experimentally observed in breast cancer cell lines, and we propose that this phenomenon is pervasive and broadly generalizable to additional cancers in which genotoxic agents are used as therapy.

To obtain measurements of numerous cell cycle regulator proteins and investigate the mechanisms of WGD in other cancers, our lab uses multiplexed immunofluorescence (mIF). Current methods of multiplexed immunofluorescence involve multiple rounds of staining, stripping, and quenching, which result in significant cell loss and reduce data quality and significance. To combat this, the lab created in situ paraffinization, which introduces paraffin layers to improve cell adherence during multiple rounds of immunofluorescence, allowing for better detection of important mechanistic details of WGD with greater sensitivity and statistical rigor.

Hypothesis:

1. **Cells in other cancer cell lines, when subject to genotoxic therapies, will produce polyploid cell populations.**
2. **The cells that go through in situ paraffinization will be more adherent, resulting in better staining and more data.**

Procedure:

1. Grew ovarian and pancreatic cell culture lines, seeded 8-well chamber slides, then administered 5-day drug treatment. OVCAR slides received either control (DMSO), cisplatin, or olaparib; PDAC slides received either control (DMSO) or Gemcitabine.
2. Prepared 2 slides in each cell type/drug treatment through in-situ paraffinization and prepared the other 2 slides through normal processing method.
3. Stained Vimentin, Cyclin A2, and pRb antibodies and performed CellDIVE imaging.
4. For Hypothesis #2: Simulate mIF through “fake rounds” using antibody diluent to simulate antibody staining and dye inactivation performed as normal, with DAPI staining for 10+ rounds. This was done on 1 in-situ slide and 1 normal slide.

Results + Conclusions:

Address to Hypothesis 1: In both cell lines, cells showed a larger nuclear area, demonstrating polyploidy due to genotoxic therapies.

Address to Hypothesis 2: Ovarian cancer cell lines showed increased adherence to the slide with in -situ paraffinization through multiple rounds of mechanistic mIF. The fluorescence intensity of Vimentin was also increased on the in-situ slides, possibly due to antigen retrieval that was performed on those slides.

Genotoxic Therapies as a Catalyst for Endoreplication & Testing the Efficacy of In-situ Paraffinization

Scholar: Sai Saharsh Gumudavelly
High School: North Allegheny Senior High School, Pittsburgh, PA
Lab: Wayne Stallaert, PhD
Mentor: Janet McLaughlin
Site: Women's Cancer Research Center

Introduction:

Genotoxic therapies (targeted and chemotherapy) are widely used as a treatment option against a variety of cancers, especially breast. The Stallaert lab has shown that breast cancer cells that survive treatment with genotoxic agents can become polyploid through endoreplication, a process in which DNA replication is decoupled from cell division. The paths towards whole genome duplication (WGD) force the cell into a state of G0, halting cell cycle progression. However, cells can exit G0, and create polyploid populations, promoting tumor evolution and progression. We wanted to show WGD is apparent in other types of cancer.

To obtain measurements of numerous cell cycle regulator proteins and investigate the mechanisms of WGD in other cancers, our lab uses multiplexed immunofluorescence (mIF). Current methods of multiplexed immunofluorescence result in significant cell loss. Our lab created in-situ paraffinization, which introduces paraffin layers to improve cell adherence, and we wanted to test its efficacy.

Hypothesis:

H1: Cells in other cancer cell lines, when subject to genotoxic therapies, will produce polyploid cell populations. + H2: The cells that go through in situ paraffinization will be more adherent, resulting in better staining and more data.

Procedure:

We grew ovarian and pancreatic cell culture lines and seeded 8-well chamber slides, then administered 5-day drug treatment. The OVCAR slides received either control (DMSO), cisplatin, or olaparib; PDAC slides received either control (DMSO) or Gemcitabine. Then, we prepared 2 slides in each cell type/drug treatment through in-situ paraffinization and prepared the other 2 slides through the normal processing method. We then stained Vimentin, Cyclin A2, and pRb antibodies and performed CellDIVE imaging. For H2, we simulated mIF through "fake rounds" using antibody diluent to simulate antibody staining and dye inactivation performed as normal, with DAPI staining for 10+ rounds. This was done on 1 in-situ slide and 1 normal slide.

Results + Conclusions:

H1: In both cell lines, cells showed a larger nuclear area, demonstrating polyploidy due to genotoxic therapies. H2: Ovarian cancer cell lines showed increased adherence to the slide with in-situ paraffinization through multiple rounds of mechanistic mIF. The fluorescence intensity of Vimentin was also increased on the in-situ slides, possibly due to antigen retrieval that was performed on those slides.

Mental Health Outcomes of Chronic Pain and Influence of Autism Spectrum Disorder Traits, Social Experiences, and Healthcare

Dr. Nev Jones, Lauren Fowler, Eidolon Kelly, Shannon Pagdon, Nixie Gyre, Carrick High School, Pittsburgh, Pennsylvania; UPMC Hillman Cancer Center Academy; CoSBBI site

Abstract

Autism Spectrum Disorder (ASD) is extremely correlated to chronic pain and illness, and is very likely to impact how it is processed and reported. Yet, this crossover is still poorly understood in clinical research. These findings suggest multiple trends that seem applicable to many kinds of chronic pain and comorbid conditions, notably social isolation and dismissal worsening both physical and mental health symptoms.

Introduction

The current existing research regarding ASD's connection to the experience of pain is somewhat limited. ASD has known links to Ehlers-Danlos Syndromes (EDS, a group of hereditary connective tissue disorders), and central nervous system (CNS) sensitivity issues. However, the amount of comorbid symptoms and conditions associated with ASD and EDS seems to surpass typical research methods that rely on extensive exclusion criteria. This study aims to gain a broader perspective on the overall ramifications of chronic pain and how ASD affects it.

Methods

A long (Approx. 95 question) online survey was distributed to 26 participants, 8 of whom were diagnosed with autism, and 12 of whom personally suspect they have autism (submissions have not yet closed, these numbers may change). The survey contained almost entirely multiple choice questions, and a few open-ended questions. All data was collected and analyzed anonymously.

Results

Some correlations were found between sensory seeking/avoiding behavior in chronic pain patients with ASD and variance in pain tolerance; as well as mental health, high frequency of adverse experiences in healthcare, and significant dismissal of pain reports in multiple settings.

Discussion

The findings of this study branch across several contexts, giving us a small yet thorough look at a larger range of shared experiences across many types of chronic pain and their comorbidity with psychological and neurodevelopmental conditions. It also provides insight into the likelihood of patients with chronic pain experiencing barriers in healthcare, including (but not limited to) the majority percentage (59%) of participants reported feeling "dismissed, gaslighted, ignored, or mistreated" by healthcare providers frequently, another 27% reporting "sometimes."

Arginine Methylation of CtIP Sustains Leukemic Cell Survival by Regulating DNA Repair and Apoptotic Signaling in MLL-AF9 Leukemia

Scholar: Najih Haider
High School: Winchester Thurston School
Lab: Wei Du, MD, PhD
Mentor: Jian Xu, Phd
Site: Cancer Biology

Background: CtIP plays a central role in DNA end resection and homologous recombination (HR)-mediated repair, yet the regulatory role of its post-translational modifications in hematologic malignancies remains poorly understood. This study investigates whether arginine methylation of CtIP is essential for sustaining leukemic cell survival and expansion, using MLL-AF9-driven leukemogenesis as a model.

Methods: A CtIP arginine methylation-deficient knock-in mouse model was combined with MLL-AF9-driven leukemogenesis. HR-mediated DNA repair and NHEJ activity were assessed, along with cell proliferation, cell cycle progression, and apoptosis in MLL-AF9 leukemic cells. Activation of the ATR-CHK1-p53 signaling axis and CtIP-BAX interaction were examined mechanistically. Findings were validated in human MLL-rearranged leukemia cell lines and primary patient samples, and correlated with clinical outcomes in human leukemia datasets.

Results: Loss of CtIP arginine methylation impaired HR-mediated DNA repair, elevated NHEJ activity, and triggered progressive replication stress-induced DNA damage accumulation. Loss of CtIP arginine methylation suppressed leukemic cell proliferation, induced cell cycle arrest, and promoted apoptosis in MLL-AF9 leukemic cells. Mechanistically, methylation-deficient leukemic cells exhibited activation of the ATR-CHK1-p53 signaling axis and aberrant interaction between CtIP and pro-apoptotic BAX, culminating in mitochondrial apoptosis. These findings were recapitulated in human MLL-rearranged leukemia cell lines and primary patient samples, and correlated with clinical outcomes in human leukemia datasets.

Conclusion: Our study shows that arginine methylation of CtIP is essential for sustaining leukemic cell survival and expansion. Loss of CtIP methylation impairs HR-mediated repair and activates the ATR-CHK1-p53-BAX axis, leading to mitochondrial apoptosis. These findings support CtIP methylation as a therapeutic vulnerability across hematologic malignancies.

Modulation of TopBP1 at the Replication Fork of Polymerase Epsilon

Scholar: Ayanna Hall

High School: Science and Technology Academy, Pittsburgh, Pennsylvania

Lab: Dr. Tatiana Moiseeva

Mentor: Rohan Harolikar

Site: Cancer Biology

Background: DNA replication is a process with many checkpoints and signals. Replication stress is a source of genome instability in pre-tumor and tumor cells. DNA replication stress-inducing drugs are effective at killing cancer cells. DNA Polymerase epsilon is an essential enzyme for DNA replication. DNA Polymerase epsilon is also responsible for synthesizing the leading strand during DNA replication. TopBP1 is an overexpressed protein in many cancer cells. FACS data shows that TopBP1 accumulates more when Polymerase Epsilon is depleted.

Methods: Osteosarcoma cell lines (U2OS, 24, & 24.2) were treated with doxycycline 100 nM, & 3-IAA 0.25mM. Cell lines 24 and 24.2 are both the same. However, 24.2 expresses the CTD of POLE1, which allows elongation in the cells without PolE. Western blots were performed to assess the strength of protein signals after treatments. Expansion was done on cells so that multiple experiments could be done without having to get a new batch of cells for every experiment.

Results: TopBP1 accumulates more on chromatin with the depletion of PolE. The western blot shows how the proteins are affected by the depletion of PolE.

Conclusion: Our study shows that with the depletion of PolE, TopBP1 accumulates more on the chromatin. This supports our hypothesis that TopBP1 is removed from the replication fork by the noncatalytic action of Polymerase Epsilon. By depleting Polymerase Epsilon, TopBP1 is not removed, and on the chromatin, it cannot dissociate. This study will help to inform replication initiation dynamics and contribute to a better understanding of replication stress-inducing drugs for future studies. For example, recent studies show that an ATR inhibitor increases the number of origins fired, so a next step would be to study how ATR inhibitors affect this accumulation.

Title: Uncovering PFIC1 Disease Mechanisms Using Patient-Derived CRISPR iPSC Models

Scholar: Adham Hendawy

High School/College/City/State: Upper Saint Clair High School, Pittsburgh, PA

PI of group/lab: Rodrigo Florentino, PhD

Mentor(s): Rodrigo Florentino, PhD

Site: Pathobiology

Background: Progressive Familial Intrahepatic Cholestasis Type 1 (PFIC1) is a severe genetic liver condition caused by ATP8B1 mutations, encoding the FIC1 protein. Pathogenesis involves loss of FIC1 flippase activity, disrupting membrane asymmetry, and loss of Farnesoid X Receptor (FXR) activity, impairing bile acid regulation. It is unknown which mechanism primarily drives the PFIC1 phenotype. To address this, our goal was to generate human induced pluripotent stem cells (iPSCs) expressing Cas12 for targeted gene modification, establishing a human-relevant model to systematically disrupt these pathways and characterize the key driver of PFIC1 pathogenesis.

Methods: Patient-derived ATP8B1 mutant iPSCs and wild-type isogenic control iPSCs were transduced with a Cas12-expressing lentivirus containing a blasticidin resistance cassette. To confirm Cas12 integration and stem cell pluripotency, they were evaluated by immunofluorescence (IF) staining targeting Cas12 and the pluripotency marker Nanog, followed by fluorescence microscopy. Total RNA was extracted from harvested cell cultures and converted into cDNA via reverse transcription to prepare templates for quantitative PCR (qPCR) analysis.

Results: Following blasticidin selection, qPCR and immunofluorescence (IF) staining demonstrated successful Cas12 protein expression across selected cells. Immunofluorescence (IF) staining confirmed strong nuclear expression of Nanog, establishing that Cas12 integration and selection did not compromise stem cell pluripotency.

Conclusion: We successfully generated a patient-derived PFIC1 CRISPR-Cas12 iPSC model. Future studies will utilize this validated system to systematically disrupt FXR and ATP8B1 pathways to identify the primary driver of PFIC1 pathogenesis.

Title: Validation of High-Frequency Ultrasound for Longitudinal Assessment of Experimental Rat Achilles Tendinopathy

Scholar: Vesta Homayoun

High School/College/City/State: University of Southern California, Los Angeles, California

PI of group/lab: Dr. Alison Bean, Musculoskeletal Regeneration Rehabilitation Lab

Mentor(s): Dr. Hiroki Kaneta

Site: Cancer Biology

Background: Achilles tendinopathy is a chronic condition characterized by tendon pain, thickening, and structural degeneration that can impair mechanical function. Although commonly observed in older populations, many preclinical studies utilize young animal models, which may not fully capture age-related disease characteristics. Furthermore, longitudinal evaluation of disease progression and comparison of different tendinopathy induction methods using non-invasive imaging remain limited. This study evaluated structural progression across multiple Achilles tendinopathy models using high-frequency ultrasound and assessed the reproducibility of ultrasound measurements between observers.

Methods: Young Sprague-Dawley and Fischer rats, as well as aged Fischer rats, underwent Achilles tendinopathy induction using collagenase injection, needling, or needling combined with treadmill exercise (n = 3–4 per group). Serial high-frequency ultrasound imaging (Vevo 3100, MX550 transducer) was performed at baseline and 4 and 8 weeks post-injury. Tendon thickness, cross-sectional area (CSA), and echogenicity were quantified. Inter-observer reliability of ultrasound measurements was assessed using the intraclass correlation coefficient (ICC).

Results: High-frequency ultrasound successfully detected longitudinal structural changes following Achilles tendon injury across the evaluated experimental models. In young Sprague-Dawley rats, collagenase injection and needling resulted in increased tendon thickness, CSA, and echogenicity that persisted throughout the 8-week study period. Similar longitudinal changes were observed following needling combined with treadmill exercise in young Fischer rats and following collagenase injection and needling combined with treadmill exercise in aged Fischer rats. Ultrasound measurements demonstrated excellent inter-observer reliability (ICC = 0.935), supporting the reproducibility of this imaging approach.

Conclusion: High-frequency ultrasound provides a reliable, non-invasive method for longitudinal assessment of Achilles tendinopathy progression across multiple experimental rat models. This technique enables reproducible, serial evaluation of tendon structural changes over time and represents a valuable tool for future studies investigating tendon degeneration and evaluating novel therapeutic interventions.

On Use of BMI to Improve Diagnosis of Myofascial Pain based on Nakagami Characterization Ultrasound Images

Saanvi Jain[1], Dr. Maryam Satarpour[2], Dr. Ajay D. Wasan[3], Dr. Andriy I. Bandos[4], PhD
[1]South Fayette Highschool, McDonald, PA; [2]University of Pittsburgh Hillman Cancer Center Academy, Pittsburgh, PA

Abstract
Myofascial pain (MP) is a significant contributor to low-back pain, which affects 70-85% of adults at some point. Satarpour et al. (2026) showed that the Nakagami characterization of ultrasound images can distinguish MP-positive from MP-negative exams. It was also confirmed that BMI was significantly associated with MP-positive exams. Here, we evaluate whether incorporating BMI can improve Nakagami-based diagnosis of MP by enabling patient-centered decisions that treat each BMI group equitably without meaningfully sacrificing overall accuracy.

Introduction
In this project, we used data from Satarpour *et al.* (2026) to evaluate how BMI could improve the Nakagami-based diagnosis of MP. For a concrete example, we focused on one of the two standard types of clinical decisions – the "rule-out" decision, which aims to spare some patients without MP from unnecessary treatment, targeting ≥90% sensitivity (or a false-negative rate ≤10%). We evaluated whether knowledge of patients' BMI could be used to create a rule-out decision that is equitable across the clinical BMI categories – ensuring that no group is systematically underserved — without substantial sacrifice of the overall performance of the decision rule.

Methods
The available data included a total of 332 exams (161 with and 171 without MP) derived from the 91 participants, where each exam represented one side of the lower back evaluated at one of up to two study visits. The study population spanned three BMI categories: healthy weight (32%), overweight (40%), and obese (29%). Empirical ROC curves were estimated using the pROC package in R [2]. Covariate-adjusted ROC curves [3] were used to assess the combined performance of BMI category-dependent decision rules for the Nakagami parameter (adjustment for the quantitative BMI was performed using ROCnReg package in R [5]). For a given threshold c, sensitivity (true positive fraction) was defined as the percentage of MP patients correctly identified above c, and specificity (true negative fraction) as the percentage of MP-negative exams correctly identified below c. For each decision rule, the threshold was set to the highest value of Nakagami parameter at which the empirical sensitivity (within the considered group) remained at least 90%.

Results
The straightforward use of a single common threshold (c=1.24) for Nakagami characterization results in a rule-out decision that can spare 25% of MP-negative subjects from unnecessary treatment while allowing no more than 10% of false negatives (i.e., 90% sensitivity). This, however, systematically underserves the healthy BMI group by resulting in 23% incorrectly ruled-out MP exams (77% sensitivity), as opposed to the targeted 10% (90% sensitivity). At the same time, using the conservative but still one-for-all threshold to ensure no more than 10% false negatives in all BMI categories (c=1.22) results in the overall specificity dropping by 14% (from 25% to 11%), and useless decisions for the Obese group (specificity of 0%). In contrast, using BMI category-specific thresholds (which ensure 90% sensitivity in each group), achieved equitable rule-out decisions with twice the aggregated specificity (22% versus 11% for the equitable but BMI-blind decision rule). In comparison to using the common threshold for inequitable rule out decision in the entire population, the overall specificity of this BMI-driven equitable decision rule dropped by only 3%, 4 of 171 exams (from 25%, 42/171, to 22%, 38/171). The ability to achieve equitable decisions at almost no aggregate cost stems from the close proximity of the pooled and BMI-adjusted ROC curves for Nakagami parameter in the high-sensitivity region.

Discussion
Our results indicate that BMI information can improve application of Nakagami characterization for supporting equitable rule-out decisions without meaningfully sacrificing overall accuracy. In ongoing work, we are evaluating whether rule-out decisions can be improved by combining BMI with Nakagami using an optimized mathematical function.

Table 1. *Sensitivity, Specificities and the corresponding numbers of correct decisions (i.e., numbers of true positives, #TP, and true negatives, #TN) for three types of rule-out decision overall and in clinical BMI categories: healthy, overweight, obese, and overall categories*

BMI categories (MP: no-MP units)	Pooled one-fits-all decision (at c=1.24)		Equitable but BMI-blind decision (at c=1.22)		Equitable decision based on BMI-specific rules (at category-specific 'c')		
	Sens (#TP)	Spec (#TN)	Sens (#TP)	Spec (#TN)	Threshold 'c'	Sens (#TP)	Spec (#TN)
Healthy (31:77)	77% (24)	35% (27)	90% (28)	17% (13)	1.22	90% (28)	17% (13)
Overweight (67:63)	93% (62)	21% (13)	99% (66)	8% (5)	1.24	91% (61)	24% (15)
Obese (63:31)	94% (59)	6% (2)	100% (63)	0% (0)	1.27	90% (57)	32% (10)
Overall (161:171)	*90% (145)*	*25% (42)*	*98% (157)*	*11% (18)*	*N/A*	*91% (146)*	*22% (38)*

Figure 1. *Nakagami-based ROC curves for individual BMI groups, the pooled ROC curve (left figure, in pink color), and the BMI-adjusted ROC curve (right figure, black color), with operating points (dots and '+') corresponding to the three types of decision rules summarized in the same order in Table 1.*

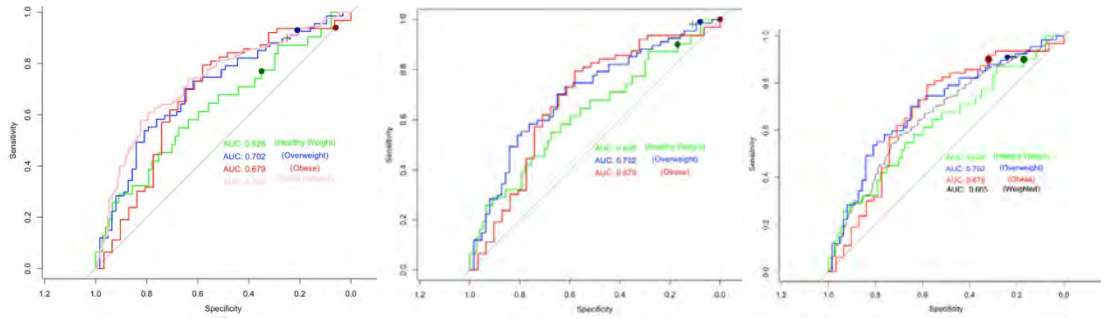

References

[1]Satarpour M, Sheng Z, Bandos A, Cormack J, Bean A, Nussbaum R, Landis-Walkenhorst E, Piccari J, Zeng Z, Pu J, Wasan A, Kim K. Three-Dimensional Quantitative Ultrasound Imaging Using Nakagami Distribution to Assess Lumbar Muscles in Chronic Low Back Pain. (Submitted to IEEE Journal of Biomedical and Health Informatics)

[2]Zhou X, Obuchowski N, McClish D. Statistical Methods in Diagnostic Medicine. 2nd ed. New Jersey, Canada: John Wiley & Sons, Inc. 2011

[3]Janes H, Pepe M. Adjusting for Covariates in Studies of Diagnostic, Screening, or Prognostic Markers: An Old Concept in a New Setting. American Journal of Epidemiology. 2008; 168(1): 89-97

[4]Robin X, Turck N, Hainard A, Tiberti N, Lisacek F, Sanchez JC, et al. pROC: an open-source package for R and S+ to analyze and compare ROC curves. BMC Bioinformatics. 2011; 12:77.

[5]Rodriguez-Alvarez MX, Inacio V. ROCnReg: an R package for receiver operating characteristic curve inference with and without covariates. R J. 2021;13(1):525-55.

Regulation of inhibitory receptors by TOX in intratumoral CD4$^+$ conventional T cells

Nathaniel J. Javorski
Brentwood Borough Middle-High School, Pittsburgh, PA
Mentors: Samuel C. Butler; Creg J. Workman, PhD; Dario A.A. Vignali, PhD

T cell exhaustion proves to be a major barrier in cancer immunotherapy. T cells under chronic antigenic stimulation become increasingly dysfunctional due to several transcriptional programs, including those regulated by TOX, decreasing their responsiveness to immunotherapies. Previous studies have detailed a critical regulatory role of TOX in the development of CD8$^+$ T cell exhaustion, enhancing expression of inhibitory receptors (IRs) and impairing effector cytokine production. Although the role of TOX is well characterized in CD8$^+$ T cell exhaustion, its functional impact in CD4$^+$ T cells is less understood. Here, we hypothesized that the loss of TOX in activated CD4$^+$ conventional T cells (T_{CONV}) will decrease expression of the IRs PD-1, LAG-3 and TIM-3. To investigate this, we generated a *Tox*$^{L/L}$*Lag3*^{CreERT2}*Rosa26*$^{LSL.tdTomato}$ murine tumor model, enabling the selective deletion of TOX in cells expressing LAG-3. Mice were inoculated with B16-F10 melanoma on Day 0, followed by the inducible activation of Cre through tamoxifen injections on Days 8, 9, and 10. Intratumoral and peripheral tdTomato$^+$ CD4$^+$ T_{CONV} cells were assessed on Days 14 and 19. We observed a significantly decreased proportion of TIM-3$^+$ and PD-1$^+$LAG-3$^+$ TOX-deficient tdTomato$^+$ CD4$^+$ T_{CONV} cells in tumors on Day 19, compared to controls. Further, we observed that the percentage of PD1$^+$ tdTomato$^+$ CD4$^+$ T_{CONV} cells in the draining lymph nodes of TOX-deficient mice was significantly decreased on Day 14, and greatly reduced on Day 19. Together, these findings suggest a potential role of TOX in reinforcing the expression of IRs in activated CD4$^+$ T_{CONV} cells. Additional investigations will be performed to corroborate these findings and assess impacts on effector cytokine production, cell survival and proliferation, and expression of related transcription factors.

Effects of EP31670 on Survival and Colony Formation of LM2 Osteosarcoma Cells

Scholar: Zhanyu Jiang
High School/College/City/State: Fox Chapel Area High School, Pittsburgh, PA
PI of group/lab: Dr. Ines Lohse, Dr. Kurt Weiss

Mentor(s): Dr. Ines Lohse
Site: Cancer Biology

Osteosarcoma (OS) is the most common primary bone malignancy in children and adolescents, yet outcomes for patients with metastatic or chemoresistant disease remain poor. This unmet need has driven interest in new molecular targets. Bromodomain and extra-terminal (BET) proteins have emerged as candidate therapeutic targets across several cancers. EP31670 is a dual inhibitor of BET proteins and the histone acetyltransferases p300/CBP. Here we investigate effects of the BET inhibitor EP31670 on the survival and proliferation of the osteosarcoma cell line LM2. SaOS-LM2 is the metastatic daughter cell line of the Sarcoma Osteogenic 2 cell line (SaOS2) and was derived through passage in the mouse.
Clonogenic assays were used to assess LM2 survival and proliferation in response to treatment with low (0.11 μM) and high (0.33 μM) doses of EP31670. Cells were seeded at 2×10^5 cells in 10cm plates and treated for 72h. Cells were then seeded for colony formation in 6-well plates and incubated for 14 days, followed by fixation with methanol/acetic acid and crystal violet staining. Due to human error, the control group was only seeded at 2.5×10^2 and 5×10^2 cells/well, and the 1×10^3 cells/well density was not included, resulting in no valid baseline colony count. Despite this limitation, data from the 5×10^3 cells/well density yielded countable data showing lower colony counts in the 0.33 μM group (mean = 198) compared to the 0.11 μM group (mean = 263), suggesting that higher drug doses result in lower colony formation. The lack of a valid control prevented calculation of plating efficiency and surviving fraction. However, the lower count at the higher dose indicates that LM2 colony formation is dose-dependent. A future repeat of this clonogenic assay will ensure a control plated at 1×10^3 cells/well to enable direct comparison with surviving fraction.

Digital twins and patient-specific computational models in women's health: a scoping review

Scholar: Ruth Joel

High School/College/City/State: Providence Day School, Charlotte, NC

PI of group/lab: Dr. Olga Kravchenko

Mentor(s): Dr. Olga Kravchenko

Site: CoSBBI

Digital twins have the potential to support personalized medical care, but their use in women's health has not been well characterized. We conducted a preliminary scoping review of PubMed literature using the National Academies of Sciences, Engineering, and Medicine (NASEM) definition of a digital twin to map how these computational models are used in women's health. Our primary question examined which digital twin or digital-twin-adjacent approaches have been developed or proposed in women's health and their clinical domains, data sources, modeling methods, and maturity levels. Our secondary research question examined the extent to which studies labeled as "digital twins" in women's health meet the NASEM definition. We used large language models to assist the initial abstract screenings to narrow down records for review. Further abstract and full-text screening is ongoing, and will be conducted manually. A total of 344 records underwent initial screening. Of these, 69 were classified as "include", 79 require further review and were classified as "maybe", and 196 were classified as "exclude". Within the 148 "include" and "maybe" records, 32 potentially met the NASEM definition of a digital twin, while 116 described digital-twin adjacent models, meaning that they only contained one or more, but not all, of the necessary components required by the NASEM definition. A total of 11 broad health domains were coded as non-mutually exclusive categories because several studies span more than one clinical area. The largest domain cluster was pregnancy and maternal-fetal health, followed by gynecologic oncology and broader health conditions relevant to women. This distribution suggests that digital twin and digital-twin-adjacent work in women's health is currently concentrated in areas with established traditions of computational physiology, multiscale modeling, treatment simulation, and patient-specific prediction. The ongoing review will refine these findings, characterize digital twins technologies across women's health, and identify areas for further research.

Title: Enumeration of Altered Retinal Network Motifs in Retinal Degeneration

Scholar: Patrick Johnson

High School/College/City/State: Science and Technology Academy, Pittsburgh, PA

PI of group/lab: Rebecca L. Pfeiffer

Mentor(s): Jie-Yu Wang, James R. Anderson, Jia-Hui Yang, Matthew L. Berardy, Bryan W. Jones, and Rebecca L. Pfeiffer

Site: VISION

Introduction:

Retinitis Pigmentosa (RP) causes the progressive degeneration of rod photoreceptors, followed by cone photoreceptor degeneration resulting in blindness. RP is caused by mutations in multiple genes, creating a need for mutation-independent treatments. This highlights the need for increased understanding of how RP alters retinal structure, function, and changes in retinal network connectivity. We evaluate these changes in synaptic connections through a series of pathoconnectomes.

Methods:

Retinas were fixed in mixed aldehydes, permeated with 1% OsO_4 and uranyl acetate, dehydrated, and embedded in Epon resin. The retinal tissues were serially sectioned at 70nm, placed on Formvar-coated slot grids, and imaged on two JEOL 1400 TEMs using SerialEM software. 1 out of every 30 sections was reserved for small molecule labeling. Images were assembled and aligned using the nornir-buildscripts custom software and analyzed using the Viking software package.

Results:

Each pathoconnectome marked a different, more progressive stage of rod degeneration. RPC1 demonstrates 50% rod degeneration, while RPC2 shows a complete loss of rods. Retinal connectome 1 (RC1) is from a healthy rabbit. Across the pathoconnectomes we find an increase in the average number of excitatory synapses. In contrast, we see a decrease in the average number of conventional post-synapses present.

Conclusions

These results provide early insight into retinal rewiring across the various stages of RP. We see that excitatory synapses increase across degeneration. Inhibitory synapses are decreased in RPC2, in contrast to results in RPC1 showing an increase in inhibition. The novel gap junctions identified in RPC1, however, persist in the RPC2 volume.

Future Directions:

These results, along with the enumeration of their connectivity within the retinal network will inform the field on the state of inner retinal circuitry across rod photoreceptor degeneration. From this, we will be able to move towards effectively integrating therapeutics for all RP mutations.

ML for CT to PET/CT Translation and Classifying Lung Cancer Subtypes

Tisha Joshi[1], Dr. In Hee Lee[2], PhD

[1]Pine-Richland High School, Gibsonia, PA; [2]University of Pittsburgh, Pittsburgh, PA

Abstract: *Two generative models - a diffusion model and a Generative Adversarial Network (GAN) - are developed and compared in terms of their performance in translating CT to PET/CT scans of patients diagnosed with lung cancer. Furthermore, a computer vision detection model, a Deep Convolutional Neural Network (CNN), is used to classify the PET/CT scans into various lung cancer subtypes: Adenocarcinoma, Small, Large, and Squamous Cell Carcinoma.*

Introduction: Positron Emission Tomography (PET) scans utilize a radioactive tracer, often fluorodeoxyglucose (FDG), and the scan reflects how much of the tracer was absorbed. FDG is particularly useful in cancer detection since cancerous cells utilize more glucose than normal cells, resulting in the scan creating bright spots in those locations to indicate increased tracer uptake and a possible tumor [1]. The scans can often be used to find changes earlier than other imaging tests, making them useful for detecting diseases [2]. Unfortunately, the availability of PET scans is limited due to how expensive, time-consuming, and inaccessible they are. Computed Tomography (CT) scans are more accessible, less expensive, and faster to obtain than PET scans. The combination of CT scans and PET scans creates the PET/CT scan. CT's anatomical precision, integrated with PET's tracer uptake indications, makes it easier to pinpoint whether there is a tumor and, more precisely, where it is located, such as lung tumors detailed in these experiments. In addition, lung cancer is the third most common cancer in the US, with more people dying from it than other types of cancer [3]. Because of a lack of noticeable symptoms, the cancer can go undiagnosed for a long time, which can further metastasize and make it hard to treat [3]. This is apparent in how nearly 44.4% of diagnosed lung cancers are diagnosed at a distant stage [4]. To combat this, in this work, a CT to PET/CT translation model and a detection model are developed to detect the presence of a subtype of lung cancerous tumor. It is hypothesized that the diffusion model will perform better than the GAN due to more stable training, but the GAN is hypothesized to take less time.

Methods: The dataset used is found in The Cancer Imaging Archive [5], containing pairs of CT and their corresponding PET/CT scans. The patients from this study were separated into 4 different categories of lung cancer subtypes: classes "A", Adenocarcinoma; "B", Small Cell Carcinoma; "E", Large Cell Carcinoma; and "G", Squamous Cell Carcinoma. After data cleaning, 1624 CT-PET/CT pairs for class A, 1345 CT-PET/CT pairs for class B, 1646 CT-PET/CT pairs for class G, and no pairs for class E are used for training the generative models. The GAN is a remnant of the conditional Pix2Pix architecture [6] with a few hyperparameter alterations, containing a UNet generator, which learns patterns from the training data to generate images (Figure One), and a CNN discriminator, which learns to distinguish ground truth training samples from the fake images the generator creates (Figure Two). The diffusion model replicates the CT2PET Diffusion Model (CPDM) proposed in [7], which follows the Brownian Bridge diffusion model architecture with the addition of attention and attenuation maps (Figure Three) to indicate where the model should generate the image and to improve the quality of image translation. Three metrics - Mean Absolute Error, Peak Signal-to-Noise Ratio, and Structural Similarity Index Measure - are used to compare the performances. A deep convolutional neural network architecture (Figure 4) is utilized for the detection model, and accuracy, cross-entropy loss, and recall are utilized as the key evaluation metrics. There are a total of 208 PET/CT images for class E, 624 after data augmentation to reduce class imbalance, that were used alongside the 1624 A, 1345 B, and 1646 G PET/CT scans to train the detection model.

Results: The original CT2PET model proposed in [7] is used in this experiment. As seen in (Figure Seven), the GAN performed the best with PSNR, while the diffusion model performed better on the other two. However, the GAN performed 2-3 hours on average on 2000 epochs on a basic CUDA on a regular computer. However, when trying to replicate the original paper's training, with only 200 epochs, it takes more than three hours on even more powerful GPUs in a lab. Additionally, for the detection model, during training, it performed perfectly, and when given fresh, new testing data, it performed near-perfectly as well, with an accuracy of 99.7%.

Discussion: SSIM is the most useful metric due to its priority in assessing how humans would truly perceive image quality by taking into account brightness, contrast, and structure. Thus, the diffusion model performs better than the GAN overall, which validates the hypothesis that the diffusion model generates better translations. Moreover, the difference in computational power and the increased training duration of the diffusion model prove that the GAN is much more efficient for training. These translation models can be used in medical settings where CT scans are available and PET scans are less accessible to translate the scans and further be used to detect and diagnose a lung cancer tumor. Future directions include offering more imaging translation models, such as CT to MRI. Additionally, the detection model can be expanded to various modes or imaging types for input and for more cancer types.

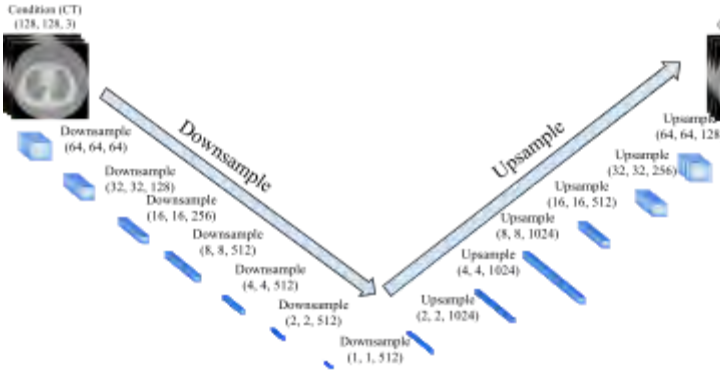

Figure One - The UNet Architecture of the GAN Generator

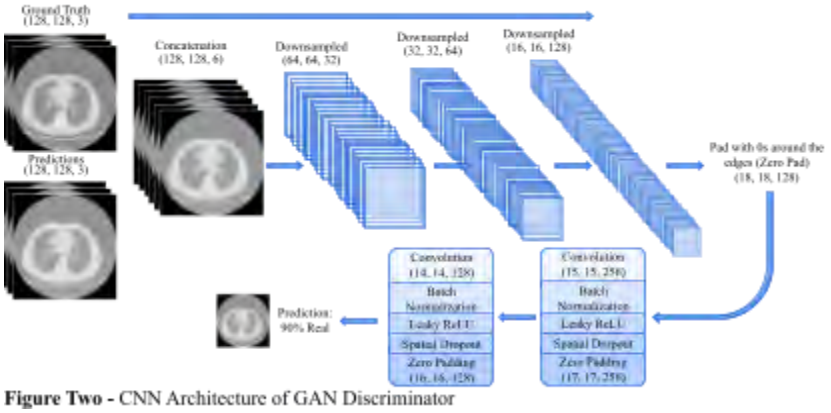

Figure Two - CNN Architecture of GAN Discriminator

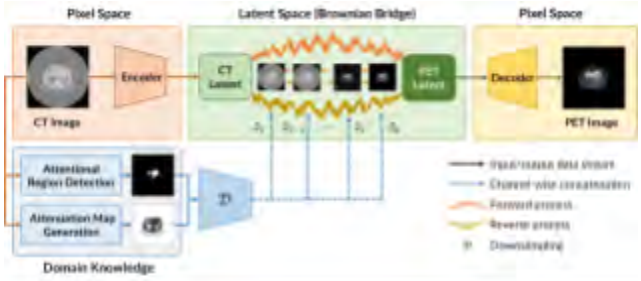

Figure Three - CT2PET Diffusion Model architecture, as detailed in [5].

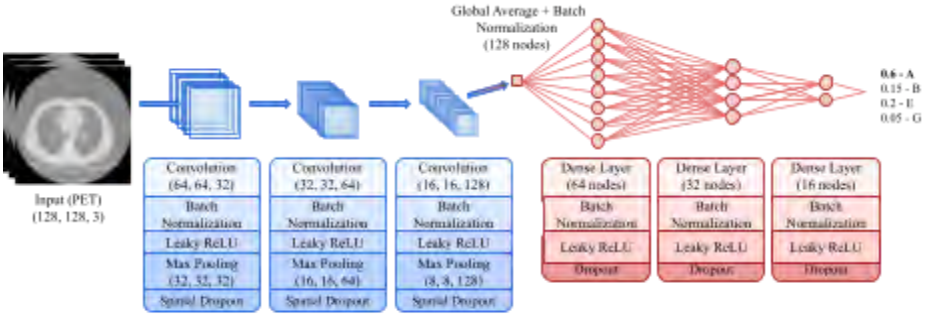

Figure Four - Deep Convolutional Neural Network Architecture

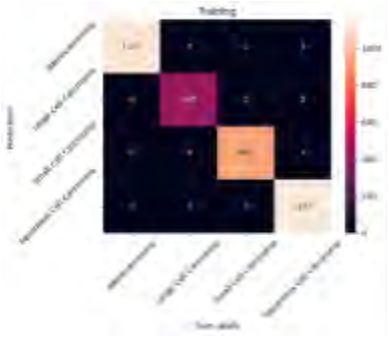

Figure Five - Best CNN Training Results
Accuracy: 1.0
Recal (Adenocarcinoma): 1.0
Recall (Small Cell Carcinoma): 1.0
Recall (Large Cell Carcinoma): 1.0
Recall (Squamous Cell Carcinoma): 1.0

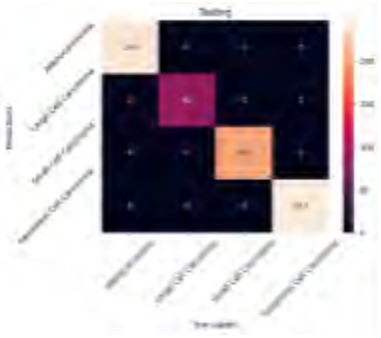

Figure Six - Best CNN Testing Results
Accuracy: 0.997
Recall (Adenocarcinoma): 0.992
Recall (Small Cell Carcinoma): 1.0
Recall (Large Cell Carcinoma): 1.0
Recall (Squamous Cell Carcinoma): 1.0

Comparing the Performances of Generative Models:

Best Performing Model	MAE ↓ (Aim: Close to 0)	SSIM ↑ (Aim: .95-1)	PSNR ↑ (Aim: 30 dB +)
GAN	0.042	0.906	**30.088**
Diffusion (From Original Paper)	**0.009**	**0.940**	29.68

Figure Seven - Comparison of the best-performing generative models. ↓: lower is better, ↑: higher is better.

References:

1. Cleveland Clinic. PET Scan: Procedure Details and Results. Cleveland, Ohio: Cleveland Clinic; 2017 Feb [cited 2026 Jun 16]. Available from: https://my.clevelandclinic.org/health/diagnostics/10123-pet-scan
2. Mayo Clinic. Positron emission tomography (PET) scan - Mayo Clinic. Mayo Clinic; 2026 Mar [cited 2026 Jun 16]. Available from: https://www.mayoclinic.org/tests-procedures/pet-scan/about/pac-20385078
3. American Lung Association. Debunking the Most Common Lung Cancer Myths. American Lung Association; 2026 Jun [cited 2026 Jul 1]. Available from: https://www.lung.org/blog/lung-cancer-myths
4. CDC. U.S. Cancer Statistics Lung Cancer Stat Bite. CDC; 2024 Jun [cited 2026 Jul 1]. Available from: https://www.cdc.gov/united-states-cancer-statistics/publications/lung-cancer-stat-bite.html
5. Li P, Wang S, Li T, Lu J, HuangFu Y, Wang D. A Large-Scale CT and PET/CT Dataset for Lung Cancer Diagnosis [Internet]. The Cancer Imaging Archive; 2020 [2026 Jun 22]. Available from: https://www.cancerimagingarchive.net/collection/lung-pet-ct-dx/
6. Isola P, Zhu J, Zhou T, Efros AA. Image-to-Image Translation with Conditional Adversarial Networks. arXiv:1611.07004v3. 2018 [cited Jul 7]: [17 p.]. Available from: https://arxiv.org/abs/1611.07004
7. Nguyen DT, Nguyen TT, Nguyen HT, Nguyen TT, Pham HH, Nguyen TH, Truong TN, Nguyen PL. CT to PET Translation: A Large-scale Dataset and Domain-Knowledge-Guided Diffusion Approach. arXiv:2410.21932v1. 2024 [cited Jun 17]: [10 p.]. Available from: https://arxiv.org/html/2410.21932v1

Title: Characterizing the Microglial Calcium Response to a Focal Two-Photon Laser Ablation Injury

Scholar: Aaditya Kasture

High Schools: Briar Woods High School, Ashburn, VA & Academies of Loudoun, Leesburg, VA

Lab: B.I.O.N.I.C. Lab

Mentors: Vanshika Singh and Dr. Takashi Kozai

Site: TechDriveX

Background: Microglia, the central nervous system's resident immune cells, rely on intracellular calcium (Ca^{2+}) signaling which is associated with functions such as process motility, phagocytosis, lysosomal regulation, and cytokine production. Resting microglia rarely exhibit spontaneous transients. Focal damage, such as laser ablation, triggers rapid, localized Ca^{2+} responses that are amplified by inflammation and evolve over several hours. However, most studies only characterize this acute response; how microglial calcium activity develops over days following a focal injury, and whether it varies with cortical depth, remains unexplored.

Hypothesis: We hypothesized that microglial calcium activity would increase following focal laser ablation, peaking around days 3–4 before returning toward baseline by day 10, independent of cortical depth.

Methods: We imaged microglia expressing red fluorophore (tdTomato) and green calcium indicator (GCaMP) by two-photon microscopy. Following the 2-photon laser ablation of one microglia at 140 µm, we recorded microglia daily from day 0 to 10 across 50–210 µm depths. Microglia cell bodies were manually segmented in ImageJ and calcium event amplitude, frequency, and duration were measured with a MATLAB script.

Results: On day 1, there were no microglial calcium events. The percent of microglia responding (16%) with calcium events peaked on day 3. The total calcium activity per microglia (signal area) was greater on day 3 than on day 1 (2.253 ± 0.667 vs. 0.110 ± 0.077). The calcium activity returned near day 1 levels on day 5 (0.360 ± 0.158).

Conclusion: The microglial calcium response to focal laser ablation injury changes dynamically across the 10-day period. Future studies will explore the significance of the microglia calcium activity peak at day 3. This work establishes a baseline for using focal laser ablation as a reproducible in vivo assay of microglial phagocytic responses, enabling future comparisons in Alzheimer's disease models.

Development and Initial Testing of Novel Placental BOLD Analysis Method

Francesco B. Keuwo[1], Dr. William Reynolds[2], PhD, Dr. Rafael Ceschin[2], PhD
[1]Olathe North High School, Olathe, KS; [2]University of Pittsburgh, Pittsburgh, PA

Abstract

Advances in fetal Magnetic Resonance Imaging (MRI) provide an opportunity to quantitatively evaluate placental morphology and spatial characteristics that may reflect alterations in oxygen transport. Our novel approach was evaluated on a cohort with Congenital Heart Disease (CHD), which has been associated with adverse outcomes, yet its correlation to placental structure and function have yet to be understood. Our approach uses custom Python code to extract spatiotemporal data from the placenta using concentric spherical shells.

Introduction

This study aims to extract regional oxygenation features and reveal differences between diseased and normal patients. BOLD images display differences in signal based on blood oxygenation levels, meaning that brighter areas have higher blood oxygenation levels and vice-versa. We hypothesize that these two groups will demonstrate altered patterns of oxygenated blood distribution, including reduced or delayed oxygen transport and increased spatial heterogeneity compared with non-exposed controls. A major challenge of reaching these discoveries is placental segmentation and orientation is difficult when applying pre-existing methods to this structure, so new methods are needed to reveal differences between at-risk cohorts. In this work, regional placental data was extracted through generated concentric spherical shells from the center of the placenta.

Methods

A review of current literature on placental MRI segmentation methods informed the segmentation protocol and study design. Fetal MRI datasets underwent manual placental segmentation using ITK-SNAP, as demonstrated in Figure 1A. Because placental boundaries are more challenging to identify than other fetal structures, preliminary training has focused on manual brain segmentation to establish proficiency with the software and fetal MRI anatomy. Following segmentation, Python-based image analysis pipelines were used to quantify placental structural characteristics and evaluate spatial patterns potentially associated with oxygen transport. Through Python, BOLD MRI images were centered to only show the placenta and spherical shells were visualized within each placenta, as depicted in Figure 1A. The center of the placental mask was calculated by identifying the midpoint between the three orthogonal imaging planes. From the centerpoint, four spherical regions of interest were generated, radiating at 4 mm increments. For each shell, temporal shell signals were extracted by calculating the mean of each time frame and normalizing by the standard deviation of the entire placenta.

Results

Once the placentas were centered, 18 of the 20 subjects were discovered to have missing time frames, likely due to inconsistent movement during MRI scans, and frames with missing data were excluded from calculations. Once the average signals of each time frame were calculated, the graphed visualization of these mean intensities revealed that Shell 4 had the highest average intensity across all patients, as well as a higher standard deviation. Figure 2 demonstrates the shell intensities across the entire cohort.

Discussion

This work developed successful spatial temporal data from the placenta. Reproducible MRI-based workflow for placental segmentation and quantitative analysis were established while improving understanding of the effects of placental function on diseases such as CHD. Despite subjects missing data at certain time frames due to movement during scans, the majority of time frames were still available and contributed to accurate results worth being analyzed. The findings may contribute to the development of imaging biomarkers capable of identifying placental alterations associated with CHD and informing future studies of fetal health and development. Additionally, the fourth shell's higher standard deviations indicate that its blood oxygenation levels were less organized and consistent when compared to the first three shells. Because the peripheral boundary of the placenta saw more variability in oxygenation, it can be concluded that blood flow dynamics near the edge of the placenta are different from the center, represented across all four shells. A further study could be conducted in different cohorts to identify whether that pattern is consistent.

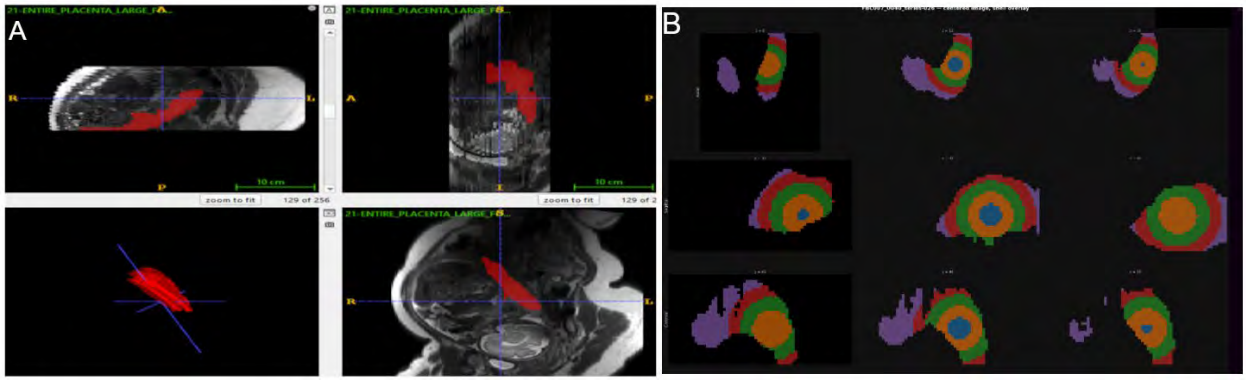

Figure 1: Segmentation Pipeline for Shell Segmentation. A: Manual Segmentation of Normal Placenta. Fetal MRI datasets underwent manual placental segmentation using ITK-SNAP. We evaluated both automated and manual methods for placental segmentations. **B: Placental shell visualization for Centered BOLD-MRI of One Patient.** The center of the placental mask was calculated by identifying the midpoint between the three orthogonal imaging planes. From the centerpoint, four spherical regions of interest were generated, radiating at 4 mm increments.

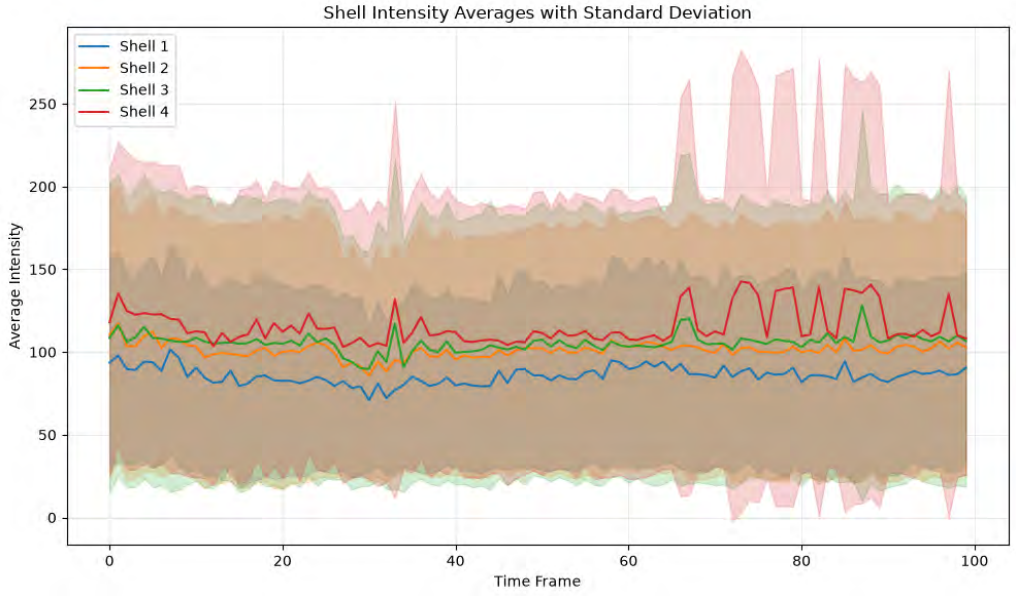

Figure 2: Average Shell Intensity for Each Time Frame Across the Entire Dataset (Pre-normalization). For each shell, temporal shell signals were extracted by calculating the mean of each time frame.

References

1. Clark A, Flouri D, Mufti N, James J, Clements E, Aughwane R, et al. Developments in functional imaging of the placenta. Br J Radiol
(2023) 10.1259/bjr.20211010.
2. Paul A. Yushkevich, Joseph Piven, Heather Cody Hazlett, Rachel Gimpel Smith, Sean Ho, James C. Gee, and Guido Gerig. User-guided 3D active contour segmentation of anatomical structures: Significantly improved efficiency and reliability. Neuroimage. 2006 Jul 1; 31(3):1116-28.

Identifying Downstream Targets of SOX2 During Ovarian Cancer Metastasis

Scholar: Helena Khalil
High School: Shady Side Academy, Pittsburgh Pennsylvania
Lab: Nadine Hempel
Mentor: Shriya Kamlapurkar
Site: WCRC

In 2026, an estimated 20,000 women in the United States will be diagnosed with ovarian cancer, and nearly 13,000 will die from the disease. This poor prognosis is largely due to early metastasis, during which ovarian cancer cells become anchorage-independent, traveling through peritoneal fluid and colonizing distant organs. Because metastatic disease accounts for the majority of ovarian cancer related death, identifying factors that promote anchorage-independent (a-i) survival may reveal therapeutic targets. Previous research from our lab demonstrated an upregulation in expression of the transcription factor SOX2 during anchorage independence. However, because SOX2 regulates essential cellular functions, it is not viable for treatment. We hypothesize that the downstream genes of SOX2 support anchorage-independent survival and may serve as potential therapeutic targets. Using multi-omic approaches (RNA-Seq and CUT&RUN), we have identified several downstream target candidates, including SOX21, ONECUT2, and AKR1B10. To validate SOX2 regulation of these candidates, we performed western blotting and qRT-PCR, followed by Live/Dead Staining. Our findings support SOX21 as a downstream target of SOX2, however, western blot analysis demonstrated that AKR1B10 had the greatest increase in protein expression in wild-type a-i conditions compared to wild-type attached cells, therefore having the strongest SOX2-dependent regulation. Similarly, qRT-PCR results showed that AKR1B10 had the largest increase in gene expression, with a 1.6-fold increase under a-i conditions, and was detected in earlier cycles compared to the other candidate genes. In addition, AKR1B10 encodes a druggable enzyme which unlike the transcription factors SOX21 and ONECUT2, makes for a better therapeutic target. We are currently using live/dead staining to assess AKR1B10’s functional role in ovarian cancer cell lines.

The Effect of Chemotherapy Drugs on Human T Cells

Kylie M. King[1], Dayana Rivadeneira, PhD[2]

[1]Moon Area High School, Coraopolis, PA; Department of Immunology, Assistant Professor, University of Pittsburgh, Pittsburgh, PA [2]

Abstract

Chemotherapy is a commonly used cancer treatment that targets highly proliferative tumor cells but can also affect the body's immune cells. Studying the proliferation of T cells after they have been treated with chemotherapy allows researchers to determine how a drug interacts with the immune system. Using this method, the amount of two donors' t cells treated with four different chemotherapy drugs, each having 6 different dosages, was recorded over 10 days.

Introduction

Chemotherapy drugs are known to cause damage to T cells due to their targeting of highly proliferative cells. However, some drugs may not affect the proliferation of these T cells as much as others. By experimentally treating T cells with different chemotherapy drugs and recording the number of cells, these differences can be analyzed.

Methods

Two donors' PBMCs (Peripheral Blood Mononuclear Cells) were collected, and the CD3 T cells were isolated through negative selection. A preliminary memory stain was taken from these cells as a comparison for later. The number of cells to be added to each condition was determined by the total number of cells left, which was found by combining 10 µl of cells and Trypan Blue in a 1:10 dilution and counting using a hemacytometer. After the correct amount was added, the cells would be treated by four different drugs, each having 6 different dosages, and left to incubate overnight. The next day, the number of cells would be counted, activated using CD3 and CD28 antibodies, and left to incubate for 48 hours after taking some to be stained. After the 48 hours were up, the number of cells would be counted again, then fed using a solution of IL2 and R10 to ensure they continued to proliferate after some were taken to be stained. From this, the cells would be counted and fed every other day until day 10. On day 10, they would be counted, then each condition would get a memory and stimulation stain to be used for comparison to the previous stains. The average of each day's counts was then recorded in a graph, and all stains were analyzed and recorded through flow cytometry.

Results

The figures show differences of proliferation between each drug, and those differences between donors in the drugs. Gemcitabine's effect on T cell proliferation is about the same between all dosages, while with 5-Fluorouracil the proliferation is much less when the cells are treated with a dosage of 4 µM or more. Oxaliplatin's effect shows about the same decrease of proliferation compared to the proliferation of the untreated cells. Paclitaxel's effect shows a struggle in recovery after treatment, with dosages 0.2 µM and 0.4 µM having a sudden drop in proliferation on day 10.

Discussion

These findings highlight different chemotherapy drugs have their own unique effects on the immune system, which can very between patients as well. This emphasizes the importance of applying patient-specific care when treating cancer, as one drug that worked for one patient may not work for the next.

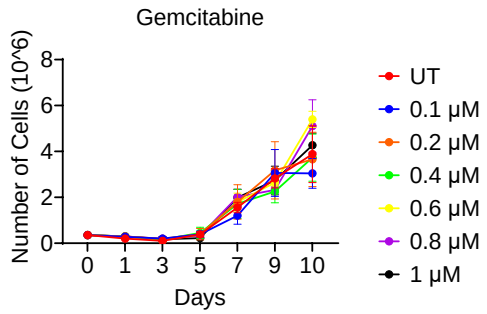

Figure 1. The average proliferation of two donors' cells when treated with Gemcitabine.

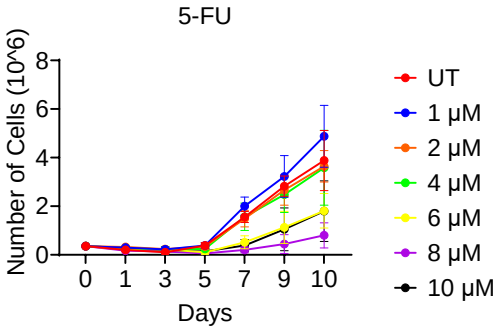

Figure 2. The average proliferation of two donors' cells when treated with 5-Fluorouracil.

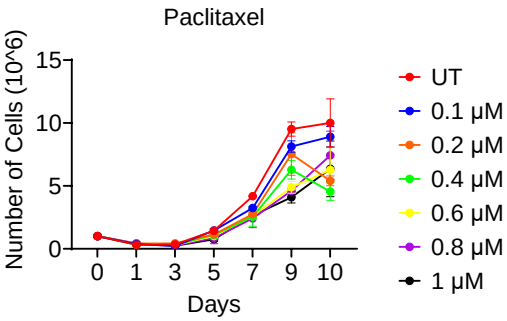

Figure 3. The average proliferation of two donors' cells when treated with Paclitaxel.

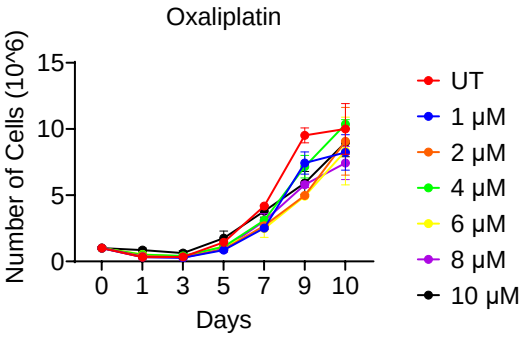

Figure 4. The average proliferation of two donors' cells when treated with Oxaliplatin.

Validating AXL protein expression in the tumor microenvironment of dedifferentiated chondrosarcoma

Scholar: Pranit Koppolu

College: Hendrix College, Conway, Arkansas

PI of Lab: Dr. Ines Lohse, PhD

Mentors: Dr. Karen Schoedel, MD; Dr. Ines Lohse, PhD

Site: Cancer Biology

Dedifferentiated chondrosarcoma (DDCS), an aggressive primary bone cancer, is characterized by rapid progression and high metastatic potential. The current treatment option available for DDCS is surgery, which highlights the urgent need for novel therapeutic approaches. The 5-year overall survival rate for patients diagnosed with DDCS is 7-24%. The receptor tyrosine kinase AXL has been studied in osteosarcoma and has been shown to be involved in dedifferentiation and metastasis. This project aims to investigate AXL expression in established chondrosarcoma cell lines using 2D monolayer and 3D spheroid cultures. LM2 osteosarcoma cells were cultured in 96-well ULA plates to form spheroids. Images of spheroids were taken every 24h for 7 days and ImageJ software was used to measure spheroid diameter.

Suitability of Honey as an Ophthalmology Research Fixative

Name: Christie Ivory Koyo
Site: Vision
School: University of Pittsburgh, Pittsburgh
Mentor: Kate Devoli
PI: Dr. Yuanyuan Chen

Background: Histological fixation is essential for preserving tissue morphology for microscopic examination. While Hartmann's fixative is the standard fixative for mouse eyes in ophthalmology research, honey has been proposed as a safer and more cost-effective alternative. Previous studies have demonstrated the effectiveness of honey as a tissue fixative in paraffin-embedded histology; however, its suitability for preserving whole mouse eyes has not been fully evaluated. This study aims to compare honey-based fixatives with Hartmann's fixative for preserving wild-type mouse eye tissue.

Methods: Wild-type mouse eyes were fixed in one of three fixatives: Hartmann's fixative, 5% honey in deionized water, or 5% honey in 30% ethanol and deionized water. Following fixation, tissues were transferred to 70% ethanol, processed, embedded in paraffin wax, sectioned at 5 µm, mounted on microscope slides, stained, and examined using light microscopy. Histological evaluation focused on preservation of ocular morphology, lens integrity, retinal structure, corneal appearance, and overall tissue quality.

Results: Initial examination revealed that some tissue sections lacked visible lenses. Following additional sectioning and staining, most sections contained intact, round lenses, suggesting that the missing lenses were likely related to sectioning or processing rather than fixation. The retina and other major ocular structures were identifiable in both the honey-fixed and alcoholic honey-fixed groups. Slight corneal thickening and localized distortion or partial collapse of the cornea and retina were observed in some sections; however, these structures remained distinguishable. Approximately five slides displayed lighter, pastel-like staining, which may have been influenced by differences in microscope imaging rather than the fixation method. Four honey-fixed and four alcoholic honey-fixed specimens demonstrated excellent preservation of ocular morphology and clear visualization of the major anatomical structures.

Conclusion: Preliminary findings indicate that both honey and alcoholic honey are capable of preserving wild-type mouse eye tissue with good overall morphology following paraffin processing. Although minor artifacts were observed in some sections, the tissue architecture remained identifiable, and several specimens demonstrated excellent preservation. Further analysis and comparison with Hartmann's fixative will determine the overall suitability of honey-based fixatives for ophthalmology research.

Effects of Microplastic Exposure on Immune Evasion in Mouse Breast Cancer and Mammary Epithelial Cells

Scholar: Veda Krishna

High School: Mount Lebanon High School, Pittsburgh, Pennsylvania

Mentor: Adam C. Soloff, PhD

Background: Microplastics are small plastic particles (<5 mm) that are increasingly prevalent throughout the environment, resulting in frequent human exposure through inhalation and ingestion. Research has raised concerns regarding potential effects on cellular and immune function. However, their effects on macrophages' ability to respond to cancer cells remain unclear. This study examines whether microplastic exposure alters macrophage's ability to detect and destroy mouse breast cancer cells compared with normal mouse mammary epithelial cells.

Methods: EO771 mouse breast cancer cells and C57MG mouse mammary epithelial cells were plated separately with 75,000 cells per well and exposed to 1µm or 4µm microplastics. Macrophages were added on day 2, with control groups included for comparison. An LDH (lactate dehydrogenase) assay was performed to measure cell death by measuring LDH released from damaged cells, and percent cytotoxicity was calculated for each condition.

Results: EO771 cells exhibited 12.37% cytotoxicity with macrophages alone, compared with 10.97% and 12.02% following the exposure to 1µm and 4µm microplastics, respectively. C57MG cells exhibited 19.59% cytotoxicity with macrophages alone, compared with 20.09% and 20.04% following the exposure to 1µm and 4µm microplastic exposure, respectively. Overall, cytotoxicity remained relatively consistent across the different microplastic exposure conditions for both the cells' lines.

Conclusions: Microplastic exposure did not produce substantial changes in cytotoxicity in either of the cell lines under the conditions tested. These findings suggest that the 1µm and 4µm microplastic exposure did not alter macrophage associated cell death significantly in this experiment. Further research will investigate additional microplastic sizes, concentrations, and exposure times to further evaluate the effect they have on macrophage function.

Diet and Immunity: The Effect of Ultra Processed Food on Host Immune Connectivity to ICI outcomes

Scholar: Melanie Lam

High School: North Hills Senior High School

Lab: Diwakar Davar, MD

Mentor: Drew Hurd, BS

Site: Cancer Biology

Immune checkpoint inhibitors (ICIs) produce durable responses in a subset of patients with solid tumors, but most patients ultimately experience disease progression. Diet has been implicated as a driver of microbiome composition, and in turn, ICI outcomes in advanced melanoma patients. Herein, we sought to evaluate whether ultra processed food (UPF) intake impacted ICI outcomes, and how this affected circulating proteome.

UPF scores were assigned using output from the DHQIII 30-day recall questionnaire of food items following NOVA system criteria. The score for each patient (n=153) was calculated as the total percentage of UPF consumption compared to total diet. Measures of abdominal visceral adiposity were quantified using CT scans. ELISA quantification of Zonulin, sCD14, and FABP2 (n = 42) evaluated host function related to diet.

Patients with increased UPF consumption showed decreased progression free survival (log rank p = 0.05). Linear modelling with host physiology demonstrates that a high UPF diet and increased abdomen fat accumulation lead to increased Zonulin (coef = 0.55, p = 0.05) with a decrease in sCD14 (coef = -0.4, p = 0.02) and FABP2 (coef = -.085, p = 0.03). Following correction for confounders, such as visceral adiposity, increased UPF intake persistently associated with inferior survival. Metagenomic composition varied between UPF status; increased intake correlated with greater between (Shannon $P = 0.019$) and within sample (PERMANOVA $P = 0.0397$) diversity.

Prior studies yielded mixed results for defining an ideal diet and underlying host mechanisms driving response. Our study explores the role of the circulating proteome in ICI outcomes mediated by a high UPF diet. Our findings, associating high UPF intake with poor ICI therapy prognosis, suggest a link to intestinal permeability biomarkers. Further research seeks to define the relationship between diet and host physiology, questioning the influence of high UPF intake and measures of physical activity.

Title: Establishment of Two Patient-Derived PFIC iPSC Lines and a Healthy Control for Disease Modelling

Scholar: Sebastian Lamana

High School: Winchester Thurston, Pittsburgh, Pennsylvania

Mentor: Lanuza Faccioli

Site: Pathobiology

Human induced pluripotent stem cells (iPSCs) are generated by reprogramming adult somatic cells into an undifferentiated, pluripotent state through the expression of defined reprogramming factors. These cells have the ability to self-renew and differentiate into a wide range of somatic cell types, including hepatocyte-like cells (iHEPs), which exhibit morphological and functional characteristics similar to primary human hepatocytes (PHHs). iPSCs provide promising opportunities to study complex liver disorders such as Progressive Familial Intrahepatic Cholestasis Type 1 (PFIC1), a genetic disorder caused by mutations in the *ATP8B1* gene that leads to liver disease. The aim of this study was to generate and characterize three iPSC lines derived from two PFIC1 patients and one healthy control.

Fibroblasts obtained from PFIC1 patients and a healthy control were reprogrammed into induced pluripotent stem cells using a Sendai vector. Genotyping was performed to confirm the presence of *ATP8B1* mutation in the PFIC1-derived iPSC lines and their absence in the healthy control. Quantitative PCR (qPCR) was used to check the expression of pluripotency genes, including NANOG, OCT3/4, LIN28, and SOX2. qPCR was also performed to evaluate the presence of the Sendai virus using the targets SEV-KOS, SEV-c-MYC, SEV-KLF4, and SEV. Immunofluorescence staining was used to identify the presence of pluripotency markers like OCT3/4, NANOG, and SSEA4.

Genotyping confirmed the presence of *ATP8B1* mutation in both PFIC1-derived iPSC lines, while no mutation was detected in the healthy control line. Pluripotency was confirmed by qPCR analysis demonstrating the expression of OCT3/4, SOX2, NANOG, and LIN28, as well as by immunofluorescence staining for OCT3/4, NANOG, and SSEA4. More than 90% of cells were positive for each pluripotency marker, indicating successful reprogramming.

Patient-derived PFIC1 iPSC lines were successfully generated and characterized. These iPSC lines provide a robust in vitro model for investigating PFIC1 disease mechanisms and evaluating potential therapeutic targets.

Isoform-specific expression of WT1 drives malignant progression of High-grade serous carcinoma

Scholar: Angelina Li

High School/College/City/State: North Allegheny Senior High School, Pittsburgh, PA

PI of group/lab: Dr. Lan G. Coffman, MD, PhD

Mentor(s): Leonard Frisbie, Dr. Lan G. Coffman

Site: WCRC

Ovarian cancer (OC) is the deadliest gynecological malignancy, accounting for the deaths of over 12,000 women each year in the US alone. High-grade serous ovarian cancer (HGSOC) accounts for the overwhelming majority of ovarian malignancies and is characterized by early diffuse metastasis, rapid development of therapeutic resistance and near ubiquitous rates of recurrence. The transcription factor Wilms Tumor 1 (WT1) is a biomarker of HGSOC, and its expression is correlated with disease progression. However, due to the complex and often contradictory function of WT1, either promoting or suppressing tumorigenesis, much of the biology of WT1 in HGSOC remains poorly understood. WT1 has four main isoforms (A, B, C, D), and in this study we aim to understand how the expression of these isoforms play a role in influencing the overall function of WT1 as a key contributor to OC progression.

Using an isoform-specific RT-qPCR assay, we measure the baseline proportions of the four main WT1 isoforms in HGSOC cell lines, primary patient-derived tumor cells and associated stroma. We further test the impact of these isoforms on driving tumor cell proliferation, chemoresistance and metastatic potential in vitro using HGSOC lines overexpressing specific WT1 isoforms. Together, we demonstrate that the HGSOC promoting function of WT1 is isoform dependent.

Optimizing digestion conditions for retinal explant dissection for drug screen using *Rho*$^{P23H/+}$ mouse model of retinitis pigmentosa

Scholar: Noa Litwin

High School/City/State: Shady Side Academy, Pittsburgh, PA

PI of lab: Yuanyuan Chen, PhD

Mentors: Saira Rizwan, PhD; Yuanyuan Chen, PhD

Site: Biology and Translational Medicine in Vision (VISION)

Background: Retinitis pigmentosa (RP), a currently untreatable group of genetic eye diseases, affects about 1.5 million people worldwide. 10-12% of Americans with RP struggle due to a P23H mutation on the *RHODOPSIN* gene. In these patients, rhodopsin misfolding overwhelms proteostasis. As rod death is accompanied by inner retinal remodeling and retinal inflammation, the retinal degeneration in RP is more complicated than rhodopsin misfolding. We developed a drug screen assay using explants from a *Rho*-P23H mouse model to find a drug treatment that stops retinal degeneration. Retinal pigmented epithelium (RPE) cells are essential for rod photoreceptor preservation, thus this study aims to find an optimized protocol for isolating retina explants together with RPE.

Methods: To determine whether papain or proteinase K results in higher RPE yield on mouse retinas, we collected genotyped P15 *Rho*$^{P23H/+}$ mice eyes. Eyes were treated with either papain or proteinase K in AMES media and incubated for 15-22 minutes at 37℃. Under the microscope, we cut along the limbus, removed the anterior part of the eye, cut the optic nerve, sliced the eye cup fourfold, and peeled the sclera off the retina and RPE. We flattened the retina in a transwell using a brush and incubated it in a well holding 600 μL of neurobasal media. We quantitatively evaluated the effect on RPE yield by Optical Coherence Tomography imaging.

Results: We were able to dissect 50% of both eyes digested in papain and proteinase K. Of the viable retinas, those digested in papain had greater RPE yield than those digested in proteinase K.

Conclusion: Our study shows that papain is the optimal solution for preserving retinas with higher RPE yield. However, future optimization of proteinase K amount may lead to different results. Small sample size and lack of technical mastery render these results inconclusive.

Transient Regulators of B-Cell Fate Revealed by FIREFate

Melody Ann Marsh[1,2], Akansha Sachan,
[1]Derry Area Highschool, Derry, PA; [2]University of Pittsburgh Hillman Cancer Center Academy

Abstract
This project uses biological input from epigenomic and transcriptomic data to conceptually advance proteomic interpretation through machine learning and stochastic modeling. Researchers can trace the biological meaning behind the model's outputs through chromatin accessibility and gene expression parameters, across transitions from naive B-cells to memory and antibody secreting B-cells. After testing B-cell fates, the Jishnu Das Lab plans to apply their framework to other immune and aging organ systems next.

Introduction
FIREFate, an AI model that uses machine learning to produce high-resolution Gene Regulation Networks (GRN) to uncover the dynamic regulatory programs and biomarkers driving cell fate decisions, was created by my mentor Akanksha Sachan, Jishnu Das, and key contributors Zarifeh Heidari and Swapnil Keshari. In this research, FIREFate was applied to B-cell differentiation to identify transcription factor episodes that determine plasmablast and germinal center fate in activated B-cells. FIREFate models regulation of continuous cell state transitions (for eg: B-cell differentiation system) to reveal how regulatory proteins (Transcription Factors: TFs) alter gene expression, driving antibody production. It identifies transcription factor patterns that act as regulatory biomarkers to signal when a B-cell state transitions. Using single-cell RNA sequencing and chromatin accessibility, FIREFate combines them within a multi-omics gene regulatory network inference framework to predict "when" a TF becomes most active and governs a state transition.

Methods
B-Cell activation and differentiation provided the foundational biological data for FIREFate. They were used as matrix inputs, which captured the genes expressed within each cell using single-cell RNA sequencing, and chromatin accessibility profiles that measured how tightly DNA is wrapped around histones. These chromatin peaks revealed whether transcription factors can bind, therefore determining which genes are active or silenced.

FIREFate used that biological data and developed a stochastic modeling technique, which identified regulatory episodes of "when" a transcription factor was consistently active within a particular cell state (State Specific), or if one was most active during a particular time during that B-cells differentiation (Episodically). Additionally, FIREFate understands epigenetic logic by predicting how much chromatin is accessible from a DNA sequence by identifying transcription factor binding sites when chromatin is opened or closed. Accordingly, we then used FIREFate to build and identify gene regulatory sub-components, which we used to predict cell-fate predisposition.

Results
Our FIREFate results showed that its multi-omic modeling successfully captured dynamic transcription factor activity during B-cell differentiation. The framework identified distinct episodes where transcription factor activation corresponded to transitions between naive, memory, and antibody-secreting B-cell states.

Discussion
These findings revealed how chromatin accessibility and RNA expression can be used jointly in contribution to immune-cell fate, offering a map of B-cell maturation and diagrams that show which transcription factors were enriched over pseudotime state specifically or episodically, and when those transcription factors were enriched during that cell's time frame. The lab plans to expand the FIREFate prediction framework to other immune (T Cell Exhaustion) and aging organ (Skeletal Muscle) systems, potentially advancing our understanding of human biology.

This information can be applied to enhance our immunotherapies and medicine by enabling early disease detection and adaptive treatment strategies.

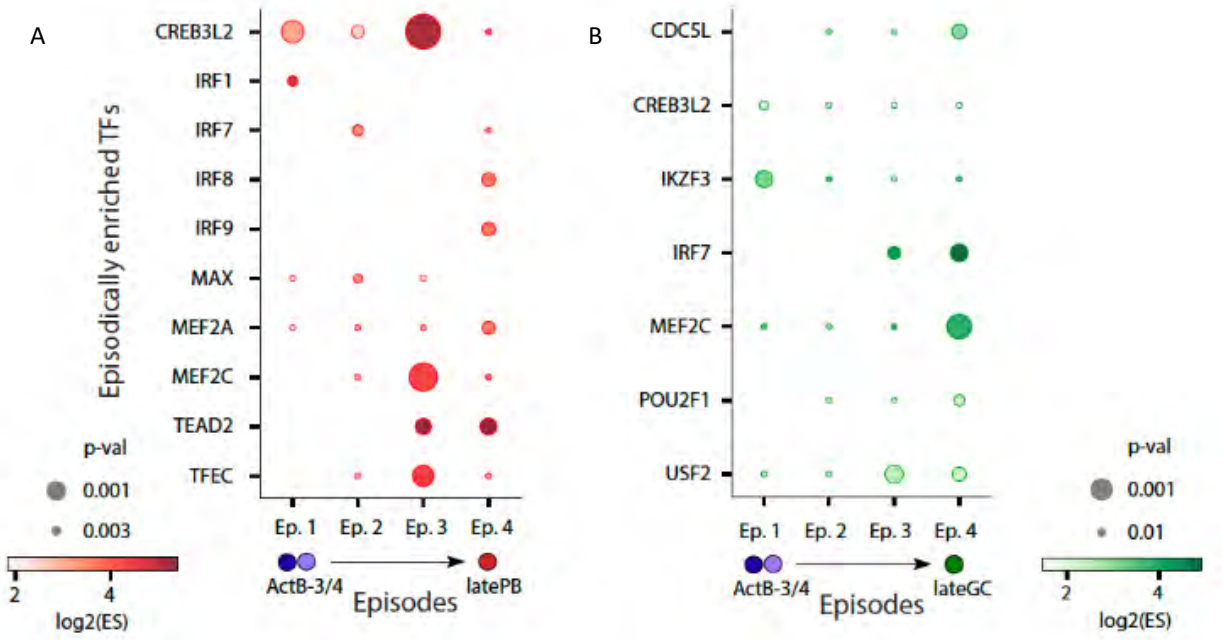

Figure 1. Temporal Shifts in Transcription Factor Enrichment (A) Episodically enriched transcription factors (TFs) identified across four stages of B-cell differentiation (Ep. 1-4). Each circle represents a p-value (p-val), with a larger p-value indicating stronger enrichment. The circle's color intensity corresponds to log2(ES), where darker shades denote higher enrichment. Transcription enrichment in plasmablast (PB) can weaken or strengthen over time. CREB3L2 showed the greatest enrichment, highlighting its potential regulatory role in plasmablast (LatePB) transition from ActB-3/4. (B) Episodically enriched transcription factors (TFs) identified across four stages of B-cell toward the late germinal center (LateGC) state. Each circle represents a p-value (p-val), with a larger p-value indicating stronger enrichment. The circle's color intensity corresponds to log2(ES), where darker shades denote higher enrichment. Many transcription factors associated with late germinal center (Late GC) cells do not appear in Episode 1, suggesting that their enrichment emerges later in development.

References

1. Pease, Nicholas A., et al. Cell cycle-coupled transcriptional network orchestrates human b cell fate bifurcation. bioRxiv, 23 Apr. 2025, doi:10.1101/2025.04.23.649973.

Altered Synaptic Connectivity in SOD1 Mice Spinal Cord Marked by Viral Tracing

Scholar: Gianna Mazer

High School/College/City/State: Shaler Area Highschool, Pittsburgh, PA

PI of group/lab: Christi Kolarcik, PhD

Mentor(s): Stefanie Taiclet, BS, Madeline Wolf

Site: Pathobiology

Background: Amyotrophic Lateral Sclerosis (ALS) is a fatal neurodegenerative disease that attacks motor neurons in the brain and spinal cord, which are responsible for voluntary movements such as walking, breathing, and speaking. As motor neurons degenerate, the pathways between the brain and the muscles are disrupted, resulting in muscle atrophy and paralysis. Over 40 genes have been linked to ALS, including the commonly mutated SOD1 gene. Therefore, SOD1 mice are widely used to study ALS progression and motor neuron degeneration. In our lab, we use SOD1 mice to investigate how ALS alters motor neurons and their connectivity throughout the spinal cord and primary motor cortex.

Methods: For this project, we injected rabies virus into the tibialis anterior hindlimb muscle of SOD1 mice and age-matched controls to act as a viral tracer. The mice were sacrificed 75 hours after injection, and their spinal cords were extracted. The lumbar region of the spinal cord was excised, embedded in paraffin, sectioned serially (1:6) at 10 μm using a microtome, and stained by immunohistochemistry (IHC) to identify rabies-positive motor neurons. DAB-stained motor neurons were then counted using predetermined criteria under 40× magnification on a light microscope.

Results: We found that SOD1 mice had fewer rabies-positive motor neurons than age-matched controls. These results support our hypothesis that synaptic connectivity from the tibialis anterior to the lumbar spinal cord is disrupted before the mice begin to show symptoms.

Conclusion: Data collection is ongoing, but current trends indicate that SOD1 mice have fewer connected motor neurons, supporting the theory that synaptic connectivity degenerates before ALS symptoms arise. These findings support future studies aimed at identifying the phenotypes and functional roles of affected neurons to better understand the mechanisms underlying motor system dysfunction and degeneration in ALS and other forms of spinal muscular atrophy.

Using X-ray Crystallography to Study Mutations in the STI1 Domain of Ubiquilins

Scholar: Ariella Mensah-Agyekum

High School/College/City/State: Westinghouse Academy, Pittsburgh, PA

PI of group/lab: Matthew Wohlever

Mentor(s): Angela Kayll, Matthew Wohlever

Site: CoSBBI

Proteins rely on their structure to function properly. When proteins are unable to fold correctly or be disposed of efficiently, they form aggregates, and diseases like cancer and ALS develop. Ubiquilins (UBQLN 1, 2, and 4) are protein coding genes, and their primary role is to regulate proteostasis. The STI1 domain is a region within Ubiquilins, but our knowledge of this area is limited. Determining the structure of the human STI1 domain will give insight on how it contributes to proteostasis and how disease-related mutations disturb its function.

Our research focuses on the structure of the STI1 domain of ubiquilins and how it contributes to amyotrophic lateral sclerosis (ALS). In this process, different Ubiquilin STI1 protein constructs are expressed, purified, crystallized, and will then go through the X-ray crystallography process. We have successfully purified 12 protein constructs and produced a number of crystallization trays. Among these trays, we've had several crystal hits that will be sent to the beamline for diffraction data and structure analysis. The information that we get from identifying the structural changes caused by mutations could give us insight on how disruption in Ubiquilin function may contribute to ALS and help us better understand ubiquilin mechanics.

Transcriptomic Profiling and Machine Learning Delineate Mechanistic Pathways and Predict Drug Response in Hepatocellular Carcinoma

Lucia Nanda[1] and Lujia Chen[2], PhD.
[1]Billerica Memorial High School, Billerica MA; [2]University of Pittsburgh, Pittsburgh PA

Abstract

This project aimed to isolate biomarkers associated with response to anti-PD-1 immunotherapy, VEGFR monotherapy, and combination therapy in hepatocellular carcinoma and apply results to machine learning based personalized drug response predictions. It analyzed bulk RNA-seq data and identified 50+ statistically significant differentially expressed genes and modules, then mapped them to biological function using pathway enrichment analysis and literature validation. In addition, an ensemble machine learning model was successfully trained to predict combination therapy drug response.

Introduction

Hepatocellular carcinoma (HCC) is a malignant primary tumor of the hepatocytes, which most commonly develops in patients with chronic liver disease or cirrhosis. Anti-PD-1 immunotherapy and VEGFR treatments are two common monotherapies used to treat HCC. Combination therapies combining both anti-PD-1 and VEGFR mechanisms boast higher objective responses compared to each monotherapy[1]. In addition, recent research reveals that patient response to these therapies is heavily influenced by specific biological and clinical indicators[2]. This project aims to identify transcriptomic biomarkers associated with response anti-PD-1 and VEGFR therapies responses in HCC, then apply these findings to personalized drug response predictions using machine learning.

Methods

First, bulk RNA-seq data from the IMbrave150 clinical trial was processed using Gene Set Variation Analysis (GSVA) to identify discriminative gene-level and module features associated with responders and non-responders in each of the three treatment groups. We then performed pathway enrichment analysis using GSVA and used functional annotation tools to identify significant Hallmark and KEGG pathways. Then, we identified the shared and unique features across treatments and cross-referenced identified key features with established literature review data. Finally, an ensemble of Glmnet, support vector machine, and feature-augmented random forest models were trained using 5-fold stratified cross-validation to predict patient-specific combination therapy response.

Results

Based on the RNA-seq data analysis, response to anti-PD-1 monotherapy (Atezolizumab) is characterized by a mix of cell-cycle progression, specific metabolic alterations, and a high proliferation profile (Figure 1). Responders show significant over-expression of SHCBP1 and BRIP1, but a steep under-expression of COG3 and USHBP1. VEGFR monotherapy (Sorafenib) responders were associated with B-cell/humoral immunity enrichment profiles. The top upregulated genes are overwhelmingly B-cell/antibody components, with epithelial-to-mesenchymal transition (EMT) being strongly associated with resistance. For combination therapy (Atezolizumab + Bevacizumab), responders presented immune-driven profiles with highly statistically significant upregulation of T-cell and B-cell related activation markers. Upregulation of TIMD4 ($p = 3.08 \times 10^{-8}$), ICOS ($p = 1.35 \times 10^{-7}$), and B-cell specific lineages like PAX5 and CD19 strongly correlate with response. The ensemble model achieved 0.72 AUC-ROC, 0.68 accuracy, and 0.58 F1 score, with the majority of prioritized features being immune-related.

Discussion

This study demonstrated that responses to each of the three treatments are characterized by unique tumor immunomicroenvironmental profiles and that advanced classifier models have the potential to accurately predict drug response in HCC. However, none of the significant genes for VEGFR therapy pass the Benjamini-Hochberg (BH) false discovery rate correction (all BH adjusted p-values are ≥ 0.149), meaning they carry a high risk of being false positives. Also, while the optimized ensemble approach demonstrates a meaningful performance increase over majority-class baselines, the cross-validated ROC-AUC ceiling of 0.716 suggests that predicting combination immunotherapy response from baseline bulk transcriptomics is inherently constrained by the data. Other limitations of this study include low sample size and potential sampling bias.. Future directions include validating findings across other HCC data cohorts, analyzing scRNA data, fine-tuning the machine learning model on more data, and exploring alternative training methods.

a)

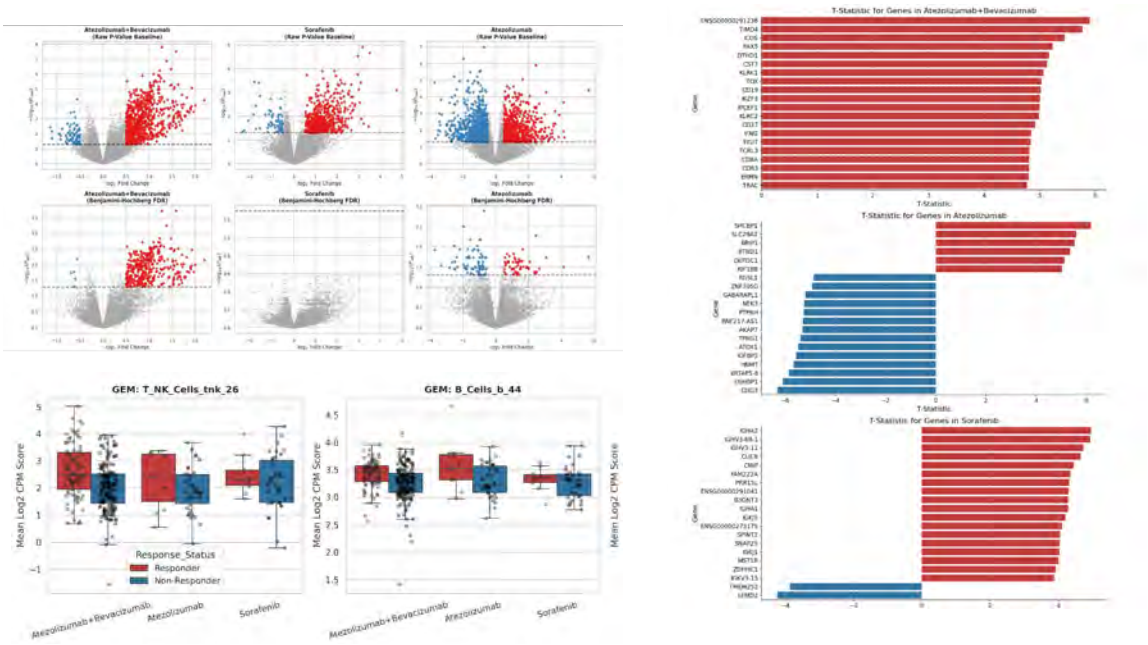

b)

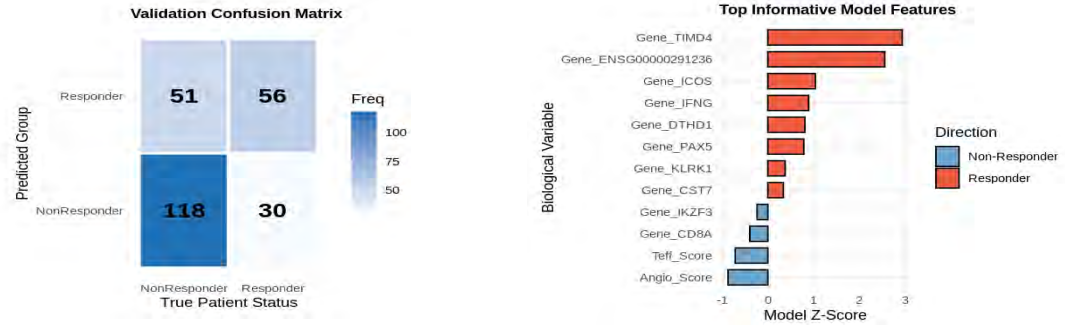

Figure 1. Significant features across responders and non-responders in the anti-PD-1, VEGFR, and combination therapy treatment arms alongside machine learning metrics. (a) Differentially expressed genes and modules (b) Ensemble model confusion matrix and prioritized features

References

1. Shigeta K, Datta M, Hato T, et al. Dual Programmed Death Receptor-1 and Vascular Endothelial Growth Factor Receptor-2 Blockade Promotes Vascular Normalization and Enhances Antitumor Immune Responses in Hepatocellular Carcinoma. *Hepatology*. 2020;71(4):1247-1261. doi:10.1002/hep.30889
2. Zhu AX, Abbas AR, de Galarreta MR, et al. Molecular correlates of clinical response and resistance to atezolizumab in combination with bevacizumab in advanced hepatocellular carcinoma. *Nat Med*. 2022;28(8):1599-1611. doi:10.1038/s41591-022-01868-2

Longitudinal Characterization of Astrocyte Calcium Activity During 10 Hz Stimulation in the Mouse Visual Cortex

Scholar: Preston Oakes

High School: Peters Township High School, McMurray, PA

PI of group/lab: Takashi D.Y. Kozai, PHD, B.I.O.N.I.C. Lab

Mentor: Anna Korol

Site: Tech Drive X

Background: Implanted neural electrodes can record and stimulate brain activity; however, implantation disrupts blood vessels, damages nearby neurons, and activates microglia and astrocytes. Astrocytes maintain the neural environment by regulating ions, metabolism, neurotransmitters, and blood flow, but their structure and function may change after injury. Studies show that astrocyte calcium activity also changes following injury. Because calcium-dependent fluorescence indirectly measures activation, we hypothesize that 10 Hz stimulation increases astrocyte calcium activity and that responses are reduced during acute injury but increase with chronic stimulation over time.

Methods: Tamoxifen-induced ALDH1L1-CreERT2 × Salsa6f mice were used to label astrocyte morphology and calcium activity. An electrode was implanted approximately 300 μm deep in layer 2/3 of the visual cortex. Two-photon microscopy collected separate 120-second 10 Hz and no-stimulation recordings throughout an 84-day study; this analysis focuses on the first 21 days. The 10 Hz recordings included 30 seconds before, 30 seconds during, and 60 seconds after stimulation; controls received no stimulation. Whole-astrocyte regions of interest were manually identified, and fluorescence was normalized as $\Delta F/F_0$ using the pre-stimulation period as F_0.

Expected Results: We expect maximum astrocyte calcium activity during 10 Hz stimulation to be significantly greater than no-stimulation controls across days. Responses should decrease from day 0 to day 3 because of acute post-implantation inflammation, then increase above day 0 by day 14 as acute inflammation resolves. Whole-astrocyte averaging should reveal overall cellular changes but may obscure distinct signaling within somas and branches.

Conclusion: These expected findings would suggest that chronic implantation alters astrocytes' functional responses to electrical stimulation. Whole-astrocyte analysis provides an initial overview of changes at the tissue–electrode interface. Future work will examine compartment-specific responses to determine how signaling within somas and branches contributes to changes in astrocyte calcium activity and the long-term performance of implanted neural devices.

Title: Metformin permeation test

Scholar: Enrique Ochoa

High School: Thomas Jefferson High School, Jefferson Hills, PA

PI of group/lab: Dr. James H-C Wang

Mentor(s): Dr. Jianying Zhang and Dr. Vasyl Pastukh

Site: Cancer Biology

Metformin is a drug commonly used to treat Type II diabetes. The development of a topical treatment option is being investigated to provide a more accessible and easier-to-use application of the drug. It is important in drug testing to find the permeation of different tissues to ensure that the drug is not toxic and can reach the target muscle, tendon, and skin tissues intended.

The goal of the HPLC experiment was to determine the concentration of Metformin that would result in a toxic reaction. We already knew that 10% Metformin lotion (ML) would result in a toxic reaction. Therefore, utilizing HPLC, we attempted to determine the concentration of Metformin that permeated the tissue samples. We expected a higher concentration in 10% ML as compared to 6% ML and expected Back Skin and Leg Skin to have relatively high concentrations of Metformin as compared to Achilles Tendon and Calf Muscle.

We examined both mice treated for 14 days (2 weeks) and for 28 days (4 weeks). The treatment groups included 10% ML, 6% ML, a Vehicle Control, and Cage Control. Achilles Tendon, Calf Muscle, Back Skin, Leg Skin, and Serum were collected. Tissue samples were collected, homogenized, and precipitated. Then we isolated Metformin, redissolved it in Mobile Phase, and processed a fixed amount through HPLC.

The 10% ML did not have a statistically significant difference in many cases when compared to the 6% ML treatment, and Leg Skin consistently had a higher concentration than the other tissue types. The Achilles Tendon had the lowest concentration. We ran ANOVA testing, and there was no significant difference in the 2-week samples; however, in the 4-week samples there was a statistically significant difference when 10% and 6% were compared to both Vehicle and Cage Controls through a one-way ANOVA and **Tukey's** HSD. In some samples of Cage and Vehicle Controls, there seemed to be Metformin contamination. Some samples indicated insignificant Metformin content, while others strangely exhibited higher levels of Metformin, which we attributed to cage contamination pre-sacrifice.

We observed a toxic reaction in male rats when they were exposed to 10% ML. Therefore, we were attempting to quantify the amount of Metformin that permeated. The next steps are attempting to find the amount of Metformin that correlates with a non-toxic reaction but also delivers Metformin as expected.

Title: Hormones and Air Pollution Effect on Raw Macrophages Cells.

Scholar: Lacqueeta Oduogo

High School/College/City/State: Mount Lebanon High School Pittsburgh, PA

PI of group/lab: Sollof Adam

Mentor(s): Sollof Adam, Noureen Naila, Udoh Hannah Mfonobong, Cheema Mohsin,

Site: ICI

Background: Fine particulate matter ($PM_{2.5}$) can bypass the upper respiratory tract's protective mechanisms. This includes the vibrissae and mucociliary clearance, and deep within the alveoli, where PM2.5 induces local inflammation. Studies have demonstrated a positive correlation between long-term $PM_{2.5}$ exposure and lung cancer risk in both men and women. Notably, among never-smokers, women appear to have a higher risk of developing lung cancer associated with air pollution exposure than men.

Methods: Murine RAW 264.7 macrophages were exposed to low, medium, and high concentrations of estrogen or testosterone while maintained at a constant concentration of diesel exhaust particles (DEP). Phagocytosis was evaluated using Texas Red–labeled Escherichia coli bioparticles and Zymosan Green fluorescent yeast particles.

Results: Exposure to diesel exhaust particles (DEP) reduced the phagocytic activity of RAW 264.7 macrophages. The addition of estrogen or testosterone further decreased phagocytic activity compared with DEP exposure alone. Treatment with AICAR, a mitochondrial activator, partially restored phagocytic function in macrophages exposed to DEP and sex hormones; however, phagocytic activity remained significantly lower than that of cells cultured under control conditions.

Conclusion: These findings demonstrate that exposure to diesel exhaust particles (DEP), in combination with estrogen or testosterone, impairs the phagocytic activity of RAW 264.7 macrophages. AICAR treatment partially restored phagocytic function but not fully reversed macrophage dysfunction. Further research is needed to understand how DEP and sex hormones impair macrophage function and whether enhancing mitochondrial activity can improve the immune response.

Lactobacillus reuteri Releasing Interleukin-22 Mitigates Radiation-Induced Intestinal Injury

Scholar: Sophie O'Toole

High School: Keystone Oaks High School, Pittsburgh, PA

Lab: Dr. Greenberger

Mentor: Dr. Mukherjee and Renee Fisher

Site: Cancer Biology

Acute intestinal injury, if left untreated, can severely compromise the body's ability to digest food, absorb nutrients and water, and eliminate waste. *Lactobacillus reuteri* engineered to release Interleukin-22 (LR-IL-22) is a second-generation probiotic radiomitigator designed to reduce damage to healthy intestinal tissue following radiation exposure. Interest in LR-IL-22 as a protective therapy stems from IL-22's established role in maintaining barrier integrity at surfaces such as the intestinal epithelium.

To test whether LR-IL-22 mitigates radiation-induced intestinal injury, we used a partial-body irradiation mouse model and assessed gene expression via RNA isolation, cDNA synthesis, and quantitative PCR (qPCR). qPCR was used to validate RNA-sequencing results by quantifying the presence and relative abundance of target transcripts; amplification data were used to generate bar graphs comparing control and treatment groups.

These analyses revealed modest but directionally consistent trends toward restoration of intestinal gene expression after radiation injury. Key markers of intestinal stem cell identity (Lgr5) and of crypt stem cell renewal, such as (Wnt3) were suppressed following partial-body irradiation and trended toward recovery in animals treated with LR-IL-22. Interestingly, this AhR dependence was not absolute: AhR-deficient mice showed some histological protection with LR-IL-22 despite the absence of a corresponding rescue in gene expression or survival. Histological examination of the small intestine showed that partial-body irradiation disrupted normal villus and crypt architecture in both male and female mice, while LR-IL-22 treatment better preserved villus height and epithelial organization, more closely resembling unirradiated controls. Together, these findings suggest LR-IL-22 promotes recovery of intestinal stem cell function and preserves epithelial integrity. Histological restoration thus links the gene expression changes to functional recovery.

Further preclinical and mechanistic studies are warranted to optimize LR-IL-22 efficacy and support its translational development as a scalable countermeasure for radiation-induced gastrointestinal injury.

Repurposing Clinically Approved EGFR Inhibitors as a Delayed Therapeutic Strategy for Acetaminophen-Induced Liver Injury

Scholar: Rhea Patel

High School: The Hill School, Pottstown, Pennsylvania

Lab: Bharat Bhushan, MS, PhD, DABT

Mentor(s): Siddih Jain, Gillian Williams

Site: Pathobiology

Background: Acetaminophen (APAP) overdose is one of the leading causes of acute liver failure worldwide. Although N-acetylcysteine (NAC) is the current standard treatment, it is most effective when administered before extensive APAP metabolism has occurred, leaving limited treatment options for patients who present later. Previous work from our laboratory demonstrated that hepatocyte-specific deletion of epidermal growth factor receptor (EGFR) reduced APAP-induced liver injury (AILI), suggesting that EGFR contributes to injury progression despite its established role in liver regeneration. Therefore, this study investigated whether clinically approved EGFR inhibitors could reduce liver injury after APAP metabolism had already occurred and whether their protective effects were independent of early glutathione (GSH) depletion.

Methods: Male C57BL/6J mice received a hepatotoxic dose of APAP followed by delayed administration of clinically approved EGFR inhibitors. Total hepatic and mitochondrial GSH levels were measured to determine whether EGFR inhibition altered early APAP metabolism. Additional experiments evaluated the therapeutic efficacy of delayed EGFR inhibitor administration at four and eight hours following APAP overdose. Liver injury was assessed using serum alanine aminotransferase (ALT) activity and histological quantification of hepatic necrosis.

Results: EGFR inhibitor treatment did not alter early depletion of either total hepatic or mitochondrial GSH following APAP administration, indicating that EGFR inhibition does not affect the initial metabolic phase of APAP toxicity. When administered four hours after APAP overdose, osimertinib significantly reduced hepatic necrosis compared with vehicle-treated mice, while serum ALT demonstrated a nonsignificant downward trend. In contrast, treatment initiated eight hours after APAP administration did not produce a statistically significant reduction in ALT, although osimertinib-treated mice demonstrated a partial reduction in liver injury compared with vehicle-treated controls.

Conclusion: These findings suggest that EGFR inhibition reduces APAP-induced liver injury without altering early GSH depletion, supporting a protective effect that occurs after the initial metabolic phase of toxicity. Furthermore, delayed administration of EGFR inhibitors remained effective when given four hours after APAP overdose, although this protective effect appeared to diminish with later treatment. Ongoing studies will further evaluate liver regeneration and define the molecular mechanisms responsible for EGFR-mediated protection.

The Role of Galectin-3 in Sex Differences in Macrophages and Stroke Outcomes

Scholar: Eric Peng

High School/College/City/State: North Allegheny Senior High School, Wexford, PA

PI of group/lab: Xiaoming Hu

Mentor(s): Jiajing Shan, Zhentai Huang

Site: ICI

Stroke is a major global health issue. It is known that young females have less severe brain injury after stroke than young males. Elucidating the mechanism behind this neuroprotection in females may reveal possible targets for therapeutic treatment. Our previous single cell RNA sequencing analyses revealed prominent sex difference in infiltrating macrophages early after stroke, and galectin-3 expression in macrophages is higher in male than that in female. The contribution of Galectin-3 to sex differences in macrophage function, especially under stroke condition is unknown. Here, we compared the phagocytic function of male and female macrophages collected from wild type (WT) and galectin-3 knockout (KO) mice using immunofluorescent staining. Female macrophages exhibited higher phagocytosis upon exposure to FITC-labeled beads or pHrodored-labeled dead neurons. Galectin-3 KO reduced phagocytic capacity of macrophages in both male and female. To further confirm our findings, we performed flow cytometry after phagocytosis. Again, female cultures had consistently higher percentages of CD11b+/FITC-A+ cells, indicating higher levels of macrophage phagocytosis. WT macrophages also outperformed galectin-3 KO ones, regardless of sex. We then treat the four groups of macrophages with damage associated molecular patterns collected from stroke brains. Male WT mice showed higher relative expression of the pro-inflammatory cytokines IL-6 and TNF-a and lower expression of the anti-inflammatory cytokine IL-10 compared to female WTs. Furthermore, galectin-3 KO led to increased expression of IL-6 and TNF-a in both genders, as well as marginally decreased expression of IL-10. Collectively, this data shows that galectin-3 and sex differences in phagocytosis appear to both independently affect phagocytosis with sex differences persisting at similar levels even after galectin-3 KO. Additionally, galectin-3 appears to act as an anti-inflammatory agent, with the knockout group showing higher levels of expression for pro-inflammatory cytokines. Future research may aim to deduce the main factor behind the observed sexual differences.

Understanding Squamous Cell Carcinoma Incidence and Mortality

Scholar: Asher Peng
High School: Fox Chapel Area High School, Pittsburgh Pennsylvania
Mentor: Robert A. Tessler, MD, FASCRS
Site: Surgery

Background: Human Papillomavirus (HPV) is a viral infection that can lead to squamous cell carcinoma (SCC) at various sites of the human body, including the anus, oropharynx, cervix, vulva, and penis. However, little is known about whether the SCC primary site is associated with mortality, and whether this association varies by race and ethnicity. In this study, we aimed to determine the association of SSC site and mortality, and whether this association varies by race and ethnicity.

Methods: Publicly available incidence and mortality data for SCC of the anus, cervix, vulva, penis, and oropharynx were obtained from the Centers for Disease Control and Prevention Wide-Ranging Online Data for Epidemiologic Research (CDC WONDER). Generalized linear models were used to evaluate the association between SCC site and mortality. Stratified analyses by race and ethnicity were performed, and interaction terms were included to assess effect modification.

Results: After excluding suppressed observations, a total of 3,452 mortality and 3,764 incidence records were included in the analysis. There was a significant interaction between SCC site and race/ethnicity for both mortality and incidence (both $p < 0.001$), showing that the relationship between cancer site and outcomes differed across racial and ethnic groups. Cervical SCC had the highest average incidence and mortality rates, while penile SCC had the lowest mortality, and oropharyngeal SCC had the lowest incidence. When each racial and ethnic group was analyzed separately, the differences in mortality by SCC sites remained significant, showing that race and ethnicity affect the relationship between SCC site and mortality.

Conclusions: Mortality among HPV-associated SCC differs significantly by primary tumor site, and these associations are modified by race and ethnicity. These findings highlight disparities in the burden of HPV-associated malignancies and underscore the need for further investigation into the biological, socioeconomic, and healthcare factors contributing to these differences to inform targeted prevention, screening, and treatment strategies.

Impact of AGR2 on Immune Cold BCLM through Fibronectin

Khanh Sunny Pham

Dr. Michelle M. Williams

Angelica Phan

Background: Breast cancer (BC) is one of the most common malignant cancers in women, and 20-30% of patients with BC will develop metastases. 50% are breast cancer liver metastasis (BCLM) patients. BCLM is one of the most deadly clinical challenges, and no treatments specific to BCLM exist. We previously showed that AGR2 expression is elevated in BCLM that lacks anti-tumor immune cells. While published works have shown that AGR2 aids cell growth and migration in different types of cancer, the role of AGR2 in BCLM remains poorly understood. My studies are testing the impact of AGR2 on tumor cell proliferation and fibronectin production, a known barrier to immune cell infiltration. I ***hypothesize*** that AGR2 promotes breast cancer cell proliferation and fibronectin production to support an immune cold state.

Methods: I performed a cell growth assay with recombinant AGR2 treatment using mouse mammary carcinoma cell lines 66Cl-4 and E0771. Next, I evaluated both Ki-67 and Cleaved PARP expression by Western blot to quantify cell proliferation and cell death in 66Cl-4 cells without and with rAGR2 treatment. To test whether our AGR2 antibody can block AGR2 activity, 66Cl-4 cells were treated with rAGR2 and varying concentrations of the AGR2 antibody.

Results: In the cell growth assay, rAGR2-treated 66Cl-4 and E0771 cells had a higher growth rate. Western blot analysis showed that cells treated with rAGR2 have an increase in Ki-67 expression and decrease in Cleaved PARP expression when normalized to B-actin. Lastly, when analyzed, the Western blot showed that the antibody is not blocking antibody.

Conclusion: My results showed that AGR2 supports cell proliferation and decreases cell death using both Western blot and a cell growth assay. Overall, AGR2 should be further researched as a new target in immune cold metastatic breast cancer.

Investigating Why DNA Repair Fails: Testing the Role of Nuclear Actin in DNA Repair

Scholar: Shamael Rahamani

High School/College: The Ellis School (‘26) & Case Western Reserve University (‘30)

PI of group/lab: Partha Roy

Mentor: Masoumeh Baghaei

Site: Women’s Cancer Research Center (**WCRC**)

Introduction

Profilin-1 (**PFN1**) is well known for its role in **actin polymerization**, but recent work suggests it also contributes to the repair of DNA double-strand breaks (**DSBs**), which cells fix through two major pathways: homologous recombination (**HR**) and non-homologous end joining (**NHEJ**). The Roy lab has found, but has yet to publish, that PFN1 depletion reduces HR and NHEJ efficiency in both 4T1 mouse mammary carcinoma cells and HEK293 human kidney cells.

Hypothesis

If actin is critical for sufficient DNA repair, then the removal or mutation of actin will replicate the defects seen in PFN1 knockout cells, confirming that a change in nuclear actin is sufficient for DNA repair deformities.

Research Methods

PFN1 was knocked out in 4T1 cells using a doxycycline-inducible Cas9 system, and transiently knocked down in HEK293 cells using siRNA; depletion was confirmed by western blot in both systems. Cells were then transfected with the PDR-GFP and pLCN-DSB/I-SceI reporter constructs to measure HR and NHEJ efficiency, respectively, by flow cytometry. As a second aim, we tested whether nuclear actin dynamics underlie this effect by expressing two nuclear-targeted actin mutants alongside the reporter system: R62D-mCherry-NLS, which cannot polymerize, and S14C-YFP-NLS, which forms unusually stable filaments.

Results

These experiments did not yet reveal a clear phenocopy of the PFN1 loss phenotype, most likely due to technical limitations rather than a true absence of effect: combining the reporter, I-SceI, and actin mutant plasmids required triple transfections that lowered overall efficiency, and spectral overlap between the mCherry/YFP tags and GFP required compensation that reduced the detectable GFP-positive population from a baseline of 8 to 15% down to roughly 2%, limiting our ability to distinguish between conditions.

Conclusion

Going forward, we propose generating stable cell lines expressing PDR-GFP and pLCN-DSB reporters to reduce the transfection burden, along with optimizing the flow cytometry panel or switching to actin mutant tags with less spectral overlap with GFP.

Outcomes of Women With Brain Metastasis from Metastatic Breast Cancer (MBC-B): Considerations of the Exposome

Scholar: Deilyla Rue.

High School: East Allegheny JR/SR High, North Versailles, PA.

PI of Group: David Boone.

Mentor: Dr. Margret (Peg) Rosenzweig. Cameron Herbst.

Site: CoSBBI.

Background: Breast cancer that spreads to the brain, known as metastatic breast cancer to the brain (MBC-Brain), is one of the most serious forms of metastatic breast cancer and is associated with poor survival. While previous studies have shown that race and socioeconomic factors can influence cancer outcomes, less is known about how neighborhood conditions, including poverty, economic opportunity, and environmental exposures, affect the development and progression of brain metastases.

Objective: This study investigated whether neighborhood socioeconomic conditions and environmental exposures were associated with the timing of brain metastasis and survival outcomes among women with metastatic breast cancer.

Methods: Clinical data from 2,108 patients diagnosed with MBC at Magee-Women's Hospital between 1999 - present were analyzed. Of these patients, 561 developed brain metastasis. Patient's characteristics included age and race. Neighborhood characteristics were measured using the Area Deprivation Index (ADI), the Distressed Communities Index (DCI), and distance from each patient's home to a nearby Polycyclic Aromatic Compounds. Comparing these factors to the time from the original breast cancer diagnosis -> to brain metastasis -> overall survival after metastatic diagnosis.

Results: Among the 561 patients, the median age for MBC-Brain diagnosis was 52.5 years. 87.3% of patients were white. 10.4% were black. Younger patients developed metastatic disease sooner. Black patients, on average, lived closer to potential chemical exposure sites, had higher ADI and DCI scores, and developed metastatic disease sooner than white patients. Although living closer to a chemical site showed weak association with earlier metastatic disease, race was the factor most consistently associated with differences in outcomes.

Conclusion: Race, not distance to toxic waste site or ADI, was most consistently associated with metastatic progression. Because race, ADI, and environmental exposures were closely related, independent effects of environmental factors remain unclear. Findings should be interpreted as hypothesis-generating given modest sample sizes, particularly among Black patients.

Protection of myoblasts from oxidative or inflammatory stress with BPC-157.

Scholar: Cruz Sanders

High School: Seneca Valley High School, Harmony Township, Pennsylvania

Lab: Bridget Deasy, PhD

Mentors: Jacob Harris, Olena Abakumova, PhD, Matthew Shi

Site: Cancer Biology

Background: BPC-157, originally isolated from gastric juice, is a synthetic peptide that has shown regenerative properties across several studies. BPC-157 has shown to activate VEGFR2 and nitric oxide synthesis via the Akt-eNOS axis. These activations promote angiogenesis, fibroblast activity, and neuromuscular stabilization. While early results show that BPC-157 can promote musculoskeletal tissue healing, more research is needed to directly examine the effects on cell types such as muscle cells and chondrocytes. Thus, this study asks if BPC-157 can protect myoblasts and chondrocytes from oxidative or inflammatory stress.

Methods: Myoblasts were cultured with and without BPC-157 (.1 ug/mL) over both long-term (28 days) and short-term (7 days) periods. Next, myoblasts with and without BPC-157 were plated with and without H2O2 (20uL). Cell count is measured each day for one week to determine cell proliferation. This short-term process was additionally done in chondrocyte containing BPC-157 with IL-1B (.1-10 ug/mL) and H2O2. Cell videos of myoblasts and chondrocytes containing BPC-157 and IL-1B were used to measure cell velocity and division time of inflammatory stress. These results were measured and graphed to determine the effect of BPC-157.

Results: Without stress, we observed a similar growth rate for myoblasts with and without BPC-157 over the long term. Additionally, we did not find a significant difference with BPC-157 in theoretical yield. When under stress, myoblasts with BPC-157 showed a larger cell proliferation than myoblast cells undergoing stress without the BPC-157. These same results are reflected in the chondrocytes. Meaning the BPC-157 was able to maintain cell proliferation under oxidative/inflammatory stress. In myoblasts treated with BPC-157, velocity increased compared to the control. But with the addition of the IL-1B and BPC-157, velocity decreased compared to the control. In chondrocytes division time significantly increased with the addition of 1uL of BPC-157. With the gradual addition of BPC-157, velocity increased in chondrocytes.

Conclusion: Our findings show that BPC-157 is effective in supporting cell proliferation in myoblasts under oxidative stress. In myoblasts, cell proliferation had similar growth rates. With inflammatory stress, BPC-157 decreased velocity, without stress BPC-157 increased velocity. The addition of 1uL BPC-157 in chondrocytes significantly increased division time. Additionally, as the dosage of BPC-157 increased, so did velocity in chondrocytes.

A Chemical Space Analysis of *De Novo* Generative Models for Drug Discovery

Saranya Saripalli[1,2], Fareeda E. Abu-Juam[3], David R. Koes[3], PhD
[1]South Fayette High School, McDonald, PA; [2]University of Pittsburgh Hillman Cancer Center, Pittsburgh, PA;
[3]Department of Computational and Systems Biology, Pittsburgh, PA

Abstract
Existing de novo generative models were evaluated for chemical space overlap to assess the biological significance of developing new generative models. Proteins BCR-ABL Kinase, KRAS, and MDM2 were each tested for the models OMTRA and TargetDiff through methods such as Tanimoto similarity, Murcko scaffolds, PCA plots, and UMAP plots. These analyses exemplified that generative models produce relatively homogeneous ligands while exploring similar regions of chemical space, though they diverge from known chemical space.

Introduction
Genetic mutations lead to changes in protein structure and function, causing diseases such as cancer[1]. Efforts to mitigate disease symptoms rely on expensive and time-consuming experiments to discover potential drugs[1]. To speed up and optimize the discovery process in comparison to experimental efforts, drugs (or ligands) can be designed using *de novo* generative models. However, many of these models are built for efficiency in producing new molecules without testing whether they deliver any real biological gain—that is, whether they explore beyond currently known drug-like molecules (chemical space). This study analyzes the relative chemical spaces of contemporary models across three cancer-associated proteins: BCR-ABL kinase (leukemia), KRAS (pancreatic cancer), and MDM2 (brain tumors), to test whether they truly explore more chemical space.

Methods
We generated 10,000 ligands using models OMTRA[2] and TargetDiff [3], for each candidate protein. After generation, each ligand from each model (for their respective protein) was tested against itself and its respective ChEMBL active set[4]. Initially, we filtered molecules for validity (Valid SMILES) and for uniqueness. We then assessed how well the valid, unique molecules sampled chemical space by comparing their fingerprints with those of randomly selected drug-like compounds and known active compounds from ChEMBL[4] and ZINC[5]. We computed Tanimoto similarity, Murcko scaffold uniqueness, Principal Component Analysis (PCA), and Uniform Manifold Approximation and Projection (UMAP) using Python.

Results
Across all three proteins, the PCA and UMAP plots showed a consistent overlap between the TargetDiff, Random ChEMBL, and Random ZINC molecules. Furthermore, the ChEMBL actives were outliers in all analyses while OMTRA molecules differed slightly from the TargetDiff, Random ChEMBL, and Random ZINC; though they still placed in the same vicinity compared to the ChEMBL active sets, across all of the proteins (Figure 1A and 1B). These findings are consistent with the Tanimoto similarity (T_C) between each generative model's set and its respective ChEMBL active set. In other words, the Tanimoto similarity between BCR-ABL Kinase ($T_C \leq 0.111$), KRAS ($T_C \leq 0.099$), MDM2 ($T_C \leq 0.096$) and their active set is closer to 0, suggesting that the molecules diverge from currently explored chemical space for each protein (Figure 1C). Furthermore, the most common Murcko scaffolds for the OMTRA and TargetDiff set suggest that generative models produce ligands that are less complex compared to ligands created in an experimental setting (ChEMBL actives set), which corroborates the similarity between the two generative models.

Discussion
We observed that the models mostly overlapped in exploring similar chemical space, as they were closer in proximity to each other as well as the Random ChEMBL and Random ZINC sets. The ChEMBL actives for each protein were outliers on the graph, suggesting that the generated molecules are not chemically similar to the experimentally validated active compounds. Additionally, the findings from the Murcko scaffold analysis revealed that the OMTRA and TargetDiff generated ligands are less complex, therefore substantiating the claim that *de novo* generative models explore similar regions of chemical space.

Figure 1. Molecules from OMTRA and TargetDiff explore similar chemical spaces as Random ChEMBL and Random ZINC and diverge from known actives. (A) PCA and (B) UMAP showcasing the overlap between TargetDiff generated molecules, Random ChEMBL, and Random ZINC molecules; ChEMBL actives' separation from generative models' chemical space; and OMTRA's distinct yet modest overlap with TargetDiff molecules. (C) Tanimoto Similarity plot showcasing the amount of similarity between its own dataset, ChEMBL actives, Random ChEMBL, and Random ZINC, showing similarity to random sets.

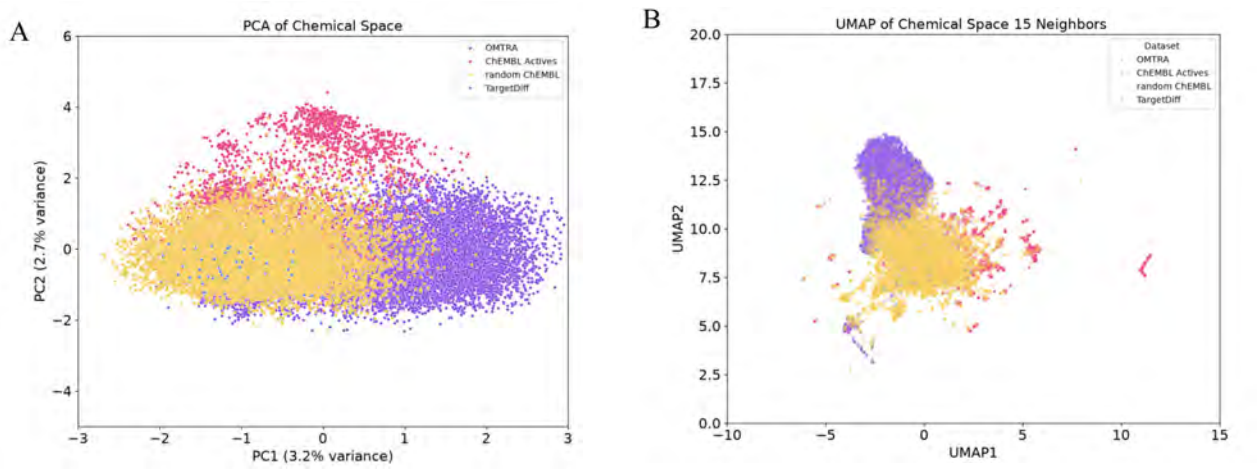

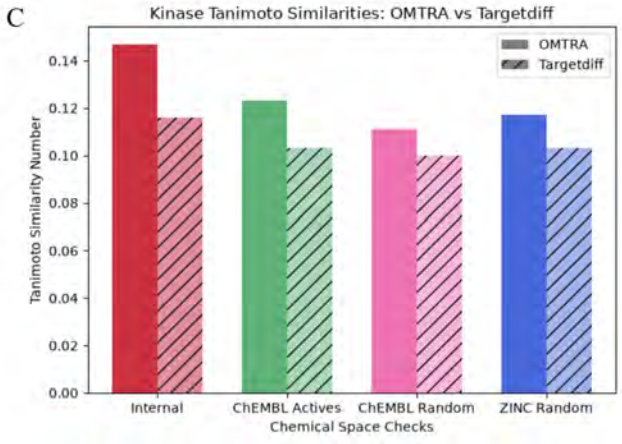

References:

1. Qiu X, Li H, Ver Steeg G, Godzik A. Advances in AI for protein structure prediction: Implications for Cancer drug discovery and development. Biomolecules [Internet]. 2024 Mar 1 [cited 2026 July 24];14(3):339. Available from: https://www.mdpi.com/2218-273X/14/3/339
2. Dunn I, Toft L, Katz T, Gupta J, Shah R, Hettiarachchi R, et al. OMTRA: A Multi-Task Generative Model for Structure-Based Drug Design [Internet]. arXiv; 2025 [cited 2026 Jul 24]. Available from: http://arxiv.org/abs/2512.05080 doi:10.48550/arXiv.2512.05080
3. Guan J, Qian WW, Peng X, Su Y, Peng J, Ma J. 3D Equivariant Diffusion for Target-Aware Molecule Generation and Affinity Prediction [Internet]. arXiv; 2023 [cited 2026 Jul 24]. Available from: http://arxiv.org/abs/2303.03543 doi:10.48550/arXiv.2303.03543
4. Gaulton A, Bellis LJ, Bento AP, Chambers J, Davies M, Hersey A, et al. ChEMBL: a large-scale bioactivity database for drug discovery. Nucleic Acids Res. 2012 Jan;40(Database issue):D1100–7. doi:10.1093/nar/gkr777 PubMed PMID: 21948594; PubMed Central PMCID: PMC3245175.
5. Tingle BI, Tang KG, Castanon M, Gutierrez JJ, Khurelbaatar M, Dandarchuluun C, et al. ZINC-22A Free Multi-Billion-Scale Database of Tangible Compounds for Ligand Discovery. J Chem Inf Model. 2023 Feb 15;63(4):1166–76. doi:10.1021/acs.jcim.2c01253

Title: Cell Stress and Communication:
The Role of Exosomes in Hepatocytes

Scholar: Honoria Saxton

High School/College/City/State: Oakland Catholic High School, Pittsburgh Pennsylvania

Lab: Dr. Melanie Scott

Mentor: Sudrisht Chaudhary

Site: Surgery

Background: The liver is one of the most important organs in the body, and hepatocytes are its main functional cells. When hepatocytes experience stress caused by low oxygen (hypoxia), inflammation, or oxidative stress, they release tiny membrane-bound particles called exosomes. These exosomes carry proteins and other molecules that allow cells to communicate with one another. The purpose of this project is to investigate how different stress conditions affect exosome release from hepatocytes and to explore whether changes in exosome-associated proteins could help identify biomarkers of liver cell injury.

Methods: Primary hepatocytes will be cultured in collagen-coated dishes and allowed to attach overnight. The cells will then be transferred to exosome-depleted culture medium and divided into four groups: untreated control, oxidative stress induced by hydrogen peroxide (H_2O_2), inflammatory stimulation using lipopolysaccharide (LPS), and hypoxia using a low-oxygen chamber. After an 18-hour treatment period, conditioned media will be collected, and exosomes will be isolated. Western blotting will be performed to detect the exosome markers CD63, CD81, and CD9, and protein expression will be compared among the different treatment groups.

Results: It is expected that hepatocytes exposed to oxidative stress, inflammation, or hypoxia will release more exosomes than untreated cells. This is anticipated to be reflected by increased expression of the exosome markers CD63, CD81, and CD9 in the treated groups.

Conclusion: This study will improve our understanding of how hepatocytes communicate during cellular stress through exosome release. Identifying stress-related changes in exosome-associated proteins may help researchers discover biomarkers of early liver injury, which could contribute to improved detection, monitoring, and future treatment of liver diseases. The project also provides valuable hands-on experience in cell culture, experimental design, exosome isolation, and protein analysis.

Trends of Publication of Osteosarcoma Over the Past Decade (2016-2026) on PubMed

Kaisra Setiawan [1], Ines Lohse, PhD [2], Kurt Weiess, MD [3], Ahmad P. Tafti, PhD [4]

[1]Mt. Lebanon High School, Pittsburgh, PA; [2]University of Pittsburgh Hillman Cancer Center, Pittsburgh, PA

Abstract

The project analyzes the publication trends in osteosarcoma research on PubMed over the past decade using MeSH terms. The publications were analyzed to identify shifts in research focus across major topics.

Introduction

Osteosarcoma is the most common type of malignant bone cancer that affects patients across the age spectrum, primarily affecting children, adolescents, and young adults. While it often starts at the bones, osteosarcoma can spread to other areas of the body, such as the lungs and other bones, making it difficult to treat. Standard treatment typically involves neo-adjuvant chemotherapy, followed by surgical removal of tumors. The effectiveness of tumor removal relies heavily on the pre-operative therapy response, as a strong treatment response allows the surgeon to remove the cancerous tumor more precisely while preserving the healthier tissues. As treatment strategies and technologies continue to evolve, understanding how osteosarcoma research has changed over time can provide valuable insight into emerging research trends, shifts in scientific priorities, and potential directions for future investigation. Examining these changes may also help identify knowledge gaps and opportunities to improve patient outcomes.

Methods

We searched the PubMed database for scientific articles on osteosarcoma published between January 1, 2016, and January 1, 2026. Searches are performed using the Medical Subject Heading [MeSH] term, MeSH Major Topic, MeSH Subheading, and Date - Publication, using the following PubMed query:

> (((((osteosarcoma[MeSH Terms]) OR (osteosarcoma tumor[MeSH Terms])) OR (osteosarcoma tumors[MeSH Terms])) OR (osteosarcoma[MeSH Major Topic])) OR (osteosarcoma[MeSH Subheading])) AND (("2016/01/01"[Date - Publication] : "2026/01/01"[Date - Publication]))

This resulted in 10,562 scientific articles published in the literature in which they have a PubMed index. Then we used natural language processing combined with large language models to turn this large column of articles into knowledge and insight.

Results

We computationally ended up with four scientific visualization components. The word cloud in Figure 1a provides a broad view of the field where the term osteosarcoma dominates the other clinical and mechanistic terms, such as chemotherapy and proliferation. While the word cloud captures what the fields emphasizes overall, the trend timeline in figure 1b shows how these topics changed over time, from molecular pathway and chemotherapy resistance in 2016-2018 to genomic, immunology, and biomarker in 2019-2021, to single-cell, spatial omics, and multiomics in 2022-2024, to finally AI, precision medicine, tumor microenvironment, and immunotherapy in 2025-2026. These topics are then organized into an ontology in Figure 2, which groups them into five categories: Biology, Technologies, Clinical, Tumor Microenvironment, and Therapeutics. The knowledge graph in figure 3 builds on from the ontology by focusing into one theme, the tumor microenvironment, and shows its connection to the three cell types (macrophage, CAFs, immune cells), which are linked to disease and context nodes (metastasis, osteosarcoma, immunotherapy), and then into methods that are used to study them (single-cell and spatial Tx for metastasis and multiomics and biomarkers for osteosarcoma.

Discussion

Osteosarcoma research over the past decade has shifted from the topics of molecule pathway and chemotherapy resistance toward immunology and spatial omics, and to more recently AI, precision medicine, and the tumor

microenvironment. Mapping these trends provides insight on how scientific priorities are changing and may guide future research and innovations in osteosarcoma care.

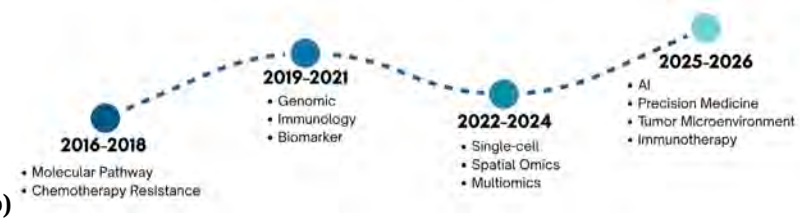

Figure 1. a) Word cloud of articles published on osteosarcoma, demonstrating the most frequently said words in the abstracts. b) Trend timeline of the major topics researched throughout the decade.

Figure 2. The ontology of research in sarcoma categorized into 5 categories: Biology, Tumor Microenvironment, Technologies, Therapeutics, and Clinical.

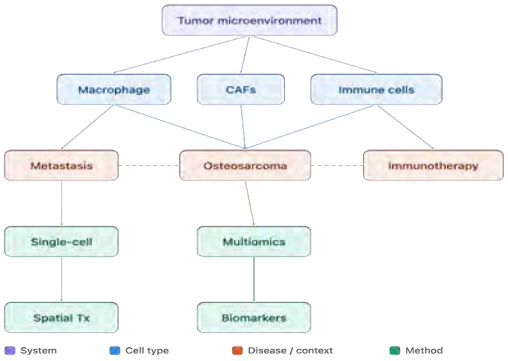

Figure 3. The knowledge graph of the theme tumor microenvironment

References

1. National Library of Medicine (US), National Center for Biotechnology Information. PubMed [Internet]. Bethesda (MD): National Library of Medicine (US); 1996- [cited 2026 Jul 25]. Available from: https://pubmed.ncbi.nlm.nih.gov/

Quantifying Cell-Cycle Heterogeneity from Live-Cell PCNA Dynamics

Allison Shi[1, 3], Gaohan Yu[2], Lu Yong[3], Jianhua Xing[2, 3]
1. Shady Side Academy, Pittsburgh, PA; 2. Department of Physics and Astronomy, University of Pittsburgh, Pittsburgh, PA; 3. Department of Computational and System Biology, University of Pittsburgh, Pittsburgh, PA

Abstract

Heterogeneity is shown on the dynamics of cell cycle progression; different cells may have different durations at each cell cycle stage. This study investigates whether sister cells sharing the same mother cell show stronger correlation than non-sister cells. Using live-cell PCNA imaging and lineage tracking, sister versus random-pair similarity were compared via Dynamic Time Warping on full trajectories. Trajectory-shape comparisons show sister cells are significantly more similar.

Introduction

Cell-to-cell heterogeneity is the natural variation in behavior, gene expression, and signaling responses that exist in identical cells. This study is meant to determine whether sister cells sharing the same mother cell show stronger correlation than non-sister cells by using Dynamic Time Warping (DTW: algorithm used to measure the similarity between two temporal sequences that vary in speed/timing) to track and compare the intensities of PCNA (proliferating cell nuclear antigen) and the duration/trends of the cell cycle phases in RPE-1 cells.

Methods

Cells expressing fluorescent reporters for PCNA were tracked using Fiji Manual Tracking via live-cell imaging, with lineage annotated to identify sister-cell pairs. Nuclei were manually segmented using Cellpose GUI and isolated before measuring PCNA intensity in each nuclear mask, with per-cell trajectories smoothed by a Savitzky-Golat filter. Cell-cycle phase transition points (G1/S, S/G2) were annotated manually to compute phase and total-cycle durations. Sister-pair similarity was tested against a distribution of random non-sibling pairings (10,000 permutations, one-sided). Analyses used 66 total cells, including 16 sister pairs (32 cells). Cell-cycle timing similarity was quantified as the Euclidean (L2) distance between paired cells in standardized duration space, and trajectory similarity as the DTW distance between group-normalized PCNA total-intensity trajectories. For each case, sister-pair distances were compared to the distribution of random-pair distances.

Results

Sister pairs were significantly closer than random pairs in cell-cycle duration space with a p-value of 0.008.

PCNA intensity trajectories had a p-value of 0.1.

Discussion

The results indicate that sister-cells inherit cell-cycle timing: the durations of the cell cycle and its phases were consistently correlated between sisters, whereas the distances were not significantly more similar. This distinction is informative for cellular memory, as what persists across division seems to be the scheduling of cell-cycle transitions rather than expression trajectory. This reflects inheritance in the broad sense; separating genetic from non-genetic contributions would require more distant lineage comparisons or genetic perturbation. Quantifying which cellular features are inherited helps show how populations diversify from a common division. Understanding this inheritance is relevant to processes where cell-to-cell variability matters, such as development, tissue homeostasis, and the emergence of drug-tolerant states in cancer.

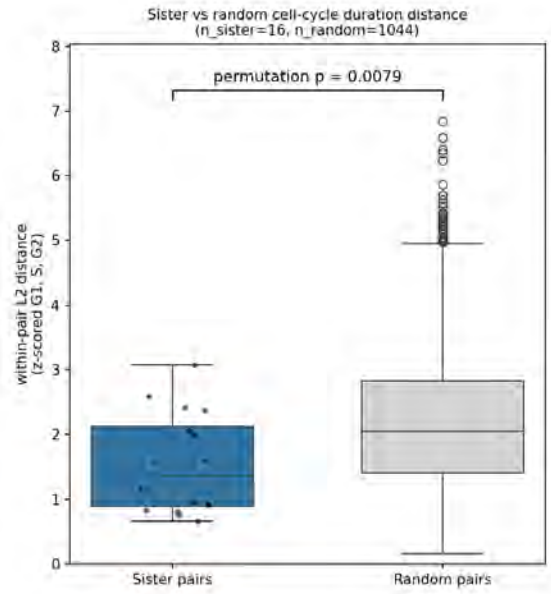

Figure 1: L2 distance in standardized (G1, S, G2) duration space for sister versus random non-sibling pairs

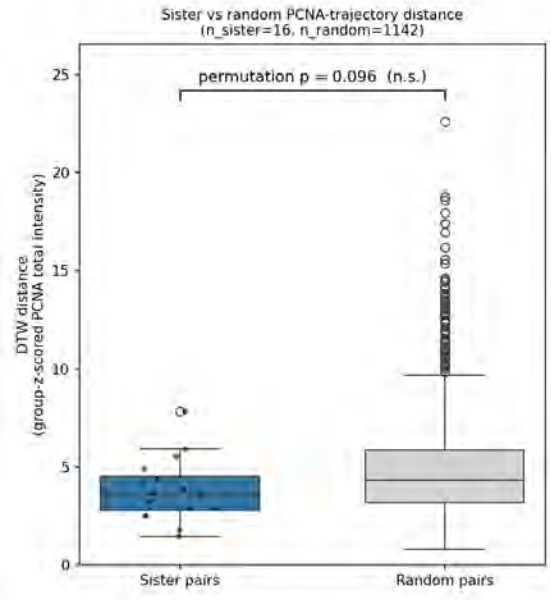

Figure 2: DTW distance of group-normalized PCNA total-intensity trajectories for sister versus random non-sibling pairs

Acknowledgements

I would like to sincerely thank and express my gratitude to Prof. Jianhua Xing, Dr. Yong Lu, and Gaohan Yu who have helped me complete this project by answering my questions and explaining complex topics to me.

Candidate Compound Testing on Multiple Mutant Zebrafish Models of Retinitis Pigmentosa

Scholar: Benjamin Shuai

High School/College/City/State: North Allegheny Senior High School, Pittsburgh, PA

PI of group/lab: Liyun Zhang, MD, PhD

Mentor(s): Liyun Zhang, MD, PhD, Molly Voit

Site: VISION

Background: Retinitis pigmentosa (RP), which affects 1.5 to 2 million people worldwide, is an inherited retinal disease causing progressive photoreceptor death. It starts with an early onset of night blindness, then gradual loss of visual field, and eventually leads to loss of central vision. Current treatments for RP are limited in part due to the vast number of different gene mutations associated with it, making it difficult to treat a large group of patients. Zebrafish have been established as an effective model for RP research because of their optical transparency, conserved retinal anatomy, and rapid reproduction and development. This study screened candidate compounds for their ability to stop or rescue retinal degeneration in multiple zebrafish models of RP.

Methods: To simulate RP in zebrafish, certain genes were previously added or deleted in the fish to create lines of zebrafish with dying rod cells. The fish were also genetically modified to have a yellow fluorescent protein (YFP) in their eyes. The 4dpf (days post fertilization) fish were loaded onto 96-well plates with the drug treatments, which consisted of 2 compounds at concentrations ranging 0.0625-1 uM, along with respective control groups. At 6dpf, clove oil was added to temporarily prevent motion so the TECAN scanner could read each well for fluorescence caused by the presence of YFP. A higher fluorescence would indicate a higher photoreceptor count. Data were analyzed using one-way ANOVA followed by Dunnett’s multiple-comparisons test.

Results: Compound A demonstrated a significant improvement in fluorescence in fish with mutations in the pde6a and rhodopsin genes, as did compound B in two of the rhodopsin mutants, rho5del and rho12del.

Conclusion: Each candidate compound demonstrated neuroprotective effects in multiple mutant models; however, further testing is necessary to verify.

FcRL5 as a therapeutic target for intratumoral memory B cell

Sofia Melani, Anabella Phelps, Charu Arora, Allison Casey, Tullia C. Bruno

Fox Chapel Area High School, Fox Chapel, PA; University of Pittsburgh Hillman Cancer Center Academy, Pittsburgh, PA

Because of the very suppressive TME associated with head and neck tumors, these cancers have very limited responses to immune checkpoint inhibition therapy, with success rates around 14%-22%. We have found that intratumoral memory B cells (MBCs) can be associated with better responses to immunotherapies in solid tumors, including head and neck tumors. MBCs are heterogeneous and generated via germinal center reactions or extrafollicular (EF) responses, with EF MBCs being dysfunctional in head and neck tumors. Our lab has previously shown that EF MBCs express multiple inhibitory receptors, including a B cell specific inhibitory receptor - FcRL5. Here, we investigate the stability of the FcRL5 molecule on the surface of B cells to gauge its value as a therapeutic target. Utilizing supernatants from in vitro FcRL5 blocking experiments, we assess the abundance of FcRL5 possibly shed from the cell surface utilizing enzyme-linked immunosorbent assays, finding that the molecule is stabilized on the membrane which would allow for long-term blockade effects. Utilizing head and neck cancer patient peripheral blood, we next assessed the ability of FcRL5+ MBCs to secrete pro-inflammatory cytokines, such as TNF-a, CXCL13, as well as inhibitory cytokine, like IL-10. We find that FcRL5+ MBCs secrete CXCL13 and TNF-a at levels higher than FcRL5- MBCs, suggesting these cells can aid in recruitment/activation of other MBCs in the tumor microenvironment. These findings help to improve our understanding of FcRL5 biology and potentially highlight FcRL5 as a candidate for future immunotherapeutics focused on B cell function.

Modulating the premetastatic niche in uveal melanoma: the role of statins in limiting metastasis

Scholar: Lotus Soletti
High School/College/City/State: Oakland Catholic High School, Pittsburgh, PA
PI of group/lab: Amanda Clark, PhD
Mentor: Amanda Clark, PhD
Site: Pathobiology

Background: Metastasis is the leading cause of mortality in uveal melanoma (UM), with approximately 90% appearing in the liver. Primary tumors communicate with distant organs, using extracellular vesicles (EVs), before cancer cells even begin to spread. These vesicles prepare the future metastatic site (pre-metastatic niche) by creating a microenvironment that is more conducive to cancer cell colonization. Prior research has shown that statins alter the production and composition of tumor-derived EVs, and attenuate the growth of metastatic tumors. Thus, we hypothesize statins suppress EV secretion by UM cells, thereby limiting premetastatic niche formation and abrogating metastatic progression.

Methods: Human UM cell lines (92.1, Mel202) were transfected with a red fluorescent protein (RFP), maintained under puromycin selection to enrich for RFP^+ cells and expression monitored by flow cytometry. Dose responses to atorvastatin (ATV) for UM cell lines were also assessed by an MTT viability assay and mouse hepatocytes (mHeps) using a crystal violet assay. Lastly, the UM^{RFP} cells were co-cultured with mHeps and examined by immunofluorescence.

Results: The $Mel202^{RFP}$ cells were successfully generated and upscaled for future cell sorting. While the 92.1^{RFP} cells were also created, these cells were not successfully upscaled. Both UM^{RFP} cells were co-cultured with and could be clearly distinguished from mHeps validating the utility of the RFP cells for future studies. Mel202 cells (IC50 6.82µM, non-toxic dose 0.048 µM) were found to have a greater sensitivity to ATV than 92.1 cells (IC50 19.5µM, non-toxic dose 8.7 µM). A non-toxic dose of at <2 µM ATV for mHeps was identified.

Conclusion: Our study created a stable UM^{RFP} cell line and determined ATV sensitivities for both UM cells and mHeps. These findings are enabling future studies evaluating the ability of statins to inhibit the production and secretion of EVs by UM cells, and limit pre-metastatic niche formation.

Molecular Subtyping of Colorectal Cancer from ResGitDR Cellular State Representations

Ayush Srivastava[1], Alex VanHelene, PhD[2], Xinghua Lu, MD, PhD[2]
[1]North Allegheny Senior High School, Wexford, Pennsylvania; [2]University of Pittsburgh, Pittsburgh, Pennsylvania

Abstract
Consensus molecular subtype (CMS) status in colorectal cancer can be predicted from gene expression; whether it is encoded in mutation-driven signaling is unknown. Using ResGitDR, tumor mutations were converted into cellular-state representations and tested for CMS recovery in 869 tumors. Unsupervised clustering agreed weakly with CMS (ARI 0.03–0.07), while a gradient-boosted classifier reached 47% accuracy against a 25% baseline, indicating partial but non-dominant CMS signal in mutation-derived representations.

Introduction
Colorectal cancer (CRC) is stratified into four consensus molecular subtypes (CMS1–4), which carry prognostic and therapeutic significance[1]. CMS can be predicted from tumor transcriptomes rather than from the somatic genome alterations (SGAs) that drive tumorigenesis. Mutations do not map cleanly onto subtypes: tumors sharing a subtype often carry distinct drivers, while distinct drivers converge on shared functional states. Because SGAs act by disrupting cellular signaling, CMS-relevant information may reside in the downstream cell state rather than in the mutations themselves. This project tested whether SGA-induced cellular-state representations learned by ResGitDR[2] recover CMS structure without using gene expression directly.

Methods
This was a retrospective computational analysis of public genomic datasets. We trained the ResGitDR model on paired somatic genome alteration (SGA) and transcriptomic data from TCGA primary tumors and GDSC cell lines (9,562 samples), yielding a transcription-factor-organized representation of perturbed cellular signaling derived from mutation input. The trained model was then used to generate cellular-state representations for a cohort of 869 CRC tumors with gold-standard CMS-annotations. Representations were evaluated under two conditions: using all representation genes and restricted to genes in the CMS classifier gene set. Two evaluation strategies were applied. First, unsupervised K-means clustering (k = 4, matching the number of CMS subtypes) partitioned the representations without access to subtype labels, and agreement with published CMS assignments was scored by adjusted Rand index (ARI). Second, a supervised gradient-boosted classifier (XGBoost) was trained to predict CMS directly from the representations using a stratified 80/20 train–test split (695/174 samples) preserving subtype proportions. Main outcome measures were ARI for clustering and accuracy on the held-out test set for supervised classification.

Results
Unsupervised clustering agreed weakly with CMS regardless of the gene set used (all-gene: ARI = 0.032; CMS-gene-filtered: ARI = 0.074). Both values fall near zero, indicating that cluster assignments were close to independent of subtype label. The supervised classifier (XGBoost) performed substantially better than chance, achieving 54% test accuracy against a 25% baseline for random four-class assignment.

Discussion
SGA-induced cellular-state representations carry detectable CMS-relevant signals, as shown by supervised classification, but this signal is not the dominant axis of variation recovered by unsupervised clustering. CMS identity therefore appears only partially encoded in mutation-derived signaling representations. Methodologically, this work demonstrates that interpretable representation-learning models such as ResGitDR offer an alternative lens for probing tumor subtype biology directly from mutation data, complementing expression-based classification. Clinically, it points toward approximating CMS-relevant biology where expression profiling is unavailable, but mutation data is accessible.

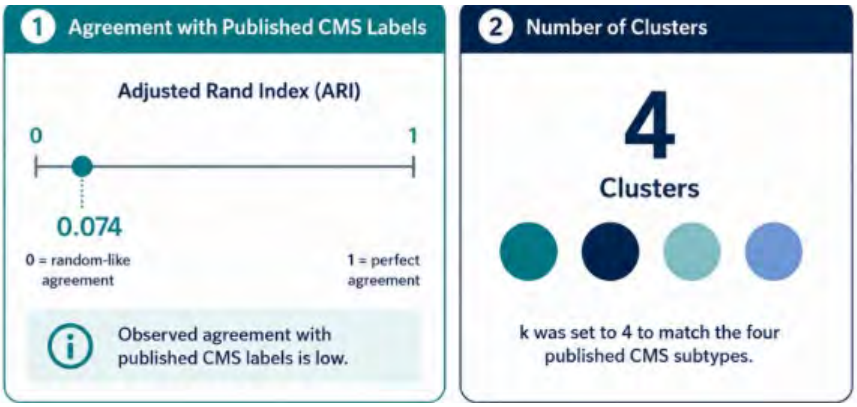

Figure 1: Unsupervised classification results

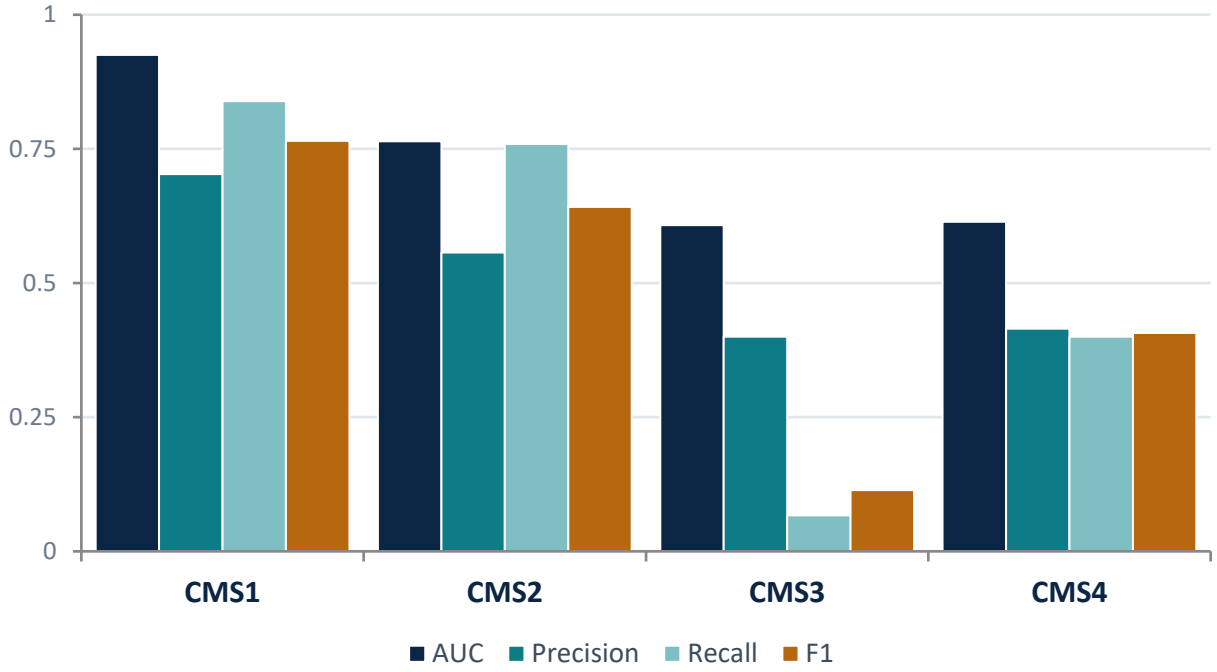

Figure 2: Extra Trees classifier performance (Supervised Classification)

References

1. Guinney J, Dienstmann R, Wang X, et al. The consensus molecular subtypes of colorectal cancer. *Nat Med.* 2015;21(11):1350-6.
2. Ren S, Cooper GF, Chen L, Lu X. An interpretable deep learning framework for genome-informed precision oncology. *Nat Mach Intell.* 2024;6(8):864-75. doi:10.1038/s42256-024-00866-y
3. Nunes L, Li F, Wu M, et al. Prognostic genome and transcriptome signatures in colorectal cancers. *Nature.* 2024;633(8028):137-46. doi:10.1038/s41586-024-07769-3
4. Colorectal Cancer Subtyping Consortium (CRCSC) identification of a consensus of molecular subtypes [dataset]. Synapse; 2015. doi:10.7303/syn2623706
5. Uppsala-Umeå Comprehensive Cancer Consortium. Whole-genome and transcriptome sequencing of Swedish primary colorectal cancers [dataset]. European Nucleotide Archive; 2024. Accession PRJEB61514. Available from: https://www.ebi.ac.uk/ena/browser/view/PRJEB61514

Title: Role of the PE8 Plasmid in Gene-Editing Applications

Scholar: Shivum Telang
High School: North Allegheny Senior High School / Pittsburgh, PA
Affiliations: Gao Lab, UPMC Vision Institute, University of Pittsburgh, Department of Ophthalmology
Mentors: Vincente Valle, Ph.D., Daniel Gao, Ph.D.

Background: Prime editing enables precise genome modification without introducing double-stranded DNA breaks, but editing efficiency remains a major limitation for many therapeutic applications. Recently, artificial intelligence-guided redesign of reverse transcriptase domains generated the PE8 family of prime editors, which demonstrated enhanced stability, expression, and editing performance compared with previous prime editing systems. To independently evaluate these redesigned editors, we compared multiple PE8 variants under identical experimental conditions using several guide RNA combinations targeting genomic loci of interest.

Methods: PEmax, PE8max, PE8a, PE8c, and PE8d plasmids were co-transfected with corresponding pegRNA and nicking guide RNA pairs into cultured mammalian cells using Lipofectamine-mediated transfection. Following a 72-hour incubation period, cells were lysed and genomic DNA was recovered by thermal lysis. Target loci were amplified using a two-step nested PCR workflow consisting of an initial flanking amplification followed by an internal PCR to increase specificity before downstream sequencing-based analysis. Editing efficiencies were compared across multiple guide pair combinations and appropriate GFP and negative controls.

Results: Successful transfection and molecular screening generated amplified target products suitable for downstream sequencing analysis of genome editing outcomes. Comparative evaluation across PE variants and guide RNA combinations enabled quantitative assessment of editing efficiency, allowing identification of the highest-performing AI-engineered PE8 editors relative to existing prime editing systems.

Conclusions: This study provides an independent experimental validation framework for AI-engineered PE8 prime editors and establishes a standardized workflow for comparing next-generation genome editing platforms. The resulting data will help determine the most efficient PE8 variant for future research and therapeutic genome editing applications while further assessing the practical advantages of AI-guided protein engineering for precision genome editing.

Assessing the generalizability of colorectal cancer epithelial subtypes to independent single-cell RNA sequencing

Divya Thirumala[1], Ethan Wolfe, PhD student[2]
[1]Fox Chapel Area High School, Pittsburgh, PA; [2]University of Pittsburgh Hillman Cancer Center Academy, Pittsburgh, PA

Abstract: In this project, an evaluation of published iCMS marker genes and gene set enrichment analysis (GSEA) was performed on reference and independent scRNA-seq datasets to assess the cross-cohort generalizability of colorectal cancer subtyping. Cross-dataset validation, dimensional reduction, and clinical distribution analyses were conducted to evaluate subtype consistency and highlight the impact of batch noise, sample limitations, and pipeline standardization on patient subtyping.

Introduction: Colorectal cancer (CRC) is a heterogeneous disease historically classified into four consensus molecular subtypes (CMSs) via bulk RNA-sequencing[2]. A recent study showed that malignant CRC cells can be classified further into two epithelial intrinsic CMSs: iCMS2 and iCMS3, discovered from scRNA-seq[1]. However, iCMS subtyping only holds scientific and clinical value if it can reliably generalize beyond its original discovery cohorts. We evaluated whether GSEA can classify independent scRNA-seq CRC cohorts using existing iCMS markers.

Methods: To evaluate the efficacy of GSEA in assigning iCMS2/iCMS3 labels using marker genes[1], we applied this method to single-cell data (GSE132465 and GSE144735[3]) and computed the F_1 score from the actual and predicted labels. We then applied it to independent scRNA-seq datasets from the Gene Expression Omnibus (GEO[4]) (GSE178341[5] and GSE200997[6]). We evaluated expression profiles using Principal Component Analysis (PCA) and Uniform Manifold Approximation and Projection (UMAP) plots to analyze the separation between predicted iCMS2 and iCMS3 clusters. We studied the distribution of the predicted iCMS clusters with respect to sidedness, microsatellite instability (MSI) status, and CMS classification, using Z-tests for comparison with group-specific proportions.

Results: Validating GSEA on reference scRNA-seq data yielded a high F_1 score of 0.8880, but applying it to independent data produced overlapping PCA and UMAP clusters rather than clear separation, driven by cross-dataset batch variation. The Z-tests revealed statistically significant deviations across most clinical feature distributions relative to reference baselines ($\alpha = 0.05$), with CMS1 and CMS2 within the predicted iCMS2 group representing the sole exceptions. The replication of Figure 3c[1] highlighted key compositional shifts in our predicted data, heavily dominated by right-sided (28/29), MSI-High (25/29), and CMS3 (3/3) features in iCMS3. In contrast, predicted iCMS2 tumors showed an unexpected representation of the CMS categories, containing CMS1 (1/13), CMS3 (3/13), and CMS4 (1/13) alongside the CMS2 majority (8/13).

Discussion: While accurate on reference data, applying our pipeline to independent data revealed shifted feature distributions and overlapping clusters, driven by cross-dataset batch noise and small sample sizes. These discrepancies show that enrichment scores struggle to generalize, underscoring the need for standardized pipelines. Future efforts may integrate multi-cohort batch correction and scalable machine learning to guide single-cell subtyping.

Figure 1: A stacked bar plot demonstrating proportions of tumor sidedness, MSI status, and CMS categories within predicted iCMS subtypes used for clinical distribution analysis.

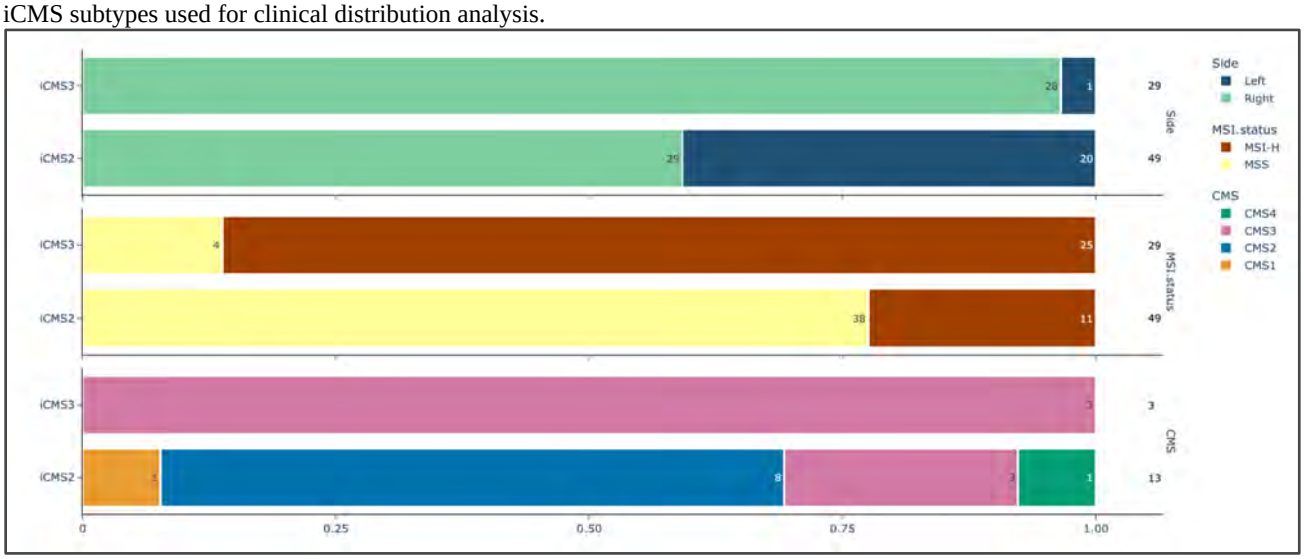

Figure 2: A UMAP plot demonstrating spatial distribution and cluster overlap of predicted iCMS2 and iCMS3 single-cell expression profiles.

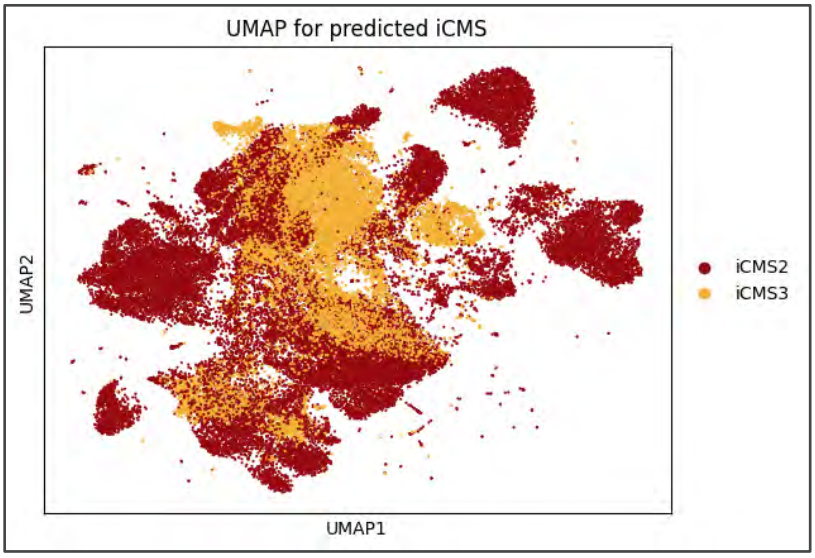

References

1. Joanito I, Wirapati P, Zhao N, Nawaz Z, Yeo G, Lee F, et al. Single-cell RNA sequencing of colorectal cancer discovers a mosaic of intrinsic tumor sub-types. Nat Genet. 2022;54(6):763–775. Available from: https://www.nature.com/articles/s41588-022-01100-4
2. Guinney J, Dienstmann R, Wang X, de Reyniès A, Schlicker A, Soneson C, et al. The consensus molecular subtypes of colorectal cancer. Nat Med. 2015;21(11):1350–1356. Available from: https://www.nature.com/articles/nm.3967
3. Lee HO, Ferguson Y, Ryba R, Jing X, Wang H, Tan AC, et al. Lineage-dependent gene expression programs influence the immune landscape of colorectal cancer. Nat Genet. 2020;52(6):594–603. Available from: https://pubmed.ncbi.nlm.nih.gov/32451460/
4. Subramanian A, Tamayo P, Mootha VK, Mukherjee S, Ebert BL, Gillette MA, et al. Gene set enrichment analysis: a knowledge-based approach for interpreting genome-wide expression profiles. Proc Natl Acad Sci U S A. 2005;102(43):15545–15550. Available from: https://academic.oup.com/nar/article/30/1/207/1332640
5. Khaliq AM, Erdogan C, Jiang Z, Bohlman S, Zhao S, Chen X, et al. Refinement of colorectal cancer molecular classification using single-cell RNA sequencing data. Genome Med. 2021;13(1):137. Available from: https://pubmed.ncbi.nlm.nih.gov/34450029/
6. Pelka K, Hofree M, Chen JH, Sarkizova S, Pirl WE, Jorgji V, et al. Spatially organized multicellular immune hubs in human colorectal cancer. Cell. 2021;184(18):4734–4752.e20. Available from: https://pubmed.ncbi.nlm.nih.gov/35538548/
7. Cancer Genome Atlas Network. Comprehensive molecular characterization of human colon and rectal cancer. Nature. 2012;487(7407):330–337. Available from: https://www.nature.com/articles/nature11252
8. Che H, Xu X, Wang Y, Zhang L, Li M, Zhou Y, et al. Single-cell mapping of human colorectal cancer evolution and microenvironment reprogramming. Nature. 2024;632(8024):390–398. Available from: https://www.nature.com/articles/s41586-024-07769-3

Title: Researcher for a building platform of adolescent health.

Scholar: Nevaeh Thompson

High School/College/City/State: Shady Side Academy, Pittsburgh, PA

PI of group/lab: Lindwe Kounga,Yueru Tu,Ana Radovic

Mentor(s): Lindwe Kounga, Yueru Tu, Ana Radovic

Site: CoSBBI

Introduction: The Youth Research Registry (YRR). As part of this project, I researched the Texas Youth Research Registry along with our Research Registry. We had identified several ideas that could help strengthen and improve the development of our own YRRduring the Texas Research. Our research highlighted the importance of involving youth in research and demonstrated how registries can connect young people with meaningful opportunities to contribute to their communities while gaining valuable experience.

Methods: To develop the Youth Research Registry, we will use a human-centered design approach that places youth perspectives at the center of the project. We will recruit approximately 15 youth participants to take part in three iterative focus group sessions. During these sessions, participants will provide feedback on the registry's design, recruitment strategies, communication methods, and ways to keep young people engaged over time.

The feedback collected from each session will be analyzed and used to improve the registry before the next focus group. This process allows us to continuously refine the registry based on youth input. We will also collaborate with University of Pittsburgh researchers and community partners to ensure the registry meets the needs of both young participants and research teams.

Conclusion: In the end of Youth research registries we will conclude that large, prospective, longitudinal data collection is critical for understanding and treating youth-specific health conditions, such as depression, diabetes, and atypical depression. These findings will highlight the need for tailored interventions and long-term monitoring for pediatric cohorts. We will also use implementation mapping methods and different types of designs to co-develop and test the registry prototype,ensuring it meets standards while meeting the parent permission standards,having minimal risk research and protecting data Every young person's story matters. Your experiences, perspectives, and ideas can help shape the future of adolescent health research.By joining the Youth Research Registry, you become part of a community working to improve healthcare through research, collaboration, and inclusion.Together, we can help create a future where every young person's voice is heard, every community is represented, and every discovery brings us one step closer to better health for all.

GLP-1RA Therapy reverses the MASH-Driven Pro-Metastatic Hepatic Niche and Reduces Colorectal Liver Metastases

Scholar: Isabel Ulis

High School/College/City/State: Allderdice High School, Pittsburgh, PA

PI of group/lab: Dr. Samer Tohme

Mentor(s): Anthony Gebran, Hamza Yazsani, Zhengyi He

Site: Surgery

Introduction: MASLD (Metabolic Dysfunction-Associated Steatotic Liver Disease) is a common liver condition that often develops in the setting of obesity and can lead to a more serious disease called MASH. People with these liver problems are more likely to experience colorectal cancer metastasis to the liver. GLP-1 receptor agonists, a new class of drugs used for weight loss, are effective at treating fatty liver disease, however, it is not yet known if they can further help stop cancer from spreading.

Methods: We fed wild type mice a high-fat diet (HFD) for eight weeks for them to develop fatty liver disease. Then, we injected the mice with either semaglutide (GLP1 drug) or a placebo for four weeks. After that, we injected colon cancer cells into the spleen, which traveled to the liver. Three weeks later, they were sacrificed,, and we assessed the mice cancer tumor sizes.

Results: The HFD mice developed fatty liver and had significantly more cancer in their livers compared to the mice that were on a regular diet. In addition, the mice treated with semaglutide had less fat in their livers, a healthier body composition, and significantly less cancer spread to the liver. Semaglutide also reduced inflammation in the liver and decreased the expression of TREM1 and TREM2 in the macrophages, two genes that we believe increase cancer progression.

Conclusion: Fatty liver disease creates an environment in the liver that makes it easier for cancer to spread there. GLP-1 drugs like semaglutide can reverse this effect, which means they could potentially be used to help prevent colon cancer from spreading to the liver in patients with fatty liver disease.

Future directions: Current and future work in the lab is aimed at understanding the protective changes that semaglutide is causing at the cellular level in the liver.

Evaluating Mechanical Scaling Strategies for Interspecies Translation of Trilayered Tissue-Engineered Vascular Grafts

Scholar: Aayushi Vardhan

High School/College/City/State: North Allegheny Senior High School, Wexford, PA

Lab: Jonathan P. Vande Geest, PhD

Mentor(s): David R. Maestas, Jr., PhD

Site: TechDrive X

Background: Cardiovascular disease remains the leading cause of global mortality. While coronary artery bypass grafting is standard, treatments rely heavily on autologous vein grafts, which suffer from mechanical compliance mismatch in arterial environments. Trilayer electrospun tissue-engineered vascular grafts (TEVGs), comprising an adventitial layer of polyester sulfobetaine urethane urea (PESBUU-50, an anti-thrombogenic material), a medial layer of 80:20 polyester urethane urea to gelatin (80:20 PEUU:gelatin), and an intimal layer of 20:80 PEUU:gelatin, achieved compliance matching in pre-clinical rodent models. However, scaling TEVG dimensions to large animal models without losing compliance matching remains a significant challenge.

Methods: This study evaluated two scaling approaches to translate rat TEVG dimensions to ovine coronary dimensions: Linear (Geometric) Scaling and Internal Pressure-Based (Law of Laplace) Scaling. Target wall thicknesses and solution volumes were calculated for both strategies. Polymer solutions were synthesized in hexafluoroisopropanol (HFIP), electrospun into trilayer conduits, and crosslinked with 0.8% genipin. Scaffolds were mounted for tubular biaxial mechanical evaluation via luminal pressurization on a CellScale device to determine compliance during the final preconditioning cycle. Custom scripts in MATLAB were utilized for data processing, compliance analysis, and visualization.

Results: Preliminary data revealed distinct compliance behaviors relative to the *in vivo* benchmark (0.000523 $mmHg^{-1}$). Linear Geometric Scaling yielded a mean compliance of $0.000510 \pm 0.000144\ mmHg^{-1}$, aligning closely with targets. Conversely, Pressure-Based Scaling exhibited hyper-compliance, averaging $0.001075 \pm 0.000094\ mmHg^{-1}$.

Conclusion: Preliminary findings indicate that, in the absence of axial tension, Linear Geometric Scaling appears to successfully achieve compliance matching with target *in vivo* values. Evaluating the influence of physiological axial pre-stretch will be critical to further validate these scaling frameworks. Future work will focus on integrating computational modeling for parametric optimization and expanding scaling frameworks toward human clinical translation.

Spatially Modeling the Quantized Signaling of Ras Activation using Particle-based Stochastic Simulation in Smoldyn

Ethan Varghese[1], Achyudhan R. Kutuva[2], James R. Faeder, Ph.D.[2]
[1]Sewickley Academy, Sewickley, PA, [2]Department of Computational and Systems Biology, School of Medicine, University of Pittsburgh, Pittsburgh, PA

Abstract: The signaling protein SOS' processivity allows a single molecule to activate up to thousands of Ras before it dissociates. This project dimensionally mapped this biological system and determined if a 2D spatial model could produce peaks of RasGTP activation as SOS levels increase. We ultimately created graphs that effectively resembled realistic Ras and SOS activity.

Introduction: Ras is an essential GTPase in the cell which, when activated, is crucial for signaling pathways involved in cell growth and survival. Ras' behavior is controlled by the guanine nucleotide exchange factor SOS, which binds allosterically to Ras causing it to switch from being inactive (GDP) to its active state (GTP). This process occurs in membrane corrals: miniature compartments of the membrane vital for cell signaling. Our project was built upon previous work that showed positive spikes in RasGTP levels as SOS increases, and the opposite as it decreases (Lee et al., 2024; Yonosh and Faeder, 2026). We were looking to see: How can we reproduce those results and what would occur as the corral size grows?

Methods: We built a basic, working Smoldyn model that would produce the same results seen in the mentioned paper: which used the BioNetGen platform for its model. This model would allow us to properly spatially map the random diffusion of SOS across the full membrane with dimensions, something we couldn't do in BioNetGen. Initially we focused on ensuring Smoldyn was able to represent the catalytic and deactivation reactions with a constant amount of SOS, using the rates discovered in past research. Then we added the binding and unbinding trait of SOS by taking the rates in the same manner. After developing a valid model with boundaries, we produced histograms of the percentage of active Ras out of total Ras for several corral sizes for comparison to the histograms produced by Lee. et al.

Result: We successfully developed a Smoldyn model that could replicate the results of the BioNetGen model seen in Lee et al. Analyzing the graphs produced by our model, we were able to confirm that as SOS binded and unbinded to the membrane anchored-Ras, RasGTP levels spiked up and down respectively. The histograms demonstrated the basic finding that as the corral size increases, the quantized distribution collapses. This was also seen in prior work.

Discussion: These results demonstrate that we can reproduce quantized activation in a 2D Smoldyn model, which can be used to examine the relationship between Ras and SOS and validate the ability of a single SOS molecule to activate hundreds of Ras molecules. We are still investigating how diffusion limitation impacts the collapse seen in the histogram.

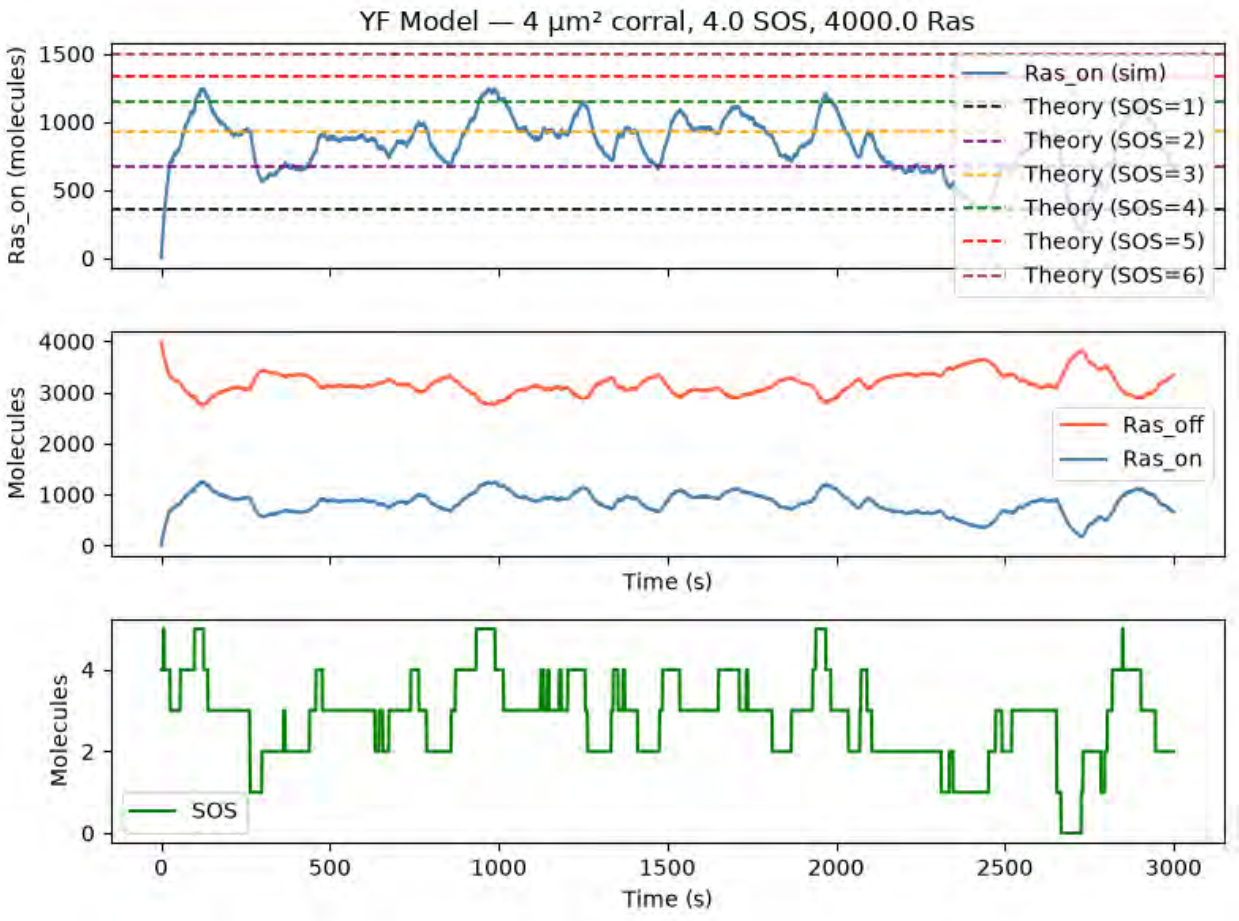

Figure A: Graphs produced by the Smoldyn simulation showing processivity of SOS.

References:

Lee, A. A. et al. Bimodality in Ras signaling originates from processivity of the Ras activator SOS without deterministic bistability. Sci. Adv. 10, eadi0707 (2024).

Katherine A. Yonosh, James R. Faeder. Mathematical modeling predicts quantization of Ras activation in membrane corrals, 21 October 2025, PREPRINT (Version 1) available at Research Square [https://doi.org/10.21203/rs.3.rs-7889340/v1]

Characterizing the Effects of Profilin-2 Depletion on Cytoskeletal Regulation in Chromophobe Renal Carcinoma Cells

Vishruth Vignesh[1], Dave Gau, PhD[2], Alison Buck, MS[2]
[1]Conestoga High School, Berwyn, PA; [2]University of Pittsburgh, Pittsburgh, PA

Background: Chromophobe renal carcinoma (ChRCC) is a rare subtype of renal carcinoma, accounting for about 5% of all renal cancer cases[1]. Although localized ChRCC is treated surgically, therapeutic options remain limited[1]. Unfortunately, surgery is a highly invasive form of treatment, with many surgical measures requiring a partial or full nephrectomy[2]. Profilin-2 (PFN2) is an actin-binding protein that plays a significant role in actin polymerization, which is the process of G-actin monomers self-assembling into long polymerized filaments known as F-actin[4]. This role is vital to cell motility and cytokinesis[3]. Knocking down PFN2 could potentially bring insight into its role during ChRCC progression. This approach could lead to future development of a therapeutic drug treatment for ChRCC.

Methods: The UOK ChRCC cell line was cultured and passaged in DMEM1X S+ media for 3-4 days until the cells became confluent. Then, the cells were plated in a 6-well plate with 200,000 cells per well, where the cells were transfected with their respective siRNA constructs to induce PFN2 knockdown. Within 24 hours of the transfection, a media change was performed. The cells were then plated onto a collagen coated plate for Immunostaining at 10,000 cells per well. These immunostained cells were imaged on a confocal 60x microscope with an oil immersion lens. Overall, ten images were taken per well for each group, and then analyzed on ImageJ Fiji by measuring intensity, to record the morphology of the cells.

Results: We quantified the actin spreading and mitochondrial area following the knockdown of PFN2 in UOK CHRCC cells. Compared to the control cells, the PFN2 knockdown did not demonstrate a statistically significant difference in the actin area (Fig.1). Furthermore, the mitochondrial assessment remained comparable between the control and PFN2 knockdown cells (Fig. 2). Based on our experimental observations, the actin fiber area and mitochondrial assessment remain uniform despite a PFN2 knockdown. Although quantification did not reflect the visual results shown in Fig. 3, future studies could attempt to further understand the actin protrusion disruption.

Conclusions: In this study, we investigated the role of PFN2 manipulation in regulating ChRCC cytoskeleton. From the quantitative analysis of the immunostaining, no significant difference was observed in the actin quantity or mitochondrial area under the conditions tested. Future studies could investigate possible compensatory mechanisms by proteins like PFN1, or the limited existence of PFN2 in the ChRCC cells. These preliminary findings suggest that PFN2 knockdown does not significantly affect total actin fiber area or mitochondrial area under the conditions tested.

However, additional experiments are needed to confirm these observations and further define the role of PFN2 in cytoskeletal regulation.

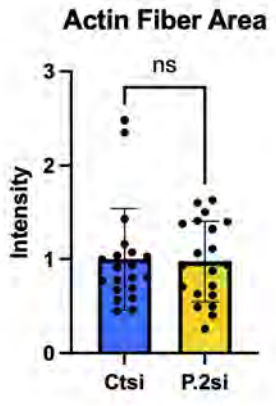

Figure 1: Quantification of actin intensity in PFN2 KD vs. Ct. UOK cells

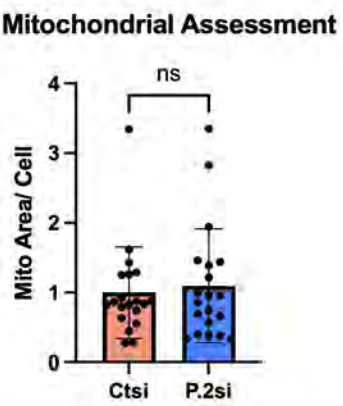

Figure 2: Quantification of mitochondrial area in PFN vs Ct. UOK cells

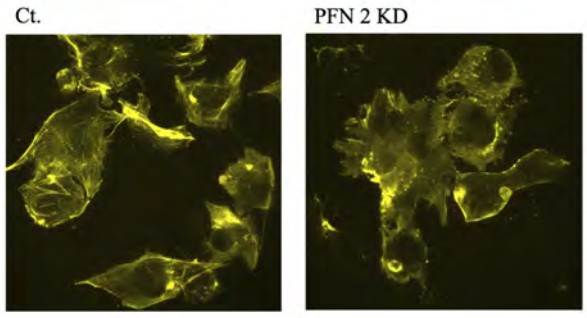

Figure 3: Immunostained confocal 60x images demonstrating actin disruption in PFN2 KD vs Ct.

References:

1. Garje, R., et al. *Comprehensive review of chromophobe renal cell carcinoma.* Critical Reviews in Oncology/Hematology. 2021.
2. *Chromophobe Renal Cell Carcinoma with Radiologic-Pathologic Correlation, Radiographics* (2021).
3. Pollard, T. D., & Cooper, J. A. *Actin, a central player in cell shape and movement.* Science.

Individual sex hormones differentially regulate skeletal muscle myogenesis in an in vitro model

Scholar: Nithila Vijayan

High School: South Fayette High School, McDonald, Pennsylvania

Lab: Amrita Sahu, PhD

Mentor: Jagruti Kosaraju, MS

Site: Technology Drive X

Background: Women are disproportionately affected by musculoskeletal injuries, yet female-specific musculoskeletal research remains limited. Hormonal contraceptives (HCs), widely used clinically, contain exogenous estrogen and/or progesterone that may enhance muscle strength and resilience, though it remains unclear how individual hormones and specific stages of muscle regeneration contribute to this effect. Our prior *in vivo* work found that high-dose combined estrogen and progesterone HCs increased skeletal muscle myofiber size in female mice, but could not isolate which hormone or which stage of myogenesis—proliferation or differentiation—drives this response, since both occur simultaneously in the whole animal. To uncouple these variables, we developed an *in vitro* model using primary female satellite cells (muscle stem cells) treated with individual hormone components at defined stages of myogenesis. The goal of this study is to determine the independent, dose-dependent, and stage-specific effects of exogenous estrogen and progestins on skeletal muscle myogenesis.

Methods: Primary female satellite cells were seeded at equal density and treated with vehicle control or synthetic hormone: ethinyl estradiol (EE; 5 pM or 10 pM, ethanol vehicle), levonorgestrel (LNG; 2 nM or 5 nM, DMSO vehicle), or desogestrel (DSG; 10 nM or 15 nM, DMSO vehicle), alongside a media-only control. To isolate the myogenic stage at which each hormone acts, treatment was administered under three parallel experimental designs: during proliferation only, during differentiation only, or throughout both proliferation and differentiation. Myogenic outcomes were assessed by immunofluorescence staining for embryonic myosin heavy chain (eMHC) and DAPI, quantifying total multinucleated fibers, fiber length and width, nuclear fusion index, number of $eMHC^+$ fibers, and total nuclei per image. Group comparisons will be made using one-way ANOVA with Tukey's honest significant difference post-hoc test ($n \geq 3$ independent biological replicates).

Results: Multinucleated fiber number, fiber length and width, nuclear fusion index, $eMHC^+$ fiber number, and total nuclei are currently being quantified across hormone type (EE, LNG, DSG), dose, and treatment window (proliferation-only, differentiation-only, or both) to determine which hormone and which stage of myogenesis is most responsive to exogenous hormone exposure.

Conclusion: This *in vitro* model will allow us to isolate the individual contributions of estrogen versus progestins to skeletal muscle myogenesis, and determine whether their effects are proliferation-driven, differentiation-driven, or both. These findings will help clarify the cellular mechanisms underlying the HC-associated increase in myofiber size observed in our prior *in vivo* work, with the ultimate goal of informing which hormone formulations and dosing strategies may best support muscle health and recovery in women.

How Genetic Variants has an effect on addiction and substance abuse disorder.

Ahana Vyas

Allderdice High School, Pittsburgh, PA.

PI: Dennis Kostka

Mentor: Elizabeth Gilfeather

Site: CompBio

Genetic variants are what makes everyone different, and sometimes they can be linked to certain disorders. Previous genetic studies have discovered that environmental factors have also been linked to certain disorders. My project asks how genetic variants affect disorders such as addiction, and substance abuse disorders. One way to understand this is through a process known as GWAS, which stands for Genomic Wide Association Study. This is the process of scanning the DNA and uncovering the genetic variant that is linked to a certain trait or disease. Furthermore, I used publicly available GWAS data to analyze the relations between genetic variants and transcription. I also noticed that environmental factors have a significant impact on disorders, which implies that other external factors are responsible for these disorders. This includes how one is brought up from their early childhood, and how certain factors affect the outcome of the present time. A lot of the information I have learned has come from recent research papers highlighting the issues I am currently researching as well. This includes the process of how genetic variants are identified. This is through the process of sequencing the DNA, which means trying to figure out the correct order of the transcription. Then this is compared and the genetic variant is identified.

Lysosomal repair pathways in B2B senescent cells

Scholar: Isha Vyawahare

High School: North Allegheny High School, Wexford, PA

PI of lab: Jay Tan, PhD

Mentor(s): Xiaojie Yu, PhD; Fangling Tian, PhD

Site: Technology Drive X

Background: The lysosome is an organelle that functions in the degradation and recycling of cellular components, helping to maintain cellular homeostasis and overall health. However, lysosomal dysfunction and damage are increasingly linked to aging. While lysosome repair pathways such as ESCRT and PITT have been discovered, their repair pathway protein recruitment in cells under stress is incompletely understood. Cellular senescence is a state that can be induced by various types of cellular damage and is characterized by cell cycle arrest while remaining metabolically active. Senescent cells accumulate as we age and are associated with impaired lysosomal function. This study investigates the recruitment of lysosome repair proteins in senescent cells.

Methods: Human bronchial epithelial cell line Beas-2B (B2B) was treated with doxorubicin to induce senescence. Senescent cells and healthy cells were treated with L-leucyl-L-leucine methyl ester (LLOMe) to induce lysosomal damage. Both senescent cells and control healthy cells were used for fixed-cell immunofluorescence staining to detect recruitment of repair pathway proteins to damaged lysosomes, with LAMP1 used as a lysosome marker.

Results: ESCRT pathway proteins IST1 and ALIX had decreased recruitment to lysosomes in senescent B2B cells compared to healthy B2B cells. PITT pathway protein ORP9 decreased recruitment as well. However, PITT pathway protein PI4K2A did not show a loss in colocalization in senescent cells when compared to controls. p62, a protein involved in lysophagy, was also found to have decreased recruitment in senescent cells.

Conclusion: This study shows that several proteins involved in ESCRT, PITT, and lysophagy processes have altered recruitment in senescent cells. This opens the door to a variety of next steps, such as investigating whether lysosome dysfunction can be explained by the changes in repair protein recruitment in aging and stressed cells.

Systematically and proactively testing variant effects for ACADM

Scholar: Hongyi Wang

High School: North Allegheny Senior High School, Pittsburgh, PA

Lab: Frederick (Fritz) P. Roth, PhD

Mentor: Warren van Loggerenberg, PhD

Site: Computational Biology

Abstract: Sequencing-based diagnosis of Medium-Chain Acyl-CoA Dehydrogenase Deficiency (MCADD) is severely limited by the difficulty of distinguishing neutral from functional variants. Although recurrent variants can be statistically associated with disease, most rare missense variants in disease genes must still be interpreted as "variants of uncertain significance" (VUS). Where a faithful assay of gene function is available, patient variants can be individually tested in a '*reactive*' manner. Alternatively, scalable functional assays can enable '*proactive*' testing of *all possible* missense variants, so that testing results are available even before first clinical presentation of a variant. Here, we propose to develop and validate a scalable, multiplexed cell-culture assay that can be applied at scale to assess the function of all possible missense variants in medium-chain acyl-CoA dehydrogenase (MCAD; encoded by *ACADM*), generating comprehensive missense variant effect map. The proposed map promises to improve diagnostic interpretation, provide training data for computational variant-effect predictors, and support the development of precision medicine therapies.

Title: Investigating the Role of FANCD2 Monoubiquitination in Regulating DNA Repair Pathway in MLL-AF9 Leukemia

Scholar: Andy Weng

College: Case Western Reserve University, Cleveland, OH

PI: Wei Du, MD, PhD

Mentor(s): Jiayang Bao, Oliver Freund

Site: Cancer Biology

Background: Fanconi anemia (FA) is a hereditary DNA repair disorder that causes bone marrow failure, genomic instabilities, and an increased leukemia risk. FANCD2 is a key FA pathway protein activated by monoubiquitination to coordinate DNA repair. Previous studies show FANCD2 regulates DNA double-strand repair in MLL-AF9 leukemia by competing with non-homologous end joining (NHEJ) factors of Ku70/80 binding to the MLL-AF9 fusion, influencing DNA repair pathway selection. However, whether monoubiquitination of FANCD2 is essential for this interaction is unclear. This study examines the role of FANCD2 ubiquitination in DNA repair pathway selection and its clinical implications in leukemia pathogenesis and treatment.

Methods: Utilizing PD20 cells as a blank test bed, we introduced wild-type FANCD2 (WT-D2) and FANCD2 mutant (KR-D2, K561R) using viral transduction, which was then followed by selection using puromycin to establish our stable cell lines. Our cells were subsequently transduced with MLL-AF9 constructs. MLL-AF9 fusion expression was confirmed by Western blot. Co-immunoprecipitation was utilized to examine the interactions between the MLL N-terminus and FANCD2, as well as Ku70/80. The differences of the protein binding between WT-D2 and KR-D2 were analyzed to determine whether the MLL-AF9 DNA repair pathway selection is affected by FANCD2 monoubiquitination.

Results: AlphaFold modeling of the isolated MLL-N1400 construct predicted that the lys561arg mutation, which prevents monoubiquitination, does not significantly affect FANCD2-MLL-N1400 interactions. Previously generated plasmids were extracted, transformed into bacteria, and their construct verified via Western blotting. We also successfully transduced various cell lines with MA9 virus, creating foundations for future studies on protein interactions. The conduction of various preliminary experiments improved handling for future experiments and projects, such as Western blots and immunoprecipitation.

Conclusion: We have established cell lines, plasmids, and experimental methods to further explore the role of monoubiquitinating FANCD2 in MLL-AF9 leukemia. While AlphaFold modeling of the MLL-N1400 construct predicts that the K561R mutation does not drastically disrupt the binding of FANCD2-MLL-N1400, future studies may provide insights into whether the loss of monoubiquitination affects protein bindings and the DNA repair pathway selections in the full MLL-AF9 fusion context.

Title: Treatment combination for multicompartment hemorrhage and midline shift
Scholar: Blake Whiteman
High School/College/City/State: University of Pittsburgh, Oakland, PA
PI of group/lab: Dr. Brown, MD
Mentor(s): Dr. Brown, MD and Dr. Leeper, MD
Site: Surgery

Background: Traumatic brain injury (TBI) is a leading cause of death after injury. Increased time to treatment results in higher mortality rates, signifying fast transport to trauma centers is ideal. Air medical transport (AMT) with helicopters is faster than ground emergency medical services (GEMS), and prior research shows AMT for selected patients with severe TBI increases survival. Oftentimes, plasma, the liquid component of blood, is administered to support the patient. It is unknown whether there is a synergistic effect of transport mode and plasma transfusion to improve patient outcomes in TBI. Our objective was to evaluate the results of the 4 different treatment combinations to determine if lower mortality is seen in AMT and plasma transfusion.
Methods: Patients in the National Trauma Databank from 2020-2023 were included that had TBI with midline shift or multicompartment hemorrhage. We excluded patients with GCS 3 and head AIS of 6 indicated non-survivable TBI. Patients were classified into one of four treatment groups: GEMS/No plasma (reference group), GEMS+plasma, AMT/No plasma, and AMT+plasma. Our primary outcome was in-hospital mortality. Multi-level logistic regression models were developed to determine the association between mortality and the treatment groups while adjusting for demographics, vital signs, injury severity score, mechanism of injury, complications, and surgical procedures. Given a large selection bias present for patients receiving plasma, inverse propensity weighting was used to account for that likelihood of receiving plasma among all patients. We separately evaluated subgroups of patients with isolated TBI and patients with polytrauma TBI (non-head region AIS≥3).
Results: A total of 256,040 patients were included, with 202,362 isolated TBI and 53,678 polytrauma TBI patients. Overall patients receiving plasma regardless of transport mode, we're significantly severely injured with lower systolic blood pressure, higher pulse, lower GCS, higher injury severity score, and more than double unadjusted mortality (Table). When compared to GEMS/No plasma patients, AMT/No plasma was associated with lower mortality (aOR 0.80; 95%CI 0.75-0.85, p<0.01). Both plasma groups had higher mortality compared to GEMS/No plasma, with a lower magnitude of mortality in the AMT+plasma group (aOR 1.37; 95%CI 1.21-1.55, p<0.01) compared to GEMS+plasma (aOR 1.46; 95%CI 1.38-1.54, p<0.01). Similar results were seen in the isolated TBI group. In the polytrauma group AMT/No plasma was also associated with lower mortality (aOR 0.72; 95%CI 0.64-0.82, p<0.01) and GEMS+plasma with higher mortality (aOR 1.56; 95CI 1.38-1.77, p<0.01). However, the mortality risk was mitigated in the AMT+plasma group (aOR 0.99; 95%CI 0.77-1.29, p=0.99).

	GEMS/No plasma	AMT/No plasma	GEMS+Plasma	AMT+Plasma	p-value
N	192950	37726	19638	6788	
Age, median (IQR)	64 (43, 77)	59 (36, 74)	53 (31, 70)	51 (31, 68)	<0.001
Blunt injury	185994 (96.4%)	35705 (94.6%)	17065 (86.9%)	6099 (89.8%)	<0.001
Penetrating injury	6956 (3.6%)	2021 (5.4%)	2573 (13.1%)	689 (10.2%)	
SBP, median (IQR)	142 (126, 162)	136 (120, 154)	125 (96, 151)	110 (88, 138)	<0.001
Pulse median (IQR)	85 (73, 100)	87 (74, 102)	99 (79, 122)	100 (81, 121.5)	<0.001
Respiratory Rate, median (IQR)	18 (16, 20)	18 (16, 21)	19 (16, 23)	19 (16, 22)	<0.001
GCS median (IQR)	14 (10, 15)	10 (3, 15)	5 (3, 14)	3 (3, 7)	<0.001
ISS, median (IQR)	17 (11, 26)	24 (16, 27)	29 (25, 38)	30 (25, 41)	<0.001
Mortality	29642 (15.4%)	8389 (22.2%)	9572 (48.7%)	3354 (49.4%)	<0.001

Conclusion: Patients receiving plasma after TBI are significantly more severely injured than patients that do not. Our results suggest that AMT in these groups of patients is likely beneficial overall. Among the most severely injured polytrauma TBI patients, there may be synergistic effects of both AMT and early plasma transfusion. Given limitations of retrospective observational data, future prospective trials are warranted to confirm the potential benefits of transport mode and plasma transfusion in severely injured patients with TBI.

Developing a Novel Small Animal Model of Pancreatic Duct Stenting

Scholar: Bradyn Whiteman

School: University of Pittsburgh, Oakland, Pennsylvania

PI of group/lab: Dr. Genia Dubrovsky

Mentor: Dr. Genia Dubrovsky

Site: Surgery

Background: Pancreatic duct (PD) stents are commonly placed via endoscopy to treat a number of medical conditions. At the time of distal pancreatectomy, PD stents have been studied in order to reduce post-operative pancreatic fistula rates. Unfortunately, current stent designs have significant limitations, including bacterial colonization, stent occlusion, and premature stent migration. In order to improve on existing PD stent designs, we sought to first develop a safe and clinically-relevant small animal model of PD stenting. We therefore tested various methods of PD stent implantation in a rat model.

Methods: 29 Sprague-Dawley retired male breeder rats (350-700 grams) were anesthetized and underwent laparotomy for stent placement into the fused bile/pancreatic duct. Five different stent designs were tested using a 1.0 cm segment of a 20 gauge catheter: a smooth stent, a smooth stent sutured to the bowel, a flanged stent, a flanged stent with sutures to push out flanges, and a flanged stent sutured to the bowel. Rat survival and need for early euthanasia was measured. The stents were monitored with weekly CT scans of the rats, and stent presence/passage was also determined at the time of euthanization.

Results: When analyzing the survival rates of the rats at the 95% confidence level, it was determined that the type of stent has no statistical significance regarding the death of the rats when comparing each design to design model #1 with a chi-squared test for independence. Design #1 vs. design #2, p=1. Design#1 vs. design #3, p=.1967. Design #1 vs. design #4, p=1. Design #1 vs. design #5, p=.7782. However, when analyzing the presence rate of the stent at 95% confidence, it was determined that the type of stent affects the movement of the stent when comparing each design to design model #1 using a chi-squared test for independence. Design #1 vs. design #2, p=.0143. Design #1 vs. design #3, p=.2850. Design #1 vs. Design #4, p=.0284. Design #1 vs. design #5, p=.0082

Conclusion: By measuring statistical significance between the migration of the stents, we can confidently say that using stent designs #2, #4, or #5 will resist migration much better than stent designs #1 or #3, meaning that stent designs #2, #4, and #5 are much better for application so that they do not pass and will not require a redo operation. We also measured that the fatality rate is not dependent on the design, rather it is dependent on spontaneity, meaning that no designs are necessarily more harmful, and death/injury likely stemming from confounding variables within the surgery process.

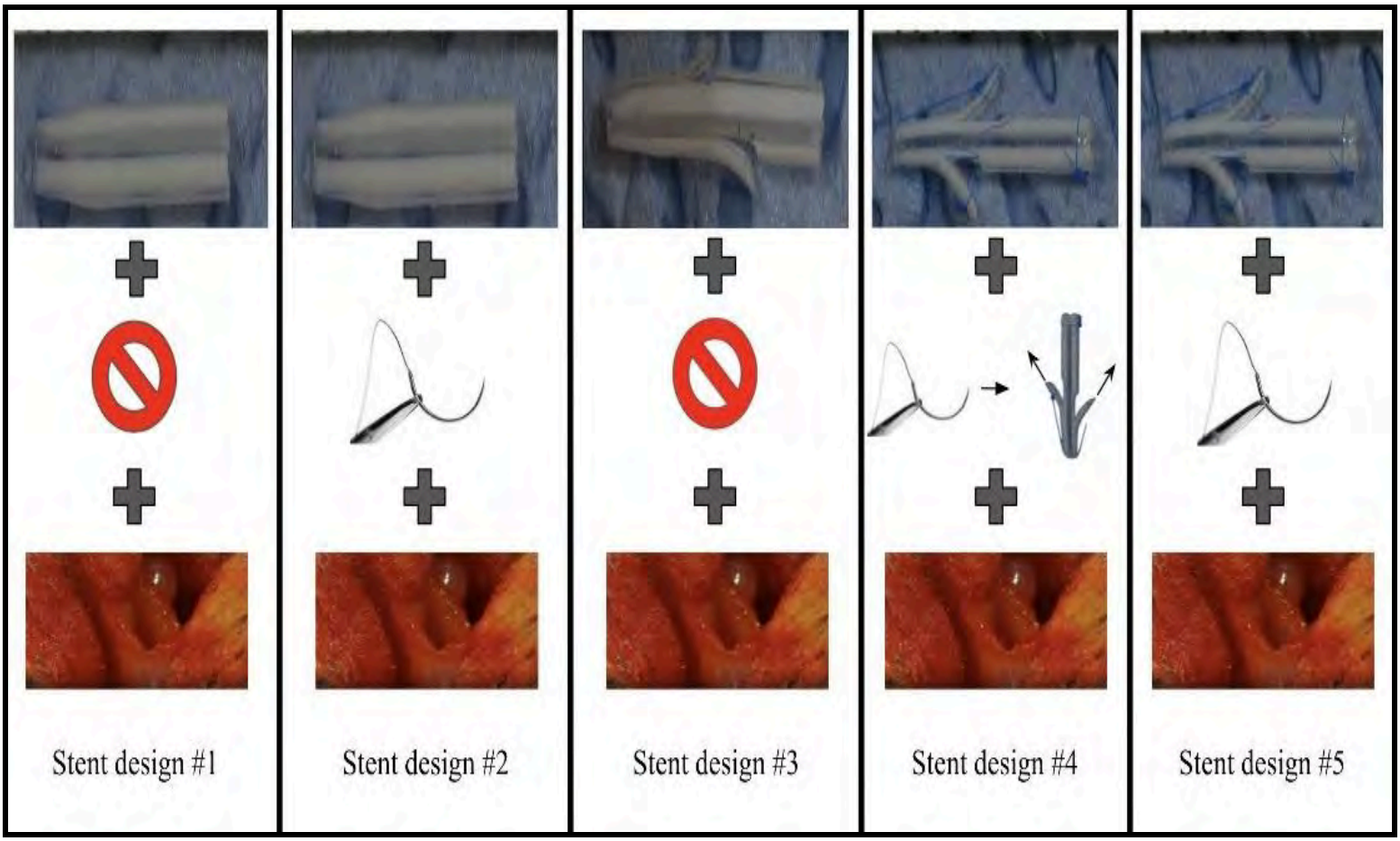
Stent design #1
Stent design #2
Stent design #3
Stent design #4
Stent design #5

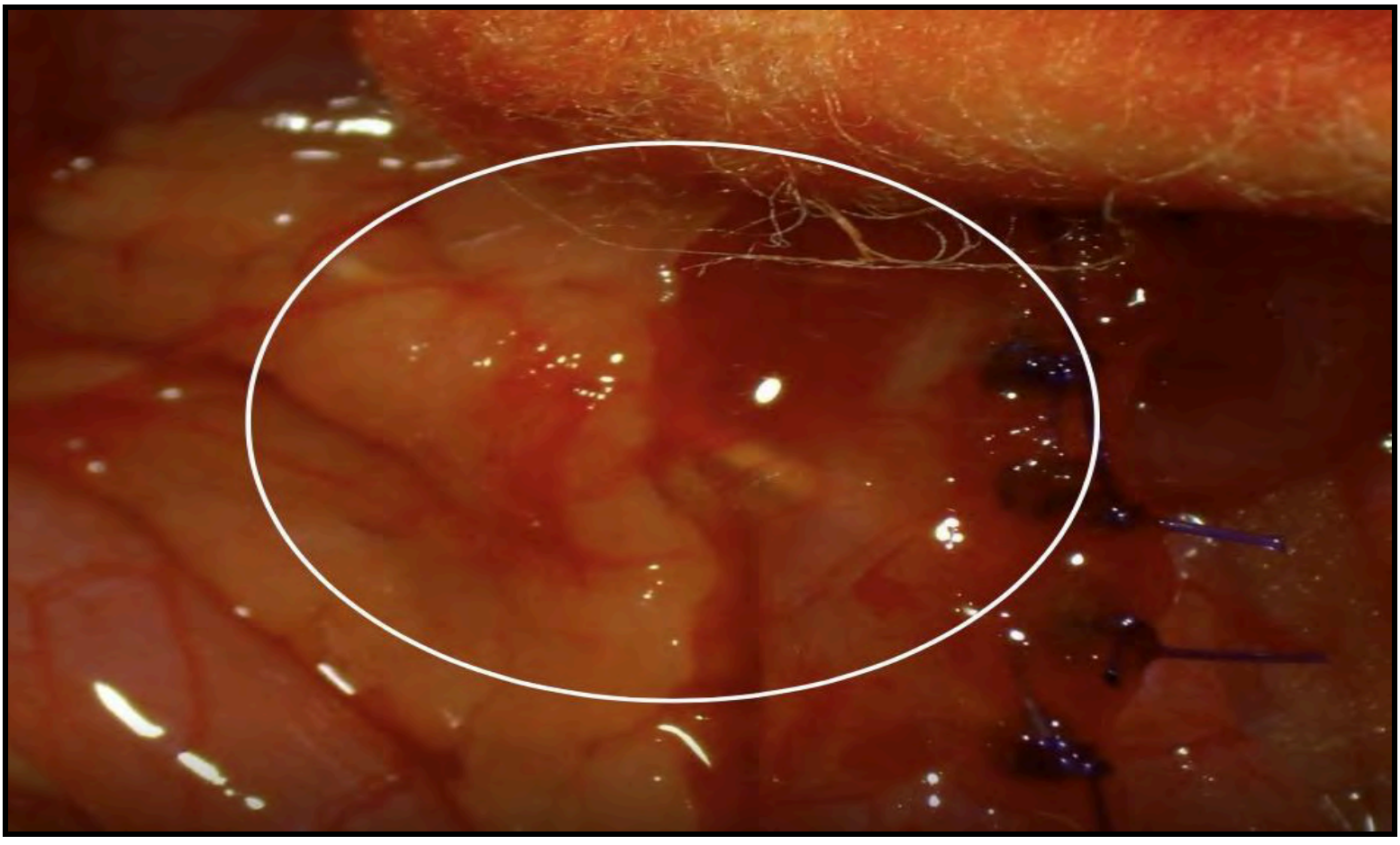

Ablation of RAGE Abrogates muco-inflammatory features of Type 2 COPD and Non-type 2 Asthma in experimental models

Gabrielle Wilkins, Oakland Catholic High School, Pittsburgh, Pennsylvania, United States.
Dr. Timothy Perkins, PhD, The University of Pittsburgh School of Medicine, UPMC Hillman Cancer Center, Pittsburgh, Pennsylvania, United States

Abstract– This project encompasses a primary goal of identifying a protein that is a perpetrator of the inflammation demonstrated in type 2 COPD and non-type 2 asthma patients. This project evaluates the effectiveness of targeting this protein, the receptor, RAGE, which drives inflammation and mucus production in the lungs. Considering the primary goal, Mice and primary human cells are subjected to various experimental models of disease with the intent of identifying proteins involved in RAGE-driven inflammation to enhance the development of potential treatments.

Introduction – COPD and asthma are both inflammatory, respiratory diseases that affect approximately 500 million people. While genetics influence susceptibility, environmental stressors such as, secondhand smoking and air pollution cause the effect of damaged cells and tissue. Thus, leading to the adverse side effects, which include, but aren't limited to, congested breathing and viscous mucus production. Damaged proteins from external factors (the environment), release from the inside of the cell to the outside, binding to a multi-ligand receptor, RAGE (Receptor for Advanced Glycation End-products) triggering a cascade of inflammation, drawing neutrophils and eosinophils to the lung tissue. The mechanism of action of this protein, which is abundantly prominent within the inflammatory response, is poorly understood and needs to be further investigated. We hypothesize that ablation of RAGE will suppress and limit inflammation and mucus production.

Methods– To achieve the primary goal, specific proteins involved in the downstream response were identified and the effects of RAGE ablation on these proteins were evaluated. This was accomplished by performing multiple western blots and Enzyme linked-immunosorbent assays (ELISA) with several different target proteins and specimens, as well as QRT-PCR analyses. We used an experimental model of non-type 2 asthma in which mice are intranasally exposed to the fungal allergen Alternaria alternata (ALT) combined with the bacterial second messenger cyclic di-GMP (CDG), which induces neutrophil-dominant airway inflammation. In addition to a healthy control group, (wild-type mice exposed to saline), we also exposed four mouse strains with ALT/CDG including wild-type, RAGE-null, ST2-null and IL-33-null. In attempts to harvest data that measures the inflammatory response, bronchoalveolar lavage fluid and lungs were extracted from every mouse group. The anatomical parts were used for the following experiments: QRT-PCR, Western blots, ELISA, and slides for a microscope to conduct cell

counting (cytospins). We stimulated non-diseased (control) and COPD human airway epithelial cells to the type 2 cytokines IL-13 or IL-4 with or without inhibition of RAGE and evaluated the effects on mucus and inflammatory markers.

Results – Allergens, which in our experiment happened to be *Alternaria Alternata* with CDG, triggered IL-33 production in mouse airways. However, when RAGE and IL-33 are eliminated from the lungs, inflammation is significantly lowered and even suppressed. An interesting finding is that when the receptor of IL-33 is removed, IL-33 is still produced, and inflammation persists. This suggests that although ST2 is known to drive IL-33 signaling, in this context of non-type 2 inflammation, there may be an alternative pathway driving IL-33 induced non-type 2 inflammation. It is now hypothesized within our lab that there is another signaling pathway that IL-33 uses to invoke non-type 2, neutrophilic inflammation in response to allergens. We found that ablation of RAGE reduced type 2 cytokine induced expression of mucus markers and secretion of inflammatory chemokines.

Discussion – RAGE is a receptor that is very complex to understand given its ability to bind to multiple ligands and activate several signaling pathways. Through examining the effects of blocking RAGE, this provides novel understanding of the receptor's function. Enhancing our understanding of RAGE promotes disease manifestation, supports treatment discovery efforts which may also help disease awareness for other diseases like high blood pressure, stroke, heart disease, and immune deficiency. Regarding this project, blocking of the receptor as well as IL-33 serves as an opportunity to develop treatment for non-type 2 asthma patients to have drugs that target the root cause of injury.

Association Between Slow Wave and Rapid Eye Movement Sleep and Cognitive Outcomes

Sarah B. Winikoff, Dr. Marrisa Gogniat

Pittsburgh Creative and Performing Arts 6-12, Pittsburgh, PA; University of Pittsburgh Hillman Cancer Center Academy, Pittsburgh, PA

Abstract

Impaired sleep architecture is a known risk factor for neurodegeneration and Alzheimer's Disease. This observational study examines a cohort of 130 cognitively healthy older adults over a week of sleep monitoring in comparison with neuropsychological testing. Sleep stages were recorded by a Fit Bit that estimates sleep stage by measuring heart rate patterns, heart rate variability, and body movement.

Introduction

Alzheimer's disease (AD) is the leading cause of dementia currently, accounting for an estimated 60-80% of all cases [1]. Accumulation of the protein amyloid beta (Aβ) outside neurons and twisted strands of the protein tau inside neurons lead to neurodegeneration and cell death in AD [2]. The neurons damaged first are those in parts of the brain responsible for memory, language, and thinking, which is why the first clinical symptoms of Alzheimer's disease tend to be cognitive problems. Age, genetics, and family history are risk factors that cannot be changed; however, approximately 35% of AD risk may be influenced by modifiable risk factors, including sleep. The consolidation of memories, learning, thinking, behaviors, and emotions are key neurobiological processes that are affected by impaired sleep. Anti-inflammatory processes, such as the clearance of toxins including amyloid beta plaques, may contribute to the cascade of events leading to AD pathogenesis, including neurodegeneration and brain atrophy.[3] The protective mechanisms of different stages of sleep in association to cognitive outcomes has yet to be well understood.

Methods

In this study, we collected sleep data using Fitbit Aspire 3, a wearable activity wristband with an embedded triaxial accelerometer. Participants at the Alzheimer's Disease Research Center (N = 130; 75.72) wore a FitBit Inspire 3, for a ~7 day consecutive period at home to estimate REM sleep and Deep Sleep. Cross-sectional linear regression models for each sleep stage were adjusted for age, sex, and education. Exclusionary criteria included a diagnosis of dementia and severe mental health disorders.

Results

SWS and REM sleep were strongly, positively correlated (r=0.635). Significant test results for measuring Deep Sleep and REM Sleep were associated with language, attention, and executive function, with greater average time spent in the sleep stage associated with better scoring, and less SWS and REM associated with worse outcome for three of the tests. An explanation for these findings is that REM and Deep sleep are associated with frontal white matter integrity, which plays an essential role in mediating the connectivity of the central nervous system.

Characteristics of Sample Population

Statistics

		age	education	avg_deep_sleep	avg_rem	sex
N	Valid	130	130	130	130	130
	Missing	0	0	0	0	0
Mean		75.72	16.12	49.79	70.79	.35
Std. Deviation		7.201	2.591	17.170	25.672	.478

Correlations

		avg_rem	avg_deep_sleep
avg_rem	Pearson Correlation	1	.635***
	Sig. (2-tailed)		<.001
	N	130	130
avg_deep_sleep	Pearson Correlation	.635***	1
	Sig. (2-tailed)	<.001	
	N	130	130

***. Correlation is significant at the 0.001 level (2-tailed).

Discussion

Variation in sleep stages and markers of increased sleep fragmentation may offer a potential noninvasive and cost-effective biomarker for dementia risk, as well as possible targets for intervention in middle-age to older adults to slow cognitive decline. Furthermore, longitudinal studies are needed to measure participants over time to observe the biological and cognitive impact of specific sleep stage duration in comparison to baseline cognition and validate these findings.

References

Patel AK, Reddy V, Shumway KR, et al. Physiology, Sleep Stages. [Updated 2024 Jan 26]. In: StatPearls [Internet]. Treasure Island (FL): StatPearls Publishing; 2026 Jan-. Available from: https://www.ncbi.nlm.nih.gov/books/NBK526132/

Aktan Süzgün M, Tang Q, Stefani A. Sleep Abnormalities and Risk of Alzheimer's Disease. Curr Neurol Neurosci Rep. 2025 Oct 13;25(1):67. doi: 10.1007/s11910-025-01451-5. PMID: 41082137; PMCID: PMC12518432.

Jiang-Xie LF, Drieu A, Bhasiin K, Quintero D, Smirnov I and Kipnis J. Neuronal dynamics direct cerebrospinal fluid perfusion and brain clearance. Nature. Feb. 28, 2024. DOI: 10.1038/s41586-024-07108-6 2025
Alzheimer's disease facts and figures. Alzheimers Dement. 2025 Apr 29;21(4):e70235. doi: 10.1002/alz.70235. PMCID: PMC12040760.

Investigating IL-13ra1 Expression to Define the Role of $CD8^+$ T Cell-Produced IL-13 in the Tumor Microenvironment

Scholar: Catherine Yang

Education: Richard Montgomery High School, Rockville, MD

PI: Amanda Poholek, PhD

Mentors: Xingjian Qiu, Aaron Yang

Site: Immunology and Cancer Immunotherapy

Enhancer of zeste homolog 2 (Ezh2) mediates trimethylation of histone 3 lysine 27 (H3K27me3), a repressive epigenetic modification that regulates gene expression and T-cell differentiation. Previous work from our lab demonstrated that Ezh2 knockout (KO) $CD8^+$ T cells demonstrate reduced exhaustion and produce increased levels of interleukin-13 (IL-13), a type 2 cytokine not typically associated with $CD8^+$ T cells. The functional consequences of $CD8^+$ T cell-derived IL-13 in the tumor microenvironment are less well understood. Identifying receptor-expressing cell populations is a first step towards clarifying possible functions.

In this study, we investigated IL-13ra1 expression across immune cell populations within the B16-GP melanoma tumor using flow cytometry. An unconjugated primary antibody and fluorescent secondary antibody were used to stain for cells expressing IL-13ra1. Analysis of immune subsets revealed clear differences in IL-13ra1 expression among cell types, with T cells serving as a largely negative population while myeloid populations, including dendritic cells and macrophages, exhibited detectable receptor expression. Comparison of wild-type and Ezh2 KO tumors showed no substantial differences in IL-13ra1 expression, suggesting that increased IL-13 production by Ezh2-deficient $CD8^+$ T cells does not alter receptor abundance.

These findings suggest that $CD8^+$ T cell-derived IL-13 may act through existing IL-13ra1 populations rather than changes in receptor expression. Future work may include staining for other specific subpopulations of immune cells, including cDC1 and cDC2 dendritic cells. In addition, comparing phosphorylated STAT6 (pSTAT6) expression between wild-type and Ezh2 KO tumors would help determine whether increased IL-13 production results in enhanced downstream IL-13 signaling despite unchanged receptor expression.

Vascular Junction Density is Significantly Reduced in APOE4 Compared to APOE3 Carriers in a Preclinical Alzheimer's Disease Model

Scholar: Grace Yang

High School: North Allegheny Intermediate High School, Wexford, PA

Lab: Bistra Iordanova, PhD

Mentor: Yucheng Shen

Site: Tech Drive X (TDX)

Background:

More than 7 million Americans are living with AD. While AD is the most common cause of dementia, there is no present cure. Apolipoprotein E (APOE) gene, which regulates lipid carriers in the body, is the strongest genetic risk factor for AD. APOE4, existing in 25% of the population, is associated with an up to 12-fold higher risk of developing AD than APOE3, the most common allele of APOE. Previous study shows APOE4 carriers are correlated with reduced cerebral blood flow (CBF) without fully understanding the underlying mechanism. We hypothesize that the abnormal CBF pattern of APOE4 carriers is a result of distinct vascular morphology.

Method:

We used Late Onset Alzheimer's mice models hAPOE3/4 with green fluorescent protein (GFP) expressed in microglia, male and female, ages 4.5 months to 11.8667 months (APOE3: n = 10, APOE4: n = 11). Acute cortical window was installed, and mice were imaged under urethane anesthesia with a multiphoton Laser Scanner. We injected a 1x PBS solution of 2 mg/mL Sulforhodamine SR101 and imaged the vasculature with two-photon laser excitation at 920 nm. We segmented the vasculature by linear unmixing between channels and binarization. Then, we extracted the skeletons of the vessel segmentations and quantified tortuosity and junction density. Two-tailed unpaired student's t-test was used to compare genotype differences.

Results:

Although there is no significant difference observed in vascular tortuosity between APOE3 and APOE4 ($p = 0.903$), our analysis shows that APOE4 group has significantly lower junction density ($p = 0.029$).

Conclusion:

This study confirms our hypothesis that APOE4 has different vascular morphology compared to APOE3 in junction density, though they share similar vascular tortuosity. This may suggest a more progressive capillary loss in APOE carriers and explain the CBF drop. Future studies can explore how these structural changes evolve in ageing.

Title: Functional Dissection of RAX Enhancers in Developing Retina

Scholar: William Zhang
High School: Hampton High School/ Pittsburgh, PA
Affiliations: Al Diri Lab, UPMC Vision Institute, University of Pittsburgh, Department of Ophthalmology
Mentors: Kamakshi Mehta Ph.D., Issam Al Diri Ph.D.

Background: Retinal neurogenesis is a tightly regulated process in which retinal progenitor cells (RPCs) exit the cell cycle and differentiate into neurons or glia under the control of complex transcriptional networks. Epigenomic studies in mice and humans have identified several non-coding elements near the Retina and Anterior Neural Fold Homeobox (Rax) gene, a key regulator of retinal development linked to diseases like anophthalmia and microphthalmia, but their roles as bona fide enhancers in the developing retina remain elusive.

Methods: Putative mouse and human *Rax* enhancer sequences were cloned into the STAGIA3 dual-reporter plasmid containing a minimal promoter. Correct insertion was verified by the sequencing method. To assess enhancer activity, STAGIA3 constructs carrying the candidate enhancers or empty vector controls were introduced into embryonic day 14.5 (E14.5) mouse retinal explants via ex vivo electroporation. Electroporated retinas were cultured for two days, followed by alkaline phosphatase (AP) staining to visualize reporter expression and determine the spatial enhancer activity.

Results: Analysis of existing ChIP-seq and ATAC-seq data revealed candidate enhancer regions for subsequent functional validation. Cloning of human *RAX* enhancer 1 and enhancer 3, as well as the mouse enhancer 3 element, into the STAGIA3 reporter vector was confirmed by Plasmidsaurus sequencing and double digestion. Sequencing showed complete alignment of the inserted enhancer sequences with the corresponding predicted sequences, verifying successful insertion and correct orientation. Additionally, successful retransformation of the plasmid constructs was confirmed prior to downstream procedural applications.

Conclusions: Our results demonstrate that the Mouse RAX-EN3 enhancer is functionally active in mouse E14.5 retina across multiple reporter assays, supporting its role in regulating gene expression during retinogenesis. Ongoing experimentation with human enhancers will determine whether these regulatory activity is conserved across species, providing insights into enhancer function and evolutionary divergence.

Generalizing the ECG-SMART-NET Architecture for Myocardial Infarction Classification on the PTB-XL Database

Erick Zhao[1], Ege Ozkoc[2], Yifan Zuo[2], Murat Akcakaya[2]

[1]*Winchester Thurston High School, Pittsburgh, PA;* [2]*University of Pittsburgh, Pittsburgh, PA*

Abstract *Myocardial infarction (MI) detection from 12-lead ECGs is challenging due to subtle patterns. ECG-SMART-NET, a deep learning architecture that separates temporal and spatial convolutions to mimic clinical ECG interpretation, had previously only been validated on a proprietary dataset. We adapted the architecture to the public PTB-XL database using a custom median beat preprocessing pipeline. On held out data the model achieved 90.34% accuracy and an AUC of 0.9618, showing it generalizes beyond its original dataset.*

Introduction Myocardial infarction (MI) remains a leading cause of cardiovascular mortality, and rapid identification from 12-lead electrocardiography (ECG) is critical for timely care. A clinically important subset of acute coronary occlusions, occlusion myocardial infarctions (OMIs), present with ECG patterns subtle enough that they do not meet traditional ST-elevation MI (STEMI) criteria, which can cause missed or delayed diagnoses. Convolutional neural networks (CNNs) offer a mechanism to automate detection of these high-risk but subtle patterns. Riek et al. recently introduced ECG-SMART-NET [3], a modified ResNet-18 architecture that first learn lead-wise temporal features through $1\times k$ temporal convolutions and then extracts cross-lead spatial concordance/discordance through a single 12×1 spatial convolution placed after the residual stages, mirroring how clinicians sequentially read individual leads before comparing them against one another. On a proprietary regional emergency medical services (EMS) cohort of 10,393 ECGs, ECG-SMART-NET achieved a test AUC of 0.953, outperforming a standard ResNet-18 and a random-forest baseline. This evaluation relied on a single closed dataset however, leaving the architecture's generalizability to independent, publicly available data untested. The objective of this study was to reproduce the ECG-SMART-NET architecture and evaluate whether it's performance holds on the public PTB-XL database, using a binary MI classification task as a generalization benchmark.

Methods *Design*: Retrospective classification study using the public PTB-XL database (PhysioNet) [1,2], a cohort of 21,799 12-lead ECGs from 18,869 patients. Records was mapped via SCP-ECG diagnostic codes into binary superclasses (MI vs. Normal, NORM) and split by unique patient using the database's built-in stratified folds into training (11,974 records), validation (1,495), and test (1,513) sets, preventing patient overlap across splits. *Preprocessing*: Because the original median-beat extraction algorithm was not published, we implemented our own: R-peaks were detected on Lead II of the 500 Hz waveform using the `wfdb` XQRS detector; 600-sample windows centered on each detected peak were stacked and reduced to a single median beat per record (attenuating noise and ectopic beats), cropped (removing 150 leading and 50 trailing samples), downsampled to 250 Hz, and normalized per lead by it's absolute maximum. Records for which R-peak detection failed were excluded, yielding 11,559/1,449/1,459 usable training/validation/test records. *Model*: We reimplemented ECG-SMART-NET as a ResNet-18 backbone (four residual stages, $64\rightarrow128\rightarrow256\rightarrow512$ channels) using $1\times k$ temporal convolutions in place of standard 2D kernels, followed by one 12×1 spatial convolution after the final residual stage, global average pooling, and a fully connected classification layer. *Training*: The model was trained with an Adam optimizer (learning rate 1×10^{-4}, weight decay 1×10^{-3}), cross-entropy loss, and a balanced sampler performing true random undersampling of the majority class without replacement each epoch to address class imbalance (34.4% MI prevalence). Training was capped at 200 epochs with early stopping on validation loss (patience = 10 epochs); the checkpoint with lowest validation loss was retained as the final model. *Main outcome measures*: Test-set accuracy, area under the receiver operating characteristic curve (AUC), average precision (AP), F1 score, precision, and recall.

Results Early stopping was triggered at epoch 11 of a maximum 200; the retained checkpoint (epoch 1, lowest validation loss) avoided the overfitting apparent in later epochs, where training accuracy exceeded 98% while validation loss rose and plateaued (Figure 1). On the independent, patient-disjoint test set (n=1,459), the model achieved an overall accuracy of 90.34%, an AUC of 0.9618, and an average precision of 0.9418 (Figure 2), exceeding the 0.953 AUC reported for ECG-SMART-NET on the original proprietary EMS cohort [3]. The model correctly classified 887/957 (92.7%) NORM records and 431/502 (85.9%) MI records, yielding a F1 score of 0.8594 (recall 0.8586, precision 0.8603); the 70 false positives and 71 false negatives were distributed roughly evenly between classes, indicating no strong directional bias in misclassification.

Discussion These results show that ECG-SMART-NET's separation of temporal (lead-wise) and spatial (cross-lead) convolutions, meant to mirror clinical ECG interpretation, generalizes beyond the single proprietary EMS dataset it was originally introduced on, achieving discrimination at least comparable to the original report (AUC 0.9618 vs. 0.953) on a independent, publicly available cohort using only median-beat inputs rather than full raw waveforms. This is meaningful because PTB-XL's MI labels reflect broad diagnostic superclasses rather than the strict occlusion-MI adjudication used in the original study, which suggest the architecture's inductive bias is robust to differences in label definition and data provenance. Limitations include the binary MI/NORM simplification relative to finer OMI distinctions, a custom median-beat pipeline that is not identical to the original authors' method, and a single train/validation/test split. Future work will extend evaluation to multiclass and OMI-specific labels within PTB-XL and benchmark against additional public 12-lead datasets. This study support ECG-SMART-NET as a reusable architecture for automated MI screening, and its performance on PTB-XL provides a reproducible benchmark for future comparisons.

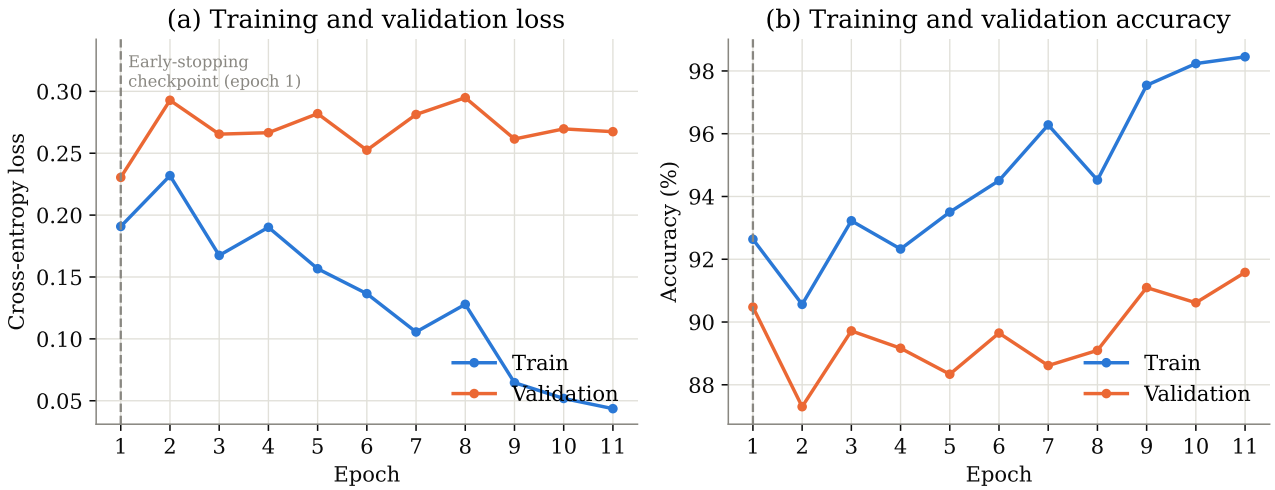

Figure 1: Training and validation (a) loss and (b) accuracy across the 11 epochs of the run in which early stopping was triggered. The dashed line marks the checkpoint retained as the final model (epoch 1, lowest validation loss); validation loss rises in later epochs even as training loss and accuracy continue to improve, indicating overfitting, which is why early stopping rather than a fixed epoch budget was necessary.

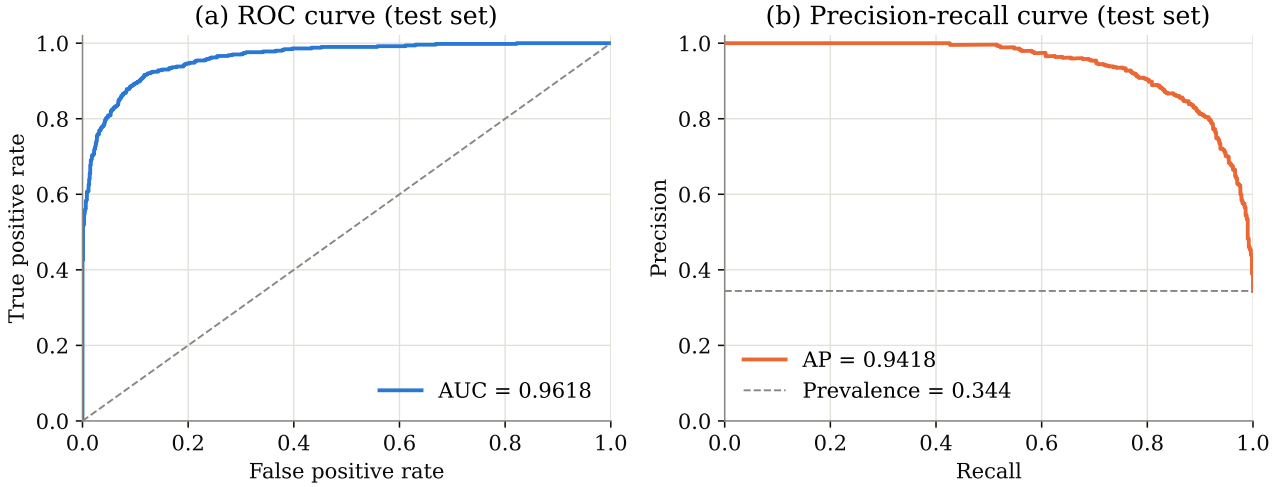

Figure 2: (a) Receiver operating characteristic curve and (b) precision-recall curve for the final model evaluated on the held-out test set (n=1,459). Precision, recall, and their harmonic mean (F1 = 0.8594) are computed at the default 0.5 probability threshold.

References

1. Wagner P, Strodthoff N, Bousseljot RD, Kreiseler D, Lunze FI, Samek W, Schaeffter T. PTB-XL, a large publicly available electrocardiography dataset. Sci Data. 2020;7:154.
2. Goldberger AL, Amaral LAN, Glass L, Hausdorff JM, Ivanov PC, Mark RG, Mietus JE, Moody GB, Peng CK, Stanley HE. PhysioBank, PhysioToolkit, and PhysioNet: components of a new research resource for complex physiologic signals. Circulation. 2000;101(23):e215-e220.
3. Riek NT, Akcakaya M, Bouzid Z, Gokhale T, Helman S, Kraevsky-Philips K, Ji RQ, Sejdic E, Zègre-Hemsey JK, Martin-Gill C, Callaway CW, Saba S, Al-Zaiti S. ECG-SMART-NET: A deep learning architecture for precise ECG diagnosis of occlusion myocardial infarction. IEEE Trans Biomed Eng. 2025.

Learning RNA Seq analysis using AI as a teaching assistant

Mia T. Zhao[1], Rahil Sethi[2], MS, Jiefei Wang[2], PhD, Uma Chandran[2], PhD, MSIS
[1]North Allegheny Senior High, Wexford, PA; [2]University of Pittsburgh Department of Biomedical Informatics, Pittsburgh, PA

Abstract

Chronic lung dysplasia is a serious lung disease caused by premature birth, typically treated with glucocorticoids such as Dexamethasone which can also cause adverse long-term neurological and behavioral side effects. The project aims are to assess Claude Chatbot's ability to teach and perform differential expression (DE) analysis of a published RNA Seq dataset of rat lung treated with Dex and another glucocorticoid, Desisobutyryl-ciclesonide (Des-CIC), which also promotes lung maturation but may have fewer adverse effects.

Introduction

AI use is becoming increasingly common in biomedical research for literature reviews, study design, and bioinformatics analysis. Novices are increasingly using AI to learn new concepts and for DIY genomics analysis, risking artifactual results and methodology errors that are difficult to detect without a domain expert. Whether AI can accurately and effectively teach advanced concepts and complex analysis remains understudied. In this RNA seq data analysis project, the goals are for a high school student to learn RNA seq data analysis under mentor supervision, using AI as an assistant to learn biological concepts (e.g. glucocorticoids in treating lung dysplasia), RNA seq workflow, hands-on RNA seq data analysis in R with Claude and evaluate AI's helpfulness in teaching or performing independent data analysis.

Methods

A published RNA seq study[1] of neonatal rat lung treated with Dex and Des-CIC provided the counts matrix and a metadata sheet used for analysis. An experienced bioinformatician mentor met with student daily to teach concepts in biology and bioinformatics, supplemented with weekly tasks for student using Claude as an assistant. Student logged AI interactions and gave verbal feedback to mentor. Learning was informally assessed across levels roughly aligned with Bloom's taxonomy, from concepts understanding to evaluating biological conclusions. Claude's analytical accuracy was also evaluated by comparison to results generated in R.

Results

Counts and metadata files were loaded into R to perform DE analysis and data visualization, while a parallel Claude data explorer taught the purpose of visualization methods (volcano plots, heat maps and dot plots). Claude's DE analysis, pathway analysis, Dex vs Des-CIC comparisons and accuracy were benchmarked against the R/EnrichR analysis. Overall, it was extremely challenging to learn concepts using AI: it requires 100s of prompts, and answers were long and ilogical. It was particularly weak at teaching statistical concepts such as p values, FDR and fold change. However, it was very helpful for troubleshooting R installation/execution errors, generating DE results for EnrichR, and comparing and explaining why Dex produced broader effects than DES-CIC. As an analytical tool, Claude's results differed slightly from the R/EnrichR analysis, and was not transparent about the differences unless directly prompted.

Discussion

Claude has strengths and weaknesses in teaching bioinformatics to novices. Strengths include reduced demand on mentor time to teach fundamental concepts in biology and bioinformatics, and effectively troublteshooting R errors. Weaknesses include inadequate teaching depth, unstructured/erroneous responses and limited transparency in analysis. AI does not adequately replace a structured curriculum (e.g. workshops or classroom teaching by an instructor). These results could inform methods to incorporate AI more effectively in teaching bioinformatics.

References

1. Jaumotte JD, El Khoury N, Min CK, Wang J, Madigan C, Jano A, Russo Kobylski RJ, Solt LA, Dhavan RS, Short KL, Lei T, Chandran U, Cole TJ, Monaghan-Nichols AP, Sampath V, Houtman R, Nettles KW, DeFranco DB. Physiologic and structural characterization of desisobutyryl-ciclesonide, a selective glucocorticoid receptor modulator in newborn rats. PNAS Nexus. 2024 Dec 26;4(1):pgae573